UNITED NATIONS UNIVERSITY
GEOTHERMAL TRAINING PROGRAMME

ORKUSTOFNUN

Öskurhóll, Hveravellir at Kjölur

Erlindo C. Angcoy Jr.

GEOCHEMICAL MODELLING OF THE HIGH-TEMPERATURE MAHANAGDONG GEOTHERMAL FIELD, LEYTE, PHILIPPINES

Report 1
September 2010

UNITED NATIONS UNIVERSITY
GEOTHERMAL TRAINING PROGRAMME
Orkustofnun, Grensásvegur 9,
IS-108 Reykjavík, Iceland

Reports 2010
Number 1

GEOCHEMICAL MODELLING OF THE HIGH-TEMPERATURE MAHANAGDONG GEOTHERMAL FIELD, LEYTE, PHILIPPINES

MSc thesis
School of Engineering and Natural Sciences
Faculty of Earth Sciences
University of Iceland

by

Erlindo C. Angcoy Jr.
Resource Management Division, Technical Services Sector
Energy Development Corporation - EDC
Merritt Road, Fort Bonifacio, Taguig City
Metro Manila
PHILIPPINES
e_angcoy@yahoo.com

United Nations University
Geothermal Training Programme
Reykjavík, Iceland
Published in September 2010

ISBN 978-9979-68-281-3
ISSN 1670-7427

This MSc thesis has also been published in March 2010 by the
School of Engineering and Natural Sciences, Faculty of Earth Sciences
University of Iceland

INTRODUCTION

The Geothermal Training Programme of the United Nations University (UNU) has operated in Iceland since 1979 with six month annual courses for professionals from developing countries. The aim is to assist developing countries with significant geothermal potential to build up groups of specialists that cover most aspects of geothermal exploration and development. During 1979-2010, 452 scientists and engineers from 47 countries have completed the six month courses. They have come from Asia (42%), Africa (29%), Central America (15%), and Central and Eastern Europe (14%). There is a steady flow of requests from all over the world for the six month training and we can only meet a portion of the requests. Most of the trainees are awarded UNU Fellowships financed by the UNU and the Government of Iceland.

Candidates for the six month specialized training must have at least a BSc degree and a minimum of one year practical experience in geothermal work in their home countries prior to the training. Many of our trainees have already completed their MSc or PhD degrees when they come to Iceland, but several excellent students who have only BSc degrees have made requests to come again to Iceland for a higher academic degree. In 1999, it was decided to start admitting UNU Fellows to continue their studies and study for MSc degrees in geothermal science or engineering in co-operation with the University of Iceland. An agreement to this effect was signed with the University of Iceland. The six month studies at the UNU Geothermal Training Programme form a part of the graduate programme.

It is a pleasure to introduce the 21st UNU Fellow to complete the MSc studies at the University of Iceland under the co-operation agreement. Mr. Erlindo C. Angcoy Jr., BSc in Chemical Engineering, of the Energy Development Corporation (EDC), Philippines completed the six month specialized training in Chemistry of Thermal Fluids at the UNU Geothermal Training Programme in October 2006. His research report was entitled: "An experiment on monomeric and polymeric silica precipitation rates from supersaturated solutions". After two years of geothermal research work in the Philippines, he came back to Iceland for MSc studies at the Faculty of Earth Sciences of the University of Iceland in August 2008. In February 2010, he defended his MSc thesis presented here, entitled "Geochemical modelling of the high-temperature Mahanagdong geothermal field, Leyte, Philippines". His studies in Iceland were financed by the Government of Iceland through a UNU-GTP Fellowship from the UNU Geothermal Training Programme. We congratulate him on his achievements and wish him all the best for the future. We thank the Faculty of Earth Sciences at the School of Engineering and Natural Sciences of the University of Iceland for the co-operation, and his supervisors for the dedication.

Finally, I would like to mention that Erlindo´s MSc thesis with the figures in colour is available for downloading on our website *www.unugtp.is* under publications.

With warmest wishes from Iceland,

Ingvar B. Fridleifsson, director
United Nations University
Geothermal Training Programme

ACKNOWLEDGEMENT

My heartfelt gratitude, sincere appreciation and lifetime indebtedness…

… to the Government of Iceland for awarding this Fellowship through the United Nations University Geothermal Training Programme under the dedicated and esteemed staff of Dr. Ingvar B. Fridleifsson (Director), Mr. Lúdvík S. Georgsson (Deputy Director), Ms. Thórhildur Ísberg and Ms. Dorthe H. Holm…

… to the management and staff of Energy Development Corporation for extending technical and personal support in the various stages of the study. My special mention to a) my colleagues who helped me outsmart the winds and rains of Mahanagdong in collecting the fluid samples: Rodrigo Arante, Teofilo Buena-agua, Paul Bertumen, Aldrin Miaga and Nimitz Oraiz, and b) the LRMD Laboratory staff whose skilful hands and minds in turn extracted the numbers from these fluids…

… to Ingvi Gunnarsson of Reykjavik Energy, Dr. Andri Stefánsson, Hanna Kaasalainen and Eydís Eiríksdóttir at the Institute of Earth Sciences, University of Iceland for guiding me through the analytical techniques and providing constructive inputs…

… to the wizards behind the speciation programs of WATCH (Dr. Jón Örn Bjarnason) and SOLVEQ (Mark Reed and Jim Palandri), for reaching out to make sure that I understand the inconvenient truths written in between the lines…

… and finally to my supervisor, Prof. Stefán Arnórsson. I may not closely approach equilibrium with his brilliance, but I can at least saturate with a similar passion to unceasingly learn, impart knowledge and provide permeability to spread the universal concept of goodness in different ways.

ABSTRACT

The high-temperature and liquid-dominated Mahanagdong geothermal field has supplied steam since 1997 to power plants with total installed capacity of 180 MWe. A geochemical assessment of the field is presented based on analytical data of fluids sampled at the wellheads of 26 wet-steam wells. The pH of the liquid samples ranges from 3 to 8 as measured on-site. Analyses of the water samples include major and minor elements. With the aid of speciation programs, the analytical data were used to model individual species activities in the initial aquifer fluids that feed the wells. The modelling indicates that excess discharge enthalpy of wells is mostly caused by phase segregation of the vapour and liquid phases in producing aquifers. The modelled aquifer fluid compositions were used to assess how closely equilibrium is approached between solution and various minerals.

At inferred Mahanagdong aquifer temperatures (250-300°C), the concentrations of H_2S and H_2 in the initial aquifer fluids, assuming they are purely liquid, are somewhat higher than those at equilibrium with hydrothermal mineral assemblages, one of which incorporates grossular, pyrite, magnetite and wollastonite, and the other hematite, magnetite and pyrite. The equilibrium constant for both buffers is very similar. The observed distribution of the data points for the gases is attributed to the presence of equilibrium vapour in the aquifer fluid. The concentrations of $H_{2,aq}$ show more scatter. Aquifer fluid concentrations of $CO_{2,aq}$ are slightly above equilibrium curve for both of the assemblages considered (czo+cal+qtz+gro and czo+cal+qtz+pre). However, variation in the composition of the solid-solution minerals may also contribute as well as departure from the model selected to calculate the gas concentration in the initial aquifer fluid. The aquifer liquid is in close saturation with various calcium-bearing, Fe-sulphide and Fe-oxide minerals but is significantly undersaturated with fluorite, grossular and wollastonite, all of which are rare at Mahanagdong. Departure from equilibrium for the Fischer-Tropsch and NH_3-N_2-H_2 reactions is high. To move the system towards equilibrium, H_2 concentrations need to increase, or in the case of the Fischer-Tropsch reaction, CH_4 must decrease.

Initial aquifer vapour fractions were derived assuming equilibrium between $H_{2,aq}$ and the gro+mag+qtz+epi+wol assemblage at the chosen mineral composition. Selecting the hem+mag mineral assemblage will give similar results. H_2S_{aq} concentrations, considering equilibrium vapour fraction in the initial aquifer fluid, are significantly above the equilibrium curves for the gro+pyr+mag+qtz+epi+wol or the hem+mag mineral assemblages. However for $CO_{2,aq}$, they closely approach equilibrium with either of the two mineral assemblages considered. Derived aquifer vapour fractions are highest in the upflow region (~4%) and in the collapse area (1-3%). The aquifer fluids east of the upflow region, which are at ~300°C, have equilibrium vapour fractions of ~1%. This area has characteristics of an upflow as suggested by systematics of the rare alkali analyses. Earlier data and those produced for this study both indicate maximum vapour loss in the western peripheral wells and vapour gain in wells when brine injection was dispersed farther from the production zone.

The most mobile elements in Mahanagdong fluids are Cl, As, Na, S, Rb, K, Li and Br. Ti and Al have the lowest mobility, both in neutral pH and acidic fluids. The acidic discharges have high metal content. Zn and Mg are probably mobilized from the reservoir rocks whereas Fe, Mn, Pb, Cu, Ni and Co in acidic waters are likely to come, at least partly, from well casing material. The only chemical differences between acidic and neutral pH waters, apart from pH and the mentioned metals, are higher levels of SO_4 and Mg in the former. The modelled aquifer pH (~4.5) of two acidic samples is lower by about 1 unit compared to the other aquifer fluids. The acidity at the surface of the Cl-SO_4-type waters is mainly caused by the dissociation of HSO_4- as the fluids cool by depressurization boiling when they flow from the aquifer to the wellhead. The molar ratios of H_2S and SO_4 in the aquifer fluids, if they still retain the signal of their magmatic sources, suggest that the disproportionation of SO_2 at subcritical conditions and hydrolysis of native sulphur contribute to acidity of fluids discharged in some wells.

TABLE OF CONTENTS

LIST OF FIGURES

LIST OF TABLES

1. INTRODUCTION

Since lighting the first bulb in 1967 using geothermal energy, the Philippines has risen to become the second largest electrical power producer in the world that harness this indigenous, environment-friendly and enormous energy resource (IGA, 2009). In 2008, geothermal power plants contributed about 18% of the total power generation mix despite constituting only 12% of the total installed power plant capacity in the country (DOE, 2009). At the forefront of Philippine geothermal development is Energy Development Corporation (EDC), a company fully-privatized in 2007 after three decades of operating as a subsidiary and geothermal arm of the government-owned and controlled Philippine National Oil Corporation (PNOC). As of 2009, EDC operates a combined capacity of ~1,200 MWe from its geothermal steamfields (Figure 1) accounting 61% of the country's total geothermal capacity (EDC, 2009).

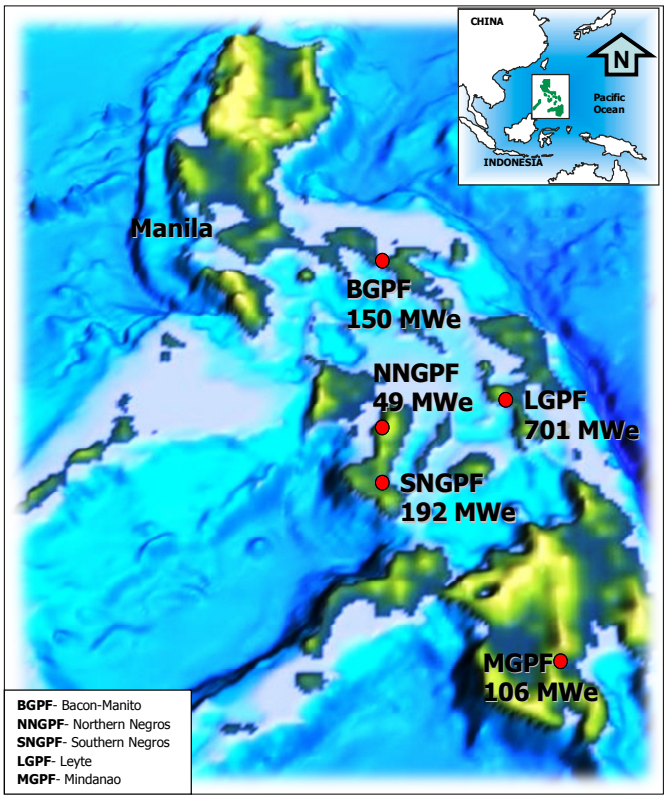

FIGURE 1: Geothermal production fields (GPF) operated by EDC and their installed capacities

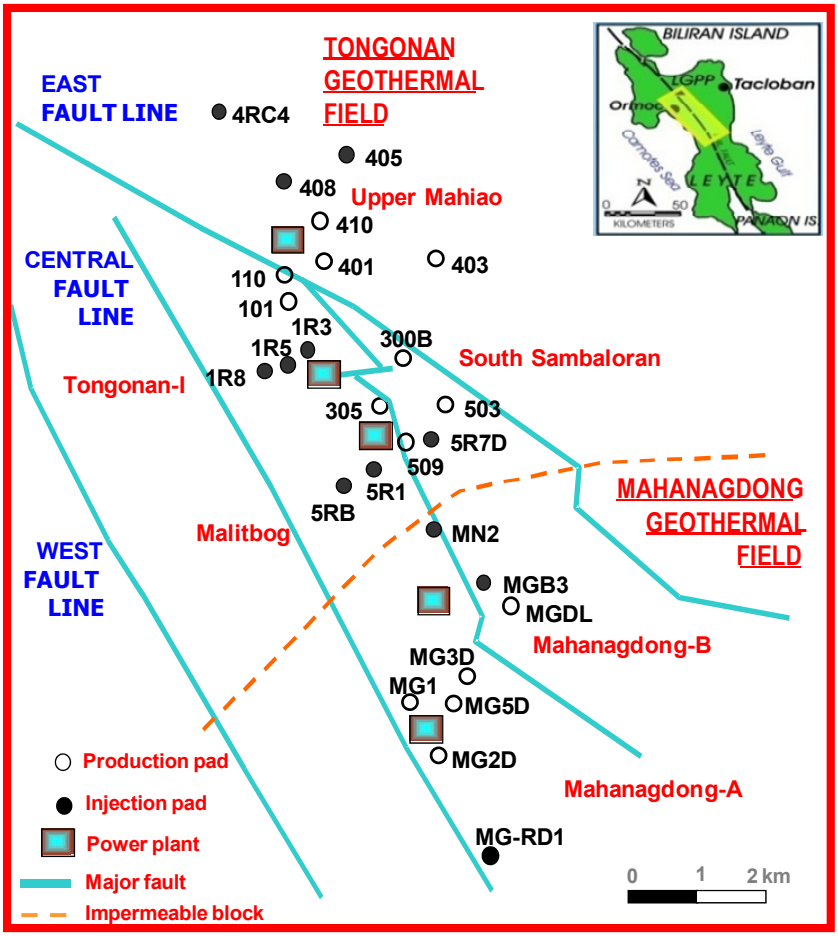

FIGURE 2: Tongonan and Mahanagdong geothermal fields in the island of Leyte, Philippines

One of EDC's pioneering geothermal ventures in 1977 is the development of the Greater Tongonan Geothermal Field in the province of Leyte, central Philippines (Figure 2). The Tongonan Geothermal Field in the north started commercial production in 1983 to supply steam to a 112 MWe power plant. The Mahanagdong Geothermal Field in the south was developed about a decade later after EDC entered into 10-year Build-Operate-Transfer contracts with private investors to construct additional power plants. Mahanagdong Geothermal Field currently supplies the steam requirements of the 120 MWe Mahanagdong-A and 60 MWe Mahanagdong-B power plants. The Greater Tongonan Geothermal Field is currently the country's largest geothermal field with a total installed capacity of

~700 MWe. EDC operates all the steamfields and power plants in this area by 2010.

The reservoir response and management of the Greater Tongonan Geothermal Field within ~25 years of field operation is well documented. A common consequence of long-term utilization is an increase of vapour to liquid ratio in the discharges of producing wells due to reservoir pressure drawdown. The production zones of most wells in Mahanagdong are below 1200 m thus higher overburden pressure prevented fieldwide boiling (Salonga, 2004). The role of gas geochemistry in assessing the reservoir becomes more relevant especially when extensive boiling leads to the decline and even disappearance of liquid phases. D'Amore (1991) and Arnórsson (2000) provide comprehensive discussions how the gas content of well discharges are evaluated and correlated with the reservoir conditions. In gas geochemistry studies, the cornerstone is the assumption of close approach to equilibrium in the aquifer either among specific reactive gases commonly present in geothermal well discharges (e.g., CO_2, H_2S, H_2, NH_3, CH_4, N_2) or between some reactive gases and potential mineral buffers in the geothermal field.

Demonstrations of gas equilibria in Mahanagdong were earlier conducted by Salonga and Auman (1997) and Siega et al. (1999). Both works used the approaches of Giggenbach (1980) and D'Amore and Truessdell (1995) which consider the gas analyses obtained in the surface as representative of the reservoir values. D'Amore (1991) lists some conditions when such assumption may be invalid. One is when the vapour phase moves faster than the liquid phase as the fluid rises to the surface. Consequently, the vapour phase sampled in the surface may reveal higher gas concentrations than what were originally in the aquifer. The extent of phase segregation is affected by vapour to liquid ratio in the fluid, the effects of capillary pressure and the relative permeability of the fluid phases in the reservoir (e.g. Horne et al., 2000; Pruess, 2002). Some wells displaying an apparent "excess enthalpy" (i.e., to discharge enthalpy that is significantly greater than that of steam-saturated water at the aquifer temperature) are mostly attributed to phase segregation (e.g. Glover et al., 1981; Arnórsson et al., 2007; Giroud, 2008).

In this contribution, analyses of water and gas samples obtained from the wellheads of 26 wet-steam wells (i.e. wells discharging a mixture of vapour and liquid water) drilled in Mahanagdong were used to formulate an updated geochemical model of the field. The fluids are saline and mineralized that typically characterize fields associated with subduction zones and hosted by andesitic rocks. Modelling involves evaluating specific mineral-gas and gas-gas equilibria that may potentially control the concentrations of the prevalent reactive gases CO_2, H_2S, H_2, CH_4 and N_2 in well discharges. The "excess enthalpies" exhibited by 13 producing wells were attributed to phase segregation and were considered in calculating their aquifer conditions following the methods described by Arnórsson et al. (2007) and Arnórsson et al. (2010). Systematics of trace and minor elements from water samples complement the model to reconcile with established hydrological flow models and observed reservoir processes. Such geochemical assessments provide insights on current reservoir conditions after prolonged production, further understanding on the acidic behaviour of some wells and helpful tools in formulating resource management strategies for Mahanagdong.

2. MAHANAGDONG GEOTHERMAL FIELD

The high-temperature geothermal field of Mahanagdong is located on the island of Leyte, central Philippines, approximately 700 km south of the capital city of Manila. The ~10 km^2 field comprises the southern part of the Greater Tongonan Geothermal Field that encompasses ~40 km^2 of rolling to rugged topography. Some aspects make Mahanagdong an interesting field. Characteristics of well discharges provide opportunities for comparison either among wells discharging liquid enthalpies and "excess enthalpies" or between those fluids with acidity varying from near-neutral to more acidic levels. Since Mahanagdong is well-studied, numerous scientific data are available from field exploration and assessment (e.g. Vasquez and Tolentino, 1972; Ogena, 1988; Bayrante et al., 1992; Sta. Ana et al., 2002) up to field monitoring and management (e.g., Seastres et al., 2000; Gonzalez et al., 2005; Angcoy et al., 2008). Salonga et al. (2004) gives a thorough background of Mahanagdong prior and after commercial operation while Alcober et al. (2008) present a more updated situation of the field. Therefore, this section shall summarize and emphasize only the details that are most relevant to the present study.

2.1 Geological overview

The field lies along a NW-SE trending chain of Quaternary calc-alkaline volcanoes associated with the subduction of the Philippine Sea Plate off the eastern coast of the archipelago. Episodes of volcanism and sedimentation mostly contributed to its rock units consisting of (from bottom to surface): (1) a Pre-Tertiary metamorphic ultramafic basement (mainly serpentinite), (2) a sedimentary breccia/conglomerate complex (altered microdiorite, quartz monzodiorite and minor volcanics), (3) an impermeable claystone unit, (4) a formation of andesite lavas, hyaloclastites and tuff breccias (collectively called Mamban Formation) and (5) surface rocks dominantly composed of fresh to weakly weathered andesite lava flows intercalated with pyroclastics. The latest exposed volcanics are assigned with Pleistocene to Recent age (e.g. Herras et al., 1996).

The NW-SE trending Philippine Fault system transects the entire Greater Tongonan Geothermal Field, moving left-laterally at a minimum slip rate of 19 mm/yr (Aurelio et al., 1994). The active Philippine Fault branches into three major traces in the area (Figure 2) highly influencing permeability and defining the boundaries of the production zones. Areas to the left of Central Fault Line comprise the less mobile block and its lithology of ultramafic basement complex and extensive claystone limit permeability to the west (Caranto and Jara, 2006). Towards the east, the area is very permeable where interconnected structures allow mixing of fluids and leads natural fluid outflow towards the southeast.

All the geothermal wells in Mahanagdong produce from the lower section of Mamban Formation to within the sedimentary breccia/conglomerate complex. It is common for drilled wells to encounter multiple intrusions with the latest dikes indicating the subsurface manifestations of the youngest heat source (Reyes, 1990).

2.2 Alteration mineralogy

Similar to most geothermal fields in the Philippines, reservoir rocks in Mahanagdong are extensively altered by silicate and sulphide minerals (e.g. Zaide-Delfin and Dulce, 1996). The main suite of silicate alteration produced by neutral-pH waters consists of illitic clays and epidote associated with chlorite, quartz, calcite and anhydrite. Other common types of silicates are K-feldspar, wairakite, albite and kaolinite. They occur either as replacement minerals or vein and vug deposits. Silicates in acid fluids are relatively few with assemblages composed of pyrophyllite and dickite associated with diaspore, alunite, quartz, anhydrite and pyrite. Acid minerals occur in discrete zones. The most common sulphides and oxides found in drill cuttings include pyrite, chalcopyrite, bornite, hematite and magnetite. Covellite, chalcocite and sphalerite were also identified in rare amounts.

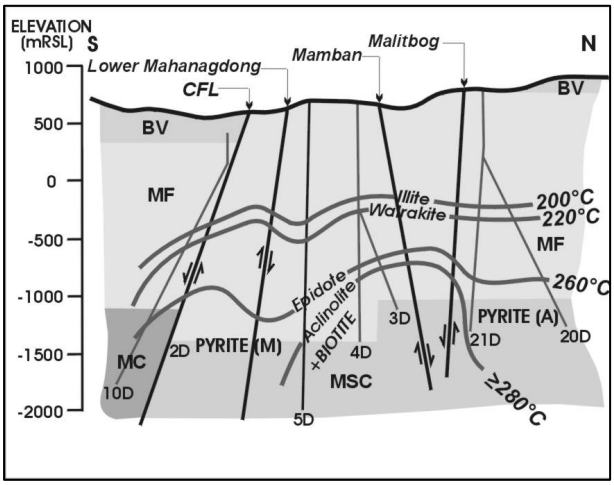

FIGURE 3: Cross section of Mahanagdong geothermal field with the first appearances of minerals and corresponding subsurface temperatures indicated (reprinted from Martinez, 1998). Abbreviations: CFL- Central Fault Line, BV- Bao Volcanics, MF- Mamban Formation, MC- Mahanagdong Claystone, MSC- Mahiao Sedimentary Complex, well names indicated at bottom of welltracks. Figure also emphasizes the abundance of pyrite in the acidic area, Pyrite (A), compared to moderate occurrences in the production zone of neutral fluids, Pyrite (M)

Parilla et al. (1997) and Martinez (1998) investigated silicate and sulphide mineral equilibria in Mahanagdong using mineral activity diagrams. They concluded that no distinct silicate and mineral assemblages can distinguish between neutral-pH and acid fluids since both types of fluids are stable with the same silicate minerals (illite, epidote, wairakite, kaolinite and K-feldspar) and sulphide minerals (pyrite, chalcopyrite and bornite). However, Dulce et al. (1995) pointed out the abundance of sulphides in acid fluids compared to neutral wells. Acidic wells with high sulphate contents have the tendency to form anhydrite veins. By using sulphur isotope systematics, Salonga et al. (2000) proposed mechanisms to explain the quantities of sulphur in the waters and rocks interacting in Mahanagdong. Calcite saturation is generally demonstrated in neutral wells with those towards the periphery of the field having the potential to develop calcite blockages within the wellbore. Figure 3 shows a general cross-section of Mahanagdong as interpreted by Martinez (1998).

In Mahanagdong, Zaide-Delfin and Dulce (1996) found that alteration mineralogy does not always correlate well with present reservoir conditions. Using secondary minerals to predict aquifer temperature and pH yield variable results. They concluded that hydrothermal alteration in Mahanagdong is pervasively relict and vein mineralogy generally reflects better the more recent hydrothermal event.

2.3 Fluid chemistry

The well discharges in Mahanagdong are generally of the neutral and mature NaCl-type of fluids. The baseline characteristics of the postulated parent fluids (MG3D, MG14D) include T_{quartz} (Fournier and Potter, 1982) at ~300°C , highest reservoir Cl (~4000 mg/kg) and SiO_2 levels (~650 mg/kg), and most isotopically enriched water of ^{18}O at -1.0 ‰. The fluids towards the major natural outflow in the southeast are homogenous with lower T_{quartz} (260-280°C) and reservoir Cl levels (2000-3000 mg/kg) and depleted ^{18}O at -2.0 ‰ to -3.0 ‰. The fluids in the northern part of the reservoir are acid Cl-SO_4 waters (pH sampled at wellhead <4) with reservoir Cl concentrations similar to wells in the upflow zone. The acidic fluids have elevated SO_4 (>100 mg/kg), Fe (>10 mg/kg) and Mg (>5 mg/kg) contents in the liquid phase and H_2S in the vapour (>25 mmoles/100 mole water). The acidic fluids have stable isotopic levels comparable to the neutral-pH fluids at the outflow regions.

Alvis-Isidro et al. (1993) proposed that geothermal fluids in both Tongonan and Mahanagdong fields are derived from mixing of magmatic water associated with local andesitic volcanism and the local meteoric waters. Studies conducted by Parilla et al. (1997) and Salonga et al. (2000) using geochemical data and stable ^{34}S and ^{18}O isotope systematics indicate that both neutral-pH and acidic fluids in Mahanagdong originate from a dominantly hydrothermal system with no active magmatic environment. The deep waters of Mahanagdong are estimated to have 32% magmatic and 68% meteoric components (Salonga and Siega, 1996). Bayon and Ferrer (2005) used stable sulphur isotope ratios to demonstrate that geothermal H_2S in Mahanagdong are either derived directly from a magmatic source or indirectly through the disproportionation of SO_2.

2.4 Well discharge enthalpies

Mahanagdong is a liquid-dominated geothermal field. By definition, it means that the aquifer fluid is either comprised purely of liquid or with a small vapour fraction, even in terms of volume (White et al., 1971). The samples in this study were obtained from 26 wells with total discharge enthalpies of about 1000-2400 kJ/kg. Some of the well discharges have liquid enthalpy (i.e. the enthalpy of the discharged fluid equals the enthalpy of vapour-saturated liquid at the aquifer temperature). In this study, 13 wells discharge variable degree of "excess enthalpies". In later sections, it will be demonstrated that phase segregation primarily accounts for the discharge enthalpy of these wells.

During the initial stage of exploitation, the field enthalpy of Mahanagdong showed indications of boiling. The increasing field enthalpy was however short-lived as soon as inflowing cooler peripheral fluids and injection returns started to take effect (Sta. Ana et al., 2002). A thick and poorly permeable layer (~1 km) of lava and pyroclastic sequence overlie the upper part of the reservoir. The productive zones are mostly below 1200 m depth and the overburden pressure prevents extensive boiling of the fluid throughout the field typically induced by reservoir pressure drawdown. The wells in this study discharging "excess enthalpy" are either in the vicinity of the upflow region or are shallow and thus only tap the upper highly two-phase production zones.

2.5 Conceptual model

Based on multi-disciplinary inputs from geology (e.g. Herras et al., 1996), geophysics (e.g. Los Baños and Maneja, 2005), reservoir engineering (e.g. Urmeneta, 1993; Sta. Ana et al., 2002) and geochemistry (e.g. Alvis-Isidro et al., 1993; Balmes, 1994), it is believed that Mahanagdong is a distinct resource separated from the northern Tongonan Geothermal Field by a cold impermeable block. The northeastern part of the field in the vicinity of wells MG3D and MG14D is the postulated upflowing region of hot, neutral-pH fluids. The major natural outflow of the reservoir is towards the southeast where interconnected structures resulted to homogenous characteristics of the neutral-pH fluids (Figure 4). A minor outflow also exists towards the north but is confined by poorly interconnected fractures thereby limiting water-rock interaction and probably factored in the emergence of acidic fluids. The Mamban Fault is inferred to be the major structure separating the acid fluids in the north and neutral-pH reservoir in the south.

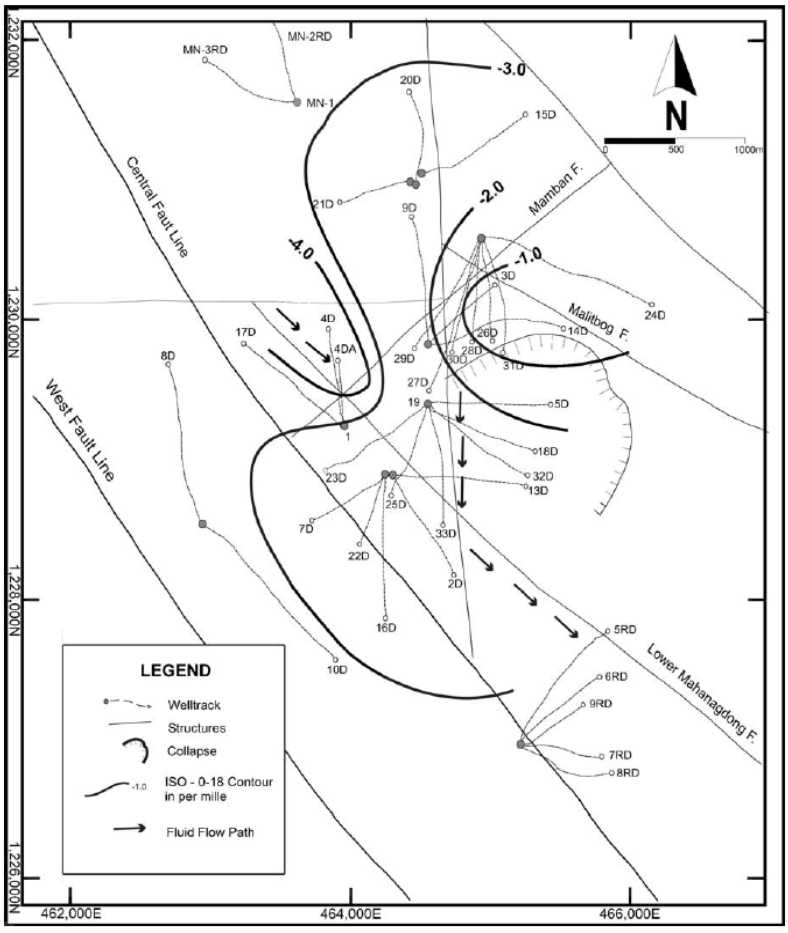

FIGURE 4: The inferred fluid flow path in Manhanagdong based on its baseline contour map of the stable isotope ($\delta^{18}O$) and geochemical signatures in 1997 (reprinted from Salong et al., 2004)

Using stable isotope systematics, Dacillo and Salonga (2004) described how the conceptual flow pattern of the deep fluids in Mahanagdong has evolved from exploration, development and exploitation stages. Their findings complemented earlier works by Salonga et al. (2004) where they demonstrated geochemical and isotopic signatures of cooler groundwater encroachment from the northwestern part of the sector and separated brine returns from the northern and southern injection fields. Herras et al. (2005) and Molina et al. (2005) attempted to quantify the rate of these processes from the results of multi-tracer tests. Some of the processes generally affecting Mahanagdong field are presented in Figure 5 as evaluated by Alcober et al. (2008).

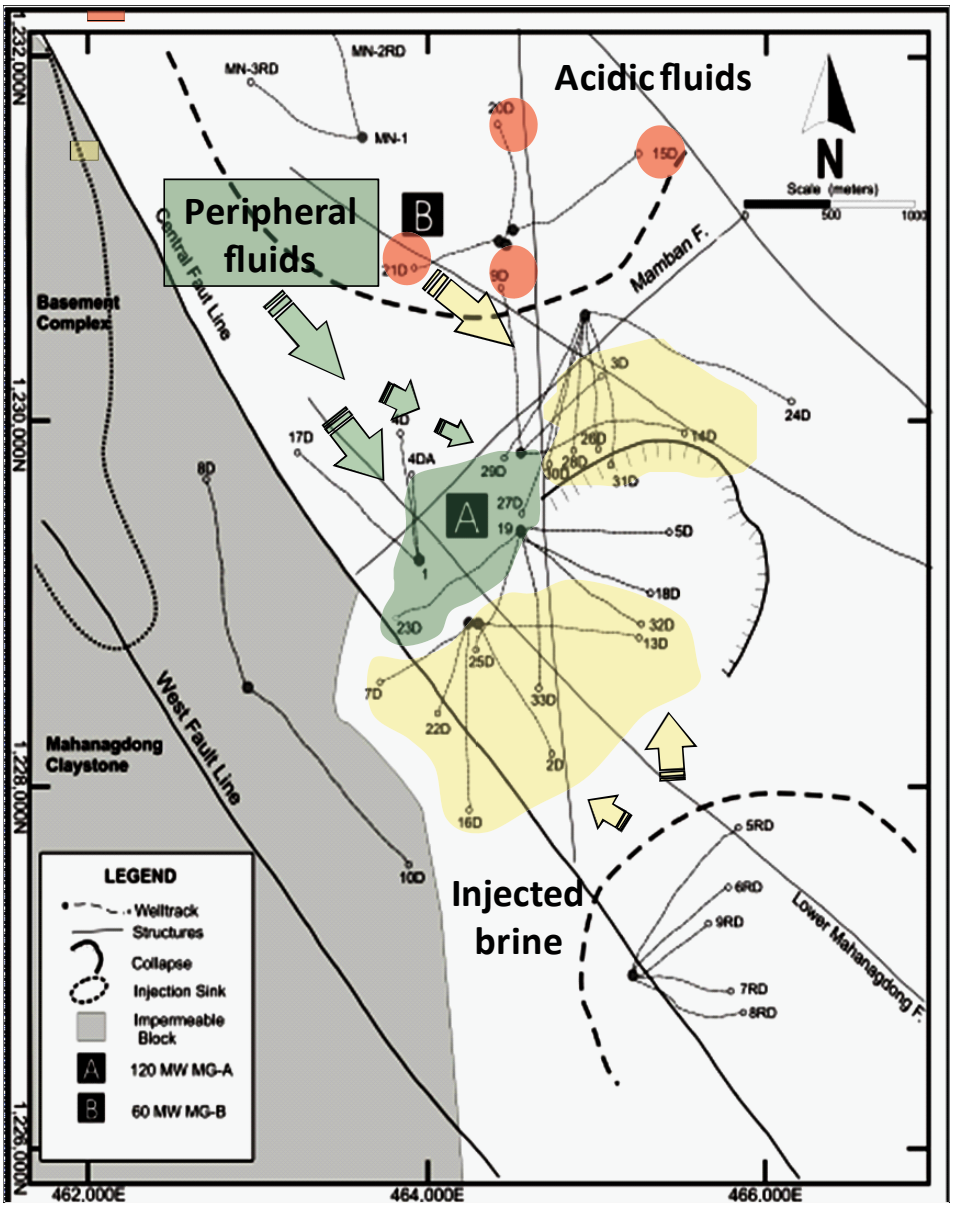

FIGURE 5: Updated processes affecting the Mahanagdong geothermal field (modified from Alcober et al., 2008)

3. METHODOLOGY

The primary data for this study were obtained from the water and gas discharges of 26 wet-steam wells drilled in Mahanagdong. All fluids were sampled during the period December 2008-January 2009 except for 3 samples collected on June-July 2009. Most of the wells were continuously supplying steam to the power plants while two (MG9D and 26D) were only discharging to silencers. MG9D was discharged with an acid inhibition system. The wells were drilled to approximate depths of 1900-2800 m. Only two wells (MG1 and 19) are drilled vertically. The wells often produce from multiple feed zones (e.g., Sta. Ana et al., 2002).

3.1 Sampling

Sampling of fluids from the wellheads of geothermal wells utilizes specific techniques in addition to normal procedures used in sampling surface and non-thermal waters. These steps ensure to obtain representative samples considering the high temperatures of the fluids and the effects of cooling or exposing the samples to the atmosphere. The Geothermal Procedural Manual (GPM) of EDC for well sampling was followed. The procedures are in principle similar to the details discussed by many references (e.g. Arnórsson, 2000 and Arnórsson et al., 2006). A double-cyclone Webre-separator is used to separate the vapour and liquid phases near the wellheads and allow liquid water and steam phases to be collected at the same sampling pressure (Figure 6). To minimize the effect of boiling, the sampling pressures are maintained within 3 lb/in^2 (0.2 bar) from the two-phase line pressure.

FIGURE 6: The double-cyclone Webre separator used to sample the well discharges

3.1.1 Vapour phase

The vapour phase from the Webre-separator is collected using two double-ended gas sampling bulbs. One gas-sampling bulb is pre-weighed, evacuated and contains freshly prepared 35% NaOH solution. The strong base is used to capture the major non-condensible gases (CO_2 and H_2S) while the residual gases (H_2, CH_4, Ar and N_2) occupy the head space. Another gas-sampling bulb collects condensed steam for analysis of the water-soluble NH_3. Only one set of gas samples was obtained for each well for analysis in Leyte Geothermal Production Field Resource Management Department (LRMD) EDC laboratory (PNS ISO/IEC 17025 accredited).

3.1.2 Liquid phase

Two sets were obtained for parallel analysis of liquid samples both in LRMD EDC laboratory and, for this study, in the Institute of Earth Sciences, University of Iceland. All liquid samples were cooled via stainless steel coil and collected in plastic bottles (HDPE or PP). On-site, samples for analysis in LRMD EDC laboratory were unfiltered whereas samples for this work were passed through 0.45 μm pore size membrane filter, except three samples from production wells (MG18D, 23D and 39D) and two samples from brine injection wells (MN3RD and MG9RD). Filtering on-site prevents contamination of the samples by suspended particles that may dissolve when the samples are acidified. The Geothermal Procedural Manual of EDC also uses the same optimum setting of Webre-separator during collection of both vapour and liquid samples. In contrast, liquid samples for this study were collected while the separator was flooded to further ensure that only the liquid phases are obtained (i.e., to prevent contamination by the vapour phase). Table 1 summarizes the different kinds of sample treatment for the various water analyses. The acid used for all sample treatment was 50% reagent

grade nitric acid (HNO_3). All water samples were transported to the University of Iceland in thermally-insulated boxes.

TABLE 1: Separated water samples

Container	Sample treatment	Analysis	Method	Laboratory
250 ml amber glass bottle	Filtered, air-free	H_2S, T-CO_2	Titration	Shortly after sampling
75 ml amber glass bottle	Filtered, air-free	T-CO_2	ICP-AES	IES*, University of Iceland
100 ml HDPE bottle	Filtered, acidified with 0.5 ml HNO_3	B, SiO_2, Cl, Na, K, Ca, Mg, SO_4, Al, Fe, Li, Br, As, Mn, Ba	ICP-AES	IES*, University of Iceland
100 ml HDPE bottle	Filtered	F, Cl, SO_4	IC	IES*, University of Iceland
200 ml HDPE bottle	Filtered, acidified with 1 ml HNO_3	Trace elements	ICP-MS	UC**-Merced
250 ml glass bottle	Unfiltered, air-free	pH, H_2S, T-CO_2/HCO_3	See text	LRMD EDC***
500 ml HDPE bottle	Unfiltered, acidified with 5 ml HNO_3	B, SiO_2, Cl, Na, K, Ca, Mg, Fe, Li, NH_3		
250 ml HDPE bottle	Unfiltered	SO_4		
*IES - Institute of Earth Science, **UC - University of California, ***LRMD EDC - Leyte Geothermal Production Field, Resource Management Department, EDC.				

3.2 Analysis

All gas analyses were carried out in LRMD EDC Laboratory (PNS ISO/IEC 17025 accredited). CO_2 and H_2S in the caustic soda were analyzed by titration while the residual gases in the head space of the gas sampling bulbs (H_2, CH_4, Ar and N_2) were analyzed on a gas-chromatograph (Shimadzu™ GC-8A or HP™ 6890). NH_3 in the steam condensate was analyzed by ion-selective electrode method. The other water analyses done by LRMD EDC laboratory include: 1) pH by electrometric method, 2) total carbonate carbon by titration, 3) H_2S by iodometry, 4) Cl by Argentometric-Potentiometric method, 5) total SiO_2 by spectrophotometry (heteropoly blue), 6) metals (Na, K, Ca, Mg, Fe, Li) by Atomic Absorption Spectrometry (AAS), 7) B by titrimetry (mannitol) and 8) SO_4^{-2} by colorimetry (barium chromate/bromophenol blue). Details of the water analyses can be found in Pang and Ármansson (2006).

In this study, the analyses of water samples are essentially in three groups: 1) on-site determination of pH, H_2S and total carbonate carbon, 2) analysis of major elements and some minor and trace elements using Spectro Ciros™ Inductively Coupled Plasma-Atomic Emission Spectrometer (ICP-AES) and Reagent Free Ion Chromatograph (RFIC™, Dionex 2000), 3) analysis of trace elements using quadrupole ICP-Mass Spectrometer (ICP-MS) at University of California, Merced.

The analyses of water samples collected from Mahanagdong are summarized in Tables 2 and 3. Table 4 gives analytical results for steam samples. Reported values in Tables 2-3 were used in the data reduction and interpretation. The ionic balances of all samples, as calculated by the WATCH speciation program (see Arnórsson et al., 1982), version 2.1 (Bjarnason, 1994), are all within ±10% with only one sample outside of ±5%. Comparison of all water analyses using different analytical methods in this study are detailed in Appendix A and summarized in Table 5. All samples were analyzed in duplicate. The percentage mean difference, which is reported in Table 5, is calculated by equation (1):

$$\%Mean\ Difference\ (\%M) = \{\ [(C_1 - C_2)]\ /\ [(C_1 + C_2)/2\ ]\ \}\ x\ 100 \qquad (1)$$

where, C_1 and C_2 are the analyses during the 1st and 2nd determinations, respectively.

TABLE 2: Measured discharge enthalpies, sampling pressures and analyses of major elements in the separated water samples[a]

Date	Well	SP[b]	H[c]	On-site		H_2S	T-CO_2	B	SiO_2	Cl	Na	K	Ca	Mg	F	SO_4	Al	Fe	NH_3	Li	Ionic Strength[d]	% Ionic Balance[d]
		barg	kJ/kg	pH	°C	mg/kg	mg/kg	mg/kg	mg/kg	mg/kg	mg/kg	mg/kg	mg/kg	mg/kg	mg/kg	mg/kg	mg/kg	mg/kg	mg/kg	mg/kg		
11Dec08	MG9D[e]	1.4	ND	3.32	23.5	ND	11.5	32.7	876	2995	1898	360	31.4	39.6	1.46	2155	2.262	840	8.09	6.26	0.15	-0.9
18Dec08	MN3RD[f]	17.9	ND	6.67	27.8	4.40	55.5	35.6	692	3367	1981	369	35.8	0.353	1.77	65.5	0.222	0.548	ND	6.24	0.10	-1.9
19Dec08	MG9RD[f]	6.19	ND	8.07	26.2	0.78	4.00	54.0	701	3913	2288	434	31.7	0.038	1.69	50.4	0.227	1.423	ND	7.07	0.11	-0.1
26Dec08	MG18D	9.4	1460	6.48	23.6	2.26	40.1	51.3	635	3653	2216	351	24.1	0.029	1.66	61.2	0.377	1.722	5.17	5.70	0.11	1.9
	MG23D	10.7	1212	6.65	22.8	1.88	43.4	42.9	634	3081	1827	333	30.3	0.022	1.64	47.2	0.393	0.251	2.85	4.69	0.09	1.1
	MG39D	10.3	1195	7.07	24.4	1.98	48.0	57.5	734	4051	2421	474	22.5	0.024	1.66	31.8	0.360	0.126	3.06	8.45	0.12	2.3
07Jan09	MG2D	9.5	1208	6.14	24.4	0.4	52.8	52.4	646	3757	2162	428	29.6	0.033	1.66	28.8	0.337	0.145	3.25	7.06	0.11	-0.5
	MG13D	10	1327	6.86	24.8	2.68	61.8	56.8	819	3741	2259	467	7.60	0.017	2.30	123	0.362	0.133	3.93	7.69	0.11	1.3
	MG7D	10.3	1177	6.27	24.1	0.42	38.3	58.6	716	4219	2424	480	40.3	0.028	1.42	23.7	0.284	0.254	2.38	7.75	0.12	-0.1
	MG16D	10.4	1379	6.08	24.3	1.45	61.5	61.7	754	4396	2551	516	38.0	0.033	1.57	22.2	0.354	0.014	2.8	8.38	0.13	0.9
	MG22D	10	1163	6.56	23.8	1.22	35.1	59.7	744	4278	2464	504	39.3	0.027	1.42	23.9	0.254	0.024	2.51	8.06	0.12	0.3
09Jan09	MG3D	9.6	1840	6.22	23.7	1.83	55.4	42.1	581	3749	2183	369	40.4	0.236	1.15	70.6	0.222	0.002	11.4	5.84	0.11	-0.7
	MG14D	9.9	1438	6.4	24.1	2.05	51.8	54.3	683	5672	3232	679	94.8	0.341	1.32	70.5	0.246	0.006	11.4	10.3	0.17	0.7
10Jan09	MG29D	8.6	1370	7.21	22.9	2.21	26.3	32.5	739	3568	2116	440	40.0	0.038	1.96	56.5	0.189	0.007	6.54	7.64	0.11	3.0
	MG27D	8.4	1084	8.13	23.0	0.87	28.6	25.7	615	1952	1276	176	9.90	0.034	1.86	75.1	0.648	0.354	3.80	3.32	0.06	4.8
	MG37D	8.1	2229	5.13	24.2	1.32	52.1	63.0	818	7455	3724	1226	240	6.94	3.01	35.2	0.146	11.95	67.3	15.2	0.22	-0.5
	MG35D	8.8	2174	5.97	23.8	2.93	71.0	74.3	916	4168	2622	507	20.0	0.742	5.43	517	0.320	0.155	33.1	8.59	0.13	0.7
13Jan09	MG36D	10.8	1193	7.01	21.1	0.61	38.0	35.6	693	2654	1711	276	16.5	0.013	1.96	45.4	0.649	0.022	3.61	5.36	0.08	7.3
	MG19	10.4	1204	6.57	21.4	0.35	74.2	49.4	696	3556	2071	416	26.1	0.016	1.42	31.9	0.389	0.005	3.20	7.78	0.10	0.1
	MG34D	10.8	2003	6.07	21.3	1.87	92.4	60.8	607	4166	2560	415	41.5	0.248	1.33	110.0	0.191	0.016	7.47	6.02	0.12	3.1
	MG32D	10.9	2399	6.79	20.7	13	225	20.4	471	609	896	90.8	7.50	0.014	2.85	928	0.800	0.142	3.99	1.34	0.05	3.3
17Jan09	MG30D	8	1253	5.89	23.2	0.76	52.0	33.4	619	3532	2110	388	44.3	0.035	1.44	44.9	0.232	0.101	5.44	6.95	0.10	3.2
	MG31D	8.9	1244	6.11	21.8	0.03	50.2	43.1	703	4091	2405	450	41.2	0.165	1.48	39.5	0.357	0.060	6.09	7.61	0.12	1.6
	MG26D	1.1	ND	7.51	21.9	0.78	21.3	33.4	689	2714	1654	259	36.8	0.070	1.82	95.7	0.370	0.025	4.90	4.12	0.08	1.8
	MG28D	8.3	2118	4.22	22.6	1.81	34.8	40.8	614	3569	2130	412	25.3	7.60	1.65	345	0.164	5.76	115	5.75	0.11	3.8
19Jan09	MG24D	8	1796	5.89	21.9	7.61	116	26.7	828	2291	1380	335	21.2	0.158	1.54	95.2	0.242	0.082	14.2	4.23	0.07	4.5
	MG1	12.8	1072	7.8	24.9	1.33	44.6	32.1	560	2286	1446	212	17.1	0.019	1.74	85.7	0.517	nil	3.54	3.93	0.07	2.5
07Jun09	MG9D[g]	1.02	ND	6.36[h]	23.4	1.46	15.5	38.5	419	3885	2393	418	14.4	12.68	1.37	439	0.185	22.5	6.99	6.22	0.12	-1.1
01Jul09	MG9D[g]	0.82	ND	5.76[h]	24.2	0.84	6.19	39.2	547	3994	2410	432	17.8	16.73	1.34	378	0.111	8.5	14.2	6.47	0.12	-1.2
27Jul09	MG40D	8.2	2265	3.98[h]	23.0	0.34	17.0	66.4	881	7159	3486	983	216	17.04	2.66	73.2	0.770	227	134	12.1	0.21	0.8

[a] see text and Appendix A for details, [b] sampling pressure, [c] discharge enthalpy from tracer flow test measurement, [d] after inputting all water analyses (except Li) and gas analyses in WATCH 2.1 and calculated at sampling temperature, [e] without caustic soda, [f] injection wells for separated brine, [g] with caustic soda, nil- not detectable, [h] shortly after sampling, ND- not determined

TABLE 3: Measured discharge enthalpies, sampling pressures and analyses of minor and trace elements in the separated water samples[a]

Date	Well	SP[b]	H[c]	pH[d]	Br	As	Rb	Cs	Sr	Mn	Ba	Ti	V	Sb	Mo	W	Ni	Ga	Be	Cu	Cr	Co	Pb	U	Zn
		barg	kJ/kg		mg/kg	mg/kg	mg/kg	mg/kg	mg/kg	µg/kg	µg/kg	µg/kg	µg/kg	µg/kg	µg/kg	µg/kg	µg/kg	µg/kg	µg/kg	µg/kg	µg/kg	µg/kg	µg/kg	µg/kg	µg/kg
11Dec08	MG9D[e]	1.4	ND	3.32	14.73	0.1415	1.757	0.6315	0.1113	12313	154.3	139.3	45.46	10.0	33.2	7.6	114.9	6.24	4.604	95.18	16.000	5.74	11.380	2.434	285.0
18Dec08	MN3R[f]	17.9	ND	6.67	15.97	2.54	2.084	0.7054	0.6812	402	197.5	58.3	52.73	15.4	36.6	10.4	13.6	15.26	1.677	1.14	2.725	0.47	0.751	0.138	nil
19Dec08	MG9R[f]	6.2	ND	8.07	17.80	4.31	2.589	0.9424	0.5579	78.0	81.8	57.9	64.47	61.2	43.3	10.4	16.0	6.32	2.125	2.07	3.795	0.39	0.445	0.068	nil
26Dec08	MG18D	9.4	1460	6.48	17.09	3.66	2.247	0.9268	0.2652	31.8	52.9	54.9	71.78	57.9	36.6	10.3	11.2	5.20	2.428	1.69	6.682	0.65	1.018	0.409	nil
	MG23D	10.7	1212	6.65	14.29	3.48	2.005	0.7551	0.4512	14.6	16.9	51.4	57.27	50.5	32.1	11.1	9.9	2.42	1.698	2.12	3.406	0.18	0.486	0.077	nil
	MG39D	10.3	1195	7.07	18.57	4.38	3.056	1.0942	0.4373	50.2	51.3	58.8	66.79	26.3	33.4	8.6	10.1	4.40	2.380	2.08	4.869	0.18	0.447	0.072	nil
07Jan09	MG2D	9.5	1208	6.14	17.37	4.18	2.625	0.9624	0.5274	59.2	50.6	50.2	57.95	56.9	42.6	8.5	11.0	2.72	2.214	1.51	4.514	0.21	0.392	0.017	nil
	MG13D	10.0	1327	6.86	17.06	3.73	3.031	1.0042	0.1594	60.9	98.1	66.1	78.56	27.7	33.5	9.5	8.0	8.26	2.495	1.61	5.288	0.07	0.324	0.014	nil
	MG7D	10.3	1177	6.27	19.29	4.87	2.768	0.9996	0.8270	94.6	66.9	55.4	65.58	87.9	44.8	10.2	10.9	4.98	2.395	1.67	3.128	0.18	0.276	0.017	nil
	MG16D	10.4	1379	6.08	19.78	4.67	2.982	1.0600	0.6775	72.7	32.4	59.4	71.35	19.4	36.7	10.3	10.4	2.89	2.496	1.99	3.984	0.18	0.284	0.013	nil
	MG22D	10.0	1163	6.56	19.59	4.95	2.990	1.0701	0.6926	62.0	57.7	57.2	63.97	99.0	39.3	9.0	10.5	2.61	2.289	1.87	3.696	0.18	0.311	0.012	nil
09Jan09	MG3D	9.6	1840	6.22	17.77	3.69	1.975	0.7001	0.7205	408	154.0	47.7	55.00	5.3	29.3	2.5	9.7	11.02	1.845	1.51	3.230	0.19	0.237	0.015	nil
	MG14D	9.9	1438	6.40	25.79	3.83	3.454	1.0609	2.0667	1786	1346.1	58.4	88.23	1.2	31.5	4.2	18.8	95.60	2.461	2.67	3.866	0.42	0.384	0.016	nil
10Jan09	MG29D	8.6	1370	7.21	16.75	2.85	2.328	0.7573	0.6888	73.8	118.8	59.7	59.17	17.0	31.6	8.7	10.2	8.47	1.366	1.36	3.145	0.21	0.246	0.014	nil
	MG27D	8.4	1084	8.13	9.21	1.65	1.036	0.3907	0.1843	17.0	50.5	47.8	40.63	25.7	26.1	10.9	5.0	5.44	1.173	0.68	1.989	0.14	0.297	0.011	nil
	MG37D	8.1	2229	5.13	37.99	4.16	6.434	1.1042	4.8297	14331	2166.3	69.6	116.56	3.1	44.9	4.2	42.1	148.78	2.991	3.66	4.952	0.96	0.620	0.017	nil
	MG35D	8.8	2174	5.97	19.57	3.32	2.840	0.9948	0.6625	2058	171.2	90.4	73.47	1.7	32.4	7.2	8.5	13.94	3.442	1.67	3.422	0.13	0.341	0.015	nil
13Jan09	MG36D	10.8	1193	7.01	12.17	2.93	1.660	0.5797	0.3882	34.5	74.4	53.6	50.83	54.5	31.0	10.6	6.5	5.48	1.506	1.15	2.312	0.12	0.449	0.011	nil
	MG19	10.4	1204	6.57	16.39	4.01	2.505	0.8967	0.4787	48.1	67.4	53.0	55.05	8.4	29.0	8.3	7.8	3.91	2.074	1.63	2.499	0.19	0.255	0.016	nil
	MG34D	10.8	2003	6.07	18.30	2.81	2.555	0.9988	0.6268	142	431.4	50.6	71.11	6.4	40.4	12.4	10.4	31.96	3.257	2.74	3.505	0.79	0.909	0.520	nil
	MG32D	10.9	2399	6.79	3.58	0.62	0.585	0.2601	0.1462	21.0	36.0	65.4	58.28	19.5	12.6	6.8	5.7	8.75	1.187	0.91	1.844	0.37	0.558	0.197	nil
17Jan09	MG30D	8.0	1253	5.89	17.33	3.64	2.211	0.7674	0.7752	57.8	90.7	48.1	57.34	68.7	33.3	7.9	13.4	6.38	1.450	1.81	2.944	0.33	0.338	0.072	nil
	MG31D	8.9	1244	6.11	19.31	2.90	2.540	0.9215	0.7918	183	278.3	53.5	65.03	4.4	30.0	8.7	10.5	19.29	2.076	2.03	3.178	0.44	0.517	0.242	nil
	MG26D	1.1	ND	7.51	12.47	2.83	1.548	0.5498	0.4357	38.3	256.4	51.9	45.32	69.8	31.6	13.7	12.3	18.99	1.802	1.31	2.605	0.68	0.838	0.598	nil
	MG28D	8.3	2118	4.22	17.11	3.55	1.929	0.6337	0.3276	2747	205.5	72.5	52.33	1.8	18.7	3.2	7.4	14.47	2.550	1.67	2.910	0.30	0.382	0.199	nil
19Jan09	MG24D	8.0	1796	5.89	12.40	1.51	1.822	0.4588	0.3828	215	137.7	59.8	36.30	13.5	21.5	7.9	6.9	8.57	1.136	0.76	2.516	0.20	0.493	0.029	nil
	MG1	12.8	1072	7.80	10.62	2.24	1.321	0.5222	0.2584	16.3	25.8	42.9	37.68	17.5	25.1	10.1	5.4	2.86	1.465	2.13	2.054	0.17	0.598	0.014	nil
07Jun09	MG9D[g]	1.0	ND	6.36	17.31	3.99	2.145	0.7429	0.0839	1980	134.3	52.8	62.23	17.6	29.7	2.9	6.8	8.85	2.823	31.61	4.484	0.39	177.086	0.112	554.72
01Jul09	MG9D[g]	0.8	ND	5.76	17.27	4.11	2.227	0.7308	0.1189	3205	237.8	58.1	59.59	79.2	22.6	2.7	50.5	15.19	2.640	17.04	7.622	1.05	116.721	0.039	305.19
27Jul09	MG40D	8.2	2265	3.98	34.89	5.28	4.856	0.9306	4.6714	51766	1932.8	84.9	102.72	61.3	48.3	8.4	81.4	80.80	3.226	28.38	10.541	4.40	191.486	0.015	97.33

[a] see text and Appendix A for more details, [b] sampling pressure, [c] discharge enthalpy from tracer flow test measurement, [d] at temperature of measurement (refer to Table 3.2), [e] without caustic soda, [f] injection wells for separated brine, [g] with caustic soda, nil- not detectable

The average and standard deviation of % mean differences of all samples in a particular analytical method are summarized in Table 5. Analytical results from laboratories of LRMD EDC and the Institute of Earth Sciences, University of Iceland compare generally well for most major components (%Mean Difference within 10%) while larger differences are observed in elements occurring at lower concentrations (e.g., Mg and Fe). The ionic balances of all water samples analyzed by LRMD EDC, as calculated by the WATCH speciation program, are all within ±5%. The succeeding sections elaborate on how the reported values in Tables 2 and 3 were chosen.

TABLE 4: Measured discharge enthalpies, sampling pressures and analyses of separated vapour samples

Date	Well	SP[a]	H[b]	mmoles/100 moles of steam						
		barg	kJ/kg	CO_2	H_2S	NH_3	H_2	CH_4	N_2	Ar
11Dec08	MG9D[c]	1.4	ND	529	30.80	0.28	26.740	0.574	213.576	2.306
26Dec08	MG18D	9.4	1460	602	20.20	6.23	1.034	0.826	19.838	0.201
	MG23D	10.7	1212	449	9.90	3.68	0.623	2.871	3.658	0.049
	MG39D	10.3	1195	412	9.00	4.18	0.051	0.435	1.388	0.018
07Jan09	MG2D	9.5	1208	797	11.70	3.50	0.327	1.964	3.101	0.033
	MG13D	10	1327	610	13.60	4.88	0.361	0.932	1.354	0.013
	MG7D	10.3	1177	322	8.60	2.90	0.016	0.09	0.131	0.001
	MG16D	10.4	1379	1142	14.00	2.81	1.787	2.16	5.387	0.050
	MG22D	10	1163	420	8.70	2.85	0.163	0.624	1.444	0.017
09Jan09	MG3D	9.6	1840	917	25.20	8.62	2.474	1.68	11.855	0.146
	MG14D	9.9	1438	767	28.30	11.50	1.848	0.99	2.446	0.022
10Jan09	MG29D	8.6	1370	470	13.30	8.29	1.178	0.851	8.014	0.115
	MG27D	8.4	1084	283	7.20	5.39	0.169	0.546	26.337	0.389
	MG37D	8.1	2229	710	58.70	5.29	1.455	1.093	1.643	0.015
	MG35D	8.8	2174	2322	43.50	8.98	1.722	6.518	3.023	0.016
13Jan09	MG36D	10.8	1193	366	8.60	5.01	0.410	0.941	19.667	0.300
	MG19	10.4	1204	563	8.20	4.67	0.126	1.209	6.135	0.079
	MG34D	10.8	2003	912	21.00	7.21	1.985	2.549	3.622	0.026
	MG32D	10.9	2399	1598	26.30	7.92	3.809	3.917	4.805	0.038
17Jan09	MG30D	8	1253	400	11.60	7.25	0.580	0.878	7.199	0.089
	MG31D	8.9	1244	630	12.00	6.55	0.700	2.845	3.619	0.040
	MG26D	1.1	ND	454	9.60	5.17	0.830	1.416	7.321	0.068
	MG28D	8.3	2118	1061	40.80	4.24	1.551	2.993	9.759	0.094
19Jan09	MG24D	8	1796	2098	39.00	8.55	1.513	5.381	1.715	0.012
	MG1	12.8	1072	240	4.20	1.76	0.070	0.583	2.566	0.031
07Jun09	MG9D[d]	0.9	ND	199	12.30	12.80	2.451	0.411	49.876	0.515
01Jul09	MG9D[d]	0.9	ND	180	12.40	3.45	0.211	0.313	33.294	-0.19
27Jul09	MG40D	8.3	2265	422	44.10	16.10[e]	2.895[e]	1.133[e]	7.088[e]	0.114[e]

[a] sampling pressure, [b] discharge enthalpy from tracer flow test measurement, [c] without caustic soda, [d] with caustic soda, [e] sample on 30Jul09 at same wellhead and sampling pressures, ND- not measured

3.2.1 pH, H_2S and total carbonate

The measurement of pH is one of the analyses most often done with the poorest precision and probably the least care (Arnórsson, 2000). Since pH is the activity of H^+, it changes with temperature. It is important to note the temperature of pH measurement in calculating the fluid conditions at higher temperatures. The water samples in this study have high SiO_2 levels (~400-900 mg/kg) making them supersaturated with amorphous silica at room temperature thereby promoting silica polymerization. In Icelandic waters, Gunnarsson and Arnórsson (2005) observed that solutions with starting pH~8 have significantly declining pH with progressive polymerization. Such can be explained when the weakly acidic silica monomers in the solution are converted to relatively more acidic oligomers (Iler, 1979). In contrast, stability tests by Urbino and Pang (2006) of a natural geothermal water from Leyte (pH=7.6) showed only a slight increase in pH and slight decrease of HCO_3^-. The pH of such water may have been buffered by weak acids other than monomeric silica.

TABLE 5: Water analyses done in this study and precision from duplicate determinations [a]

	Analytical Method	Concentration range, mg/kg		Ave. of % mean differences	SD of % mean differences	Detection limit, mg/kg
		minimum	maximum			
pH	Cole Parmer precision pH electrode, Type B	3.32	8.13	0.04[b]	0.04[b]	
H_2S	Titration with $HgAc_2$ (dithizone indicator)	0.13	4.58	7.6	12.9	0.01[c]
CO_2	Titration	4.00	225	18.1	20.1	0.5[d]
	ICP-AES Unfiltered	6.64	211	8.0	7.6	4.4[e]
	ICP-AES Filtered	4.88	165	4.0	3.0	
B	ICP-AES	20.4	74.3	1.2	0.8	0.0016[f]
	ICP-MS	18.699	62.125	20.7	4.2	
SiO_2	ICP-AES	419	916	4.8	1.6	0.1[g]
Cl	ICP-AES	609	7455	3.2	4.8	0.2[f]
	IC	584	8058	2.0	1.0	
Na	ICP-AES	896	3724	1.7	1.7	0.01[g]
K	ICP-AES	90.8	1226	1.0	1.4	0.2[g]
Ca	ICP-AES	7.52	240	1.2	1.6	0.001[g]
Mg	ICP-AES	0.0134	39.6	5.9	6.0	0.001[g]
Al	ICP-AES	0.111	2.26	2.8	1.8	0.0001[f]
	ICP-MS	0.0736	0.7996	-	-	
Fe	ICP-AES	0.02	840	9.5	11.3	0.01[g]
	ICP-MS	0.002	743	-	-	
Li	ICP-AES	1.34	15.2	2.3	2.9	0.00002[f]
SO_4	ICP-AES	23.6	2155	2.2	2.4	0.5[g]
	IC	16.9	2080	3.7	2.0	
F	IC	1.15	1.85	5.3	2.0	
Br	ICP-AES	3.58	37.99	3.0	1.7	0.027[f]
As	ICP-AES	0.181	5.28	3.5	4.0	0.0074[f]
	ICP-MS	0.142	4.43	-	-	
Sr	ICP-AES	0.081	4.896	1.3	1.5	
	ICP-MS	0.0839	4.8297	4.0	4.1	
Mn	ICP-AES	14.63[h]	51766[h]	1.9	2.9	0.0001[f]
	ICP-MS	14.826[h]	42441[h]	-	-	
Ba	ICP-AES	16.8[h]	2166[h]	5.6	5.3	0.00002[f]
	ICP-MS	14.2[h]	2490[h]	6.9	5.9	
Rb	ICP-MS	0.5851	6.4340	6.4	2.8	
Cs	ICP-MS	0.2601	1.1042	12.7	4.2	
Mo	ICP-MS	12.6[h]	48.3[h]	95.4	34.4	
W	ICP-MS	2.5[h]	13.7[h]	4.2	4.3	
Sb	ICP-MS	1.2[h]	99.0[h]	4.7	3.6	
Be	ICP-MS	1.1364[h]	4.6039[h]	165.4	28.7	
Pb	ICP-MS	0.237[h]	191.486[h]	10.4	9.2	

[a] See Appendix A for details, [b] difference, [c] Arnórsson et al. (2006), [d] Arnórsson (2000), [e] Stefánsson et al. (2007), [f] Spectro™ product presentation material, [g] Arnórsson et al. (2002), [h] in µg/kg

In this study, the pH of the water sample was measured on-site using a portable pH meter (MetroOhm™) coupled to a quick-response electrode (Cole Parmer™) and calibrated with standard buffer solutions as close as possible to the sampling temperature. The above measurements can be compared with 1) pH measured with the same pH meter in the laboratory shortly after sampling (i.e. during titration to determine carbonate carbon) and 2) pH measured by a different pH meter of LRMD EDC laboratory at a later period but within 3 days from sampling (Table 1, Appendix A). The pH values measured on-site and later in the laboratory using the same pH meter were within 0.2 pH units except for 2 samples. In comparison with pH values from LRMD EDC, the field measurements are systematically lower (Figure 7). However, differences between the two pH meters can also be a

factor. To eliminate any variable that can affect the solution pH, the values measured on-site were used for calculations.

To prevent loss of H_2S in the sample by degassing and/or oxidation, H_2S was measured on-site by titration with standard mercuric acetate solution and using dithizone as endpoint indicator (Arnórsson et al., 2006). The method is sensitive (0.01 mg/kg for 50 ml sample aliquot) but coloured precipitates in samples (e.g. when metal content is high) may make it impossible to detect the endpoint. Instability of the mercury acetate titrant and difficult field conditions during sampling also contribute to uncertainties in most of the results. For these reasons, H_2S analyses from LRMD EDC laboratory, if available, were reported in Table 2.

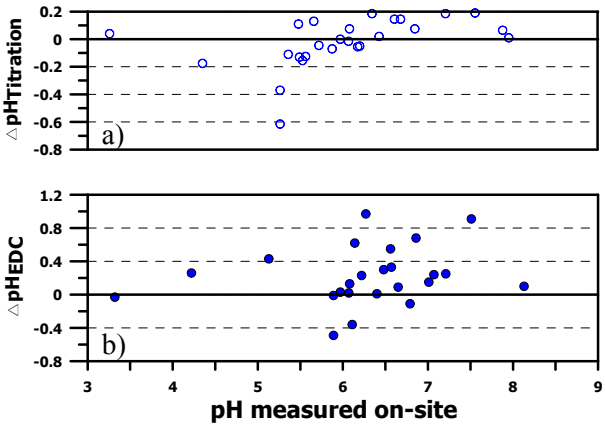

FIGURE 7: Comparison of separated water pH values measured on-site vs: a) measured shortly after sampling (open circles) and b) measured by EDC within 3 days from sampling (closed circles)

Total carbonate carbon (T-CO_2) was determined from alkalinity titration in the laboratory shortly after sampling and back titrated with standard NaOH solution to correct for interference from other weak acids in the solution (Arnórsson et al., 2006). Samples were also collected in amber glass bottles with air-tight caps for analysis of dissolved inorganic carbon (DIC) by ICP-AES (Stefánsson et al., 2007) in unfiltered and filtered samples. The results of the 2 methods are presented in Table 3 of Appendix A. T-CO_2 values from titration are on the average ~20% higher than analysis by ICP-AES using unfiltered samples. Both methods were marked with imprecision (>5% % Mean Difference) in some measurements. This occurs when the sample is exposed to the atmosphere during titration and when colloidal particles in the sample destabilize the spectral signals of ICP-AES. The filtered samples analyzed by ICP-AES improved precision but gave ~60% lower values. The average partial pressures of CO_2 in the water samples as calculated by the speciation program WATCH at sampling conditions (1.4×10^{-2} bar) are 2 orders of magnitude higher than atmospheric partial pressure of CO_2 ($\sim 4 \times 10^{-4}$ bar). Thus CO_2 degassing inevitably occurred during filtering. The reported T-CO_2 values in Table 2 are taken from titration measurement. If titration method is not possible due to acidity of the sample, values were determined from the ICP-AES analysis of unfiltered samples.

3.2.2 Major and trace elements

Major elements (B, SiO_2, Cl, Na, K, Mg, Ca, SO_4, Al and Fe) and minor/trace elements (Li, Br, Ba, Sr, Mn and As) were analyzed by ICP-AES. Seven elements analyzed by ICP-AES were also analyzed by ICP-MS (B, Al, Fe, Ba, Sr, Mn and As). Analyses with good repeatability from ICP-AES are chosen whenever ICP-MS results are lower or only have a single measurement. Lower analytical values from ICP-MS often occur when the concentration in the samples are considerably higher than the standard values. On the other hand, values from ICP-MS are selected if the ICP-AES values approach the detection limits and show big differences between duplicate determinations. The other trace elements determined only by ICP-MS are Be, Co, Ni, Cu, Ga, Rb, Cs, Pb, U, Ti, Mo, W, Cr, Sb, V and Zn. Zn is not detectable except in few samples (Table 3). Analyses of the anions F, SO_4 and Cl were also carried out using ion chromatography (RFIC^{TM}). To avoid overloading the column due to elevated Cl contents of the samples (average of ~3700 mg/kg), dilution by ~200 times was required. However, dilution affects the analyses of SO_4 and F which are ~2-3 orders of magnitude lower than Cl levels. Therefore, only F analyses were taken from IC. Reported values are usually taken from the average of duplicate determinations. But if one of the determinations is deemed faulty but not due to statistical variations, the value consistent with other analytical methods is selected.

3.3 Data handling

The analytical data of samples collected at the wellheads (Tables 2 and 3) were recalculated to the deep aquifer fluid conditions with the aid of the speciation program WATCH (Arnórsson et al., 1982), version 2.1 (Bjarnason, 1994). This procedure is relatively simple for wells discharging liquid enthalpy. In this case, the pressure drop induced by discharging the well is not enough to start boiling in the original aquifer fluid. The level of first boiling is within the well and it is reasonable to treat the aquifer and the well as an isolated system and to assume adiabatic boiling of the fluid. If the pressure produced by a discharging well is sufficient to cause extensive boiling in the producing aquifer, it is common that the discharge enthalpy of the well is significantly higher than the enthalpy of the aquifer fluid beyond the zone of depressurization around the well. The aquifer-well system is no longer isolated. The discharge enthalpy of the well can increase from its initial enthalpy in the aquifer fluid by conductive heat transfer between the aquifer rock and the flowing fluid which is cooled by depressurization boiling. The aquifer-well is a closed system since there is an exchange of energy with the surrounding but the composition of the fluid does not change (model 2 in Arnórsson et al., 2010). Thus in the isolated and closed systems, the total well discharge composition is equivalent to that of the initial aquifer fluid. In this study, phase segregation will be demonstrated as the dominant mechanism responsible for the "excess enthalpy" discharged in the wellhead. The increase in the enthalpy as the fluid flows from the undisturbed aquifer to the wellhead is primarily due to segregation of the vapour and liquid water in the aquifer. The vapour phase flows to the wellhead while liquid water is partially or totally retained in the aquifer, adhering onto mineral grain surfaces by capillary forces. The mechanism of phase segregation is therefore an open system, causing both the enthalpy and composition of the flowing fluid to change from the initial aquifer conditions to the wellhead (model 3 in Arnórsson et al., 2010). The WATCH speciation program calculates individual species activities in the aquifer fluid. This permits derivation of activity products for minerals, and from the solubility constants for these minerals, their state of saturation in the fluid can be obtained.

3.3.1 Aquifer temperatures

To process the analytical data in the wellhead, one needs first to select the reference temperature (representing the aquifer temperature) at which the composition of the deep fluid shall be calculated. This can be arbitrarily chosen but often guided by chemical and isotope geothermometers and measurements from downhole temperature surveys. Mahanagdong fluids are primarily of the mature NaCl-type and applications of many water geothermometers are successfully established (e.g., Herras et al., 1996; Balmes, 1994; Salonga et al., 2004). As summarized in Table 6, there is general agreement between the major water geothermometers for each well suggesting either a single feed zone or an almost similar temperature of multiple aquifers that feed the well. The quartz geothermometer by Gunnarsson and Arnórsson (2000), $T_{qtz,GA}$, is used in Table 6. In the temperature range applicable to Mahanagdong wells (200-300°C), $T_{qtz,GA}$ values of 200°C, 250°C and 300°C differ by about -6°C, +3°C and +15°C, respectively, compared to the more widely used calibration of Fournier and Potter (1982). Except in 2 samples of well MG9D and in wells MG32D and 37D, $T_{qtz,GA}$ of a particular well will differ by at most 20°C from the average of all water geothermometers (T_{ave} in Table 6), and on average, is within ±15°C from temperature in its major production zone measured when the well is thermally stable. Thus for most of the wells, it is reasonable to represent the aquifer temperature by quartz geothermometry. For acid well MG9D, its $T_{qtz,GA}$ values fluctuated from 287°C to 217°C within ~1.5 months of discharge. Several factors may cause this decline which may include either a shift to a more dilute zone feeding the well or loss of silica in the solution into various precipitates induced by raising the pH in the solution when caustic soda was dosed. So for the calculations of all MG9D samples, a reference temperature of 265°C is selected which is consistent with the average of all $T_{Na/K}$ values during its stable discharge. Determining the true aquifer temperature can be complex. In later sections, it is investigated how the modelling parameters are affected when the reference temperature varies within ±20°C from the assumed aquifer temperature.

In Table 6, comparing $T_{qtz,GA}$ and $T_{Na/K}$ values of wells with "excess enthalpy" serves another purpose. The solubility of quartz is affected by secondary processes such as mixing, dilution and boiling. In contrast, a geothermometer based on component ratios, such as Na/K, is practically independent of the

said processes. Thus, a proposed model that account for the "excess enthalpies" of some wells can be validated if both types of geothermometers yield comparable results. The temperatures yielded by the different water geothermometer in Table 6 are calculated from the composition of its aquifer liquid, assuming the phase segregation model for wells with "excess enthalpy". On average, $T_{qtz,GA}$ of most "excess enthalpy" wells are within ~15°C compared to the average of all $T_{Na/K}$ values suggesting that the assumption of phase segregation model is reasonable. Three wells with bigger differences (MG32D, 35D and 37D) have the highest discharge enthalpies of 2200-2400 kJ/kg. As elaborated in section 4.3, at higher discharge enthalpies the point where phase segregation is selected may result to lower calculated aquifer fluid concentration of non-volatile components, like SiO_2, explaining the bigger difference between the two geothermometers.

TABLE 6: Summary of water geothermometers (in °C) calculated from the concentrations of components in the total fluid of initial aquifer assuming no vapour fraction[a]

Well	Fournier and Truesdell	Giggenbach	Truesdell	Arnórsson et al.	Gunnarsson and Arnórsson[b]	
	$T_{Na/K/Ca}$	$T_{Na/K}$	$T_{Na/K}$	$T_{Na/K}$	T_{qtz}	T_{ave}
MG9D[c]	264	289	269	232	287	268
MG18D	260	272	243	251	267	259
MG23D	263	285	263	266	268	269
MG39D	279	292	273	277	283	281
MG2D	274	293	275	276	269	277
MG13D	296	298	282	283	295	291
MG7D	273	293	275	278	280	280
MG16D	276	296	284	281	286	285
MG22D	276	297	280	282	284	284
MG3D	258	278	252	257	258	260
MG14D	274	299	278	282	275	282
MG29D	273	298	283	282	282	283
MG27D	248	259	225	234	262	246
MG37D	301	ND	365	335	293	323
MG35D	281	291	271	272	307	284
MG36D	260	274	246	254	277	262
MG19	276	295	277	278	277	281
MG34D	259	274	246	252	263	259
MG32D	223	233	189	180	239	213
MG30D	263	286	264	267	263	269
MG31D	268	288	267	271	277	274
MG26D	246	271	241	249	261	254
MG28D	274	291	272	270	262	274
MG24D	282	315	308	300	294	300
MG1	249	265	233	241	257	249
MG9D[d]	276	281	257	257	217	258
MG9D[d]	275	284	260	260	239	264
MG40D	287	331	335	323	301	315

[a] Sources of geothermometer equations are summarized in Arnórsson (2000),
[b] Gunnarsson and Arnórsson (2000), [c] Without caustic soda, [d] With caustic soda, ND - out of range

3.3.2 Aquifer fluid compositions

The speciation programme WATCH 2.1 was used to model the deep aquifer fluid compositions. WATCH 2.1 is specifically suited to handle geochemical data from wet-steam wells. For this study, the program reads the chemical analyses of water and gas samples collected at the wellhead then computes for the chemical composition at the reference temperature (i.e. at $T_{qtz,GA}$) including pH, aqueous speciation, partial pressure of gases, redox potentials and activity products of mineral dissolution reactions. No mineral precipitation or dissolution is assumed as the fluid is modelled from the aquifer to the surface. For detailed discussions of the programme, readers are referred to Arnórsson et al. (1982) and Bjarnason (1994). SOLVEQ (Reed and Spycher, 1989), version XPT, was used to handle one acidic sample (undosed discharge of MG9D) since this water is very high in Fe (840 mg/kg) and the WATCH 2.1 program does

not handle Fe (II)/Fe (III) satisfactorily, leading to among other things erroneous aquifer water pH. In using SOLVEQ, a special version of the database SOLTHERM was utilized to consider only gas solubility reactions involving the gas species CH_4, H_2, N_2 and NH_3 but not associated redox gas-equilibria reactions (see for example Akaku et al., 1991).

Arnórsson et al. (2007) and Arnórsson et al. (2010) provide thorough procedures to calculate the chemical composition of aquifer fluids from the analyses obtained in the wellhead using different reasonable sets of assumptions. In this study, the concepts applicable to the open system phase segregation model are adopted (see model 3 in Arnórsson et al., 2010). In the equations that follow, X is a steam fraction, m refers to a concentration, the subscript represents a component (*i*- any component, *r*- non-volatile, *s*- volatile), the first superscript denotes the location of the fluid (*d*-discharge, *f*- initial aquifer, *e*/*g*- a point right before/after a zone between aquifer and wellhead) and the second superscript refers to the fluid phase (*l*-liquid, *v*-vapour, *t*-total fluid). The procedure is straightforward for liquid enthalpy wells since their initial aquifers are considered to be purely liquid. The system between initial aquifer conditions and the wellhead can be approximated as isolated (no transfer of mass and energy with the surroundings) such that the total discharge enthalpy ($h^{d,t}$) is equal to the enthalpy of the initial aquifer fluid ($h^{f,t}$) and for any component *i*, its total concentration at the aquifer ($m_i^{f,t}$) and the wellhead ($m_i^{d,t}$) are also equal. If the aquifer fluid is sub-boiling water, $h^{d,t} = h^{f,l}$ leading to:

$$m_i{}^{f,t} = m_i{}^{f,l} = m_i{}^{d,t} = m_i{}^{d,l}(1 - X^{d,v}) + m_i{}^{d,v} X^{d,v} \quad (2)$$

$$X^{d,v} = (h^{f,l} - h^{d,l}) / (h^{d,v} - h^{d,l}) \quad (3)$$

$m_i^{d,l}$ and $m_i^{d,v}$ are the concentrations of any component *i* in the liquid and vapour sampled at the wellhead, respectively. $X^{d,v}$ is the steam fraction at the sampling conditions. Its value can be obtained from the specific enthalpies of the liquid aquifer at the assumed aquifer temperature ($h^{f,l}$) and of saturated liquid and vapour at sampling pressure ($h^{d,l}$ and $h^{d,v}$, respectively). In equation (2), only carbonate carbon and sulphide sulphur have significant concentrations in both liquid and vapour phases. Other volatiles have negligible amount in the liquid ($m_i^{d,l} \approx 0$) while non-volatile components partition only to the liquid phase ($m_i^{d,v} = 0$).

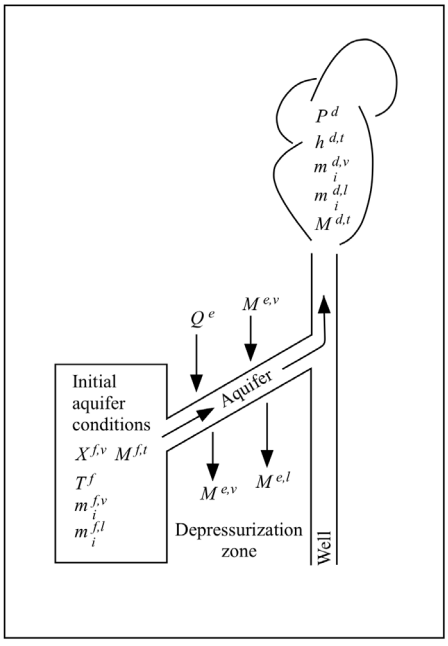

FIGURE 8: Schematic diagram describing the processes occurring in the depressurization zone around wells that may cause changes in the flowing fluid enthalpy (from Arnórsson et al., 2010)

Continuously producing geothermal fields like Mahanagdong often undergo extensive boiling in aquifers feeding the wet-steam wells. Some of the wells have discharge enthalpies that are significantly greater than that of steam-saturated water at their aquifer temperatures (i.e., $h^{d,t} > h^{f,l}$). In liquid-dominated fields, there are three possible causes for the excess enthalpy: 1) conductive heat transfer driven by a temperature gradient from the hot aquifer rock to a cooled flowing fluid due to its depressurization boiling, 2) partial or total retention of the liquid phase in the aquifer by its adhesion onto mineral grain surfaces by capillary forces and 3) addition of vapour phase to the flowing fluid by boiling of the capillary water. As mentioned earlier, the first mechanism corresponds to a closed system thus follows the same conservation of mass equations applicable to liquid enthalpy wells but has an input of additional heat. The second and third mechanisms represent open systems. In modelling the 3 scenarios, a point between the aquifer and the discharge is chosen where addition of heat, phase segregation and/or addition of vapour occurs (Figure 8).

It is possible that either all of the mentioned factors contribute to the "excess enthalpy" or one may dominate over the others. By the method of Glover et al. (1981), the trends of a non-volatile and conservative component (e.g. Cl)

plotted against discharge enthalpy suggest that phase segregation dominates in producing the "excess enthalpy" in Mahanagdong. Data from two representative wells currently discharging variable degree of "excess enthalpy" are shown in Figure 9. MG3D ($h^{d,t}$≈1800 kJ/kg) is drilled near the inferred upflow zone while MG32D ($h^{d,t}$≈2400 kJ/kg) is located in an area with high pressure drawdown. Silica trend was plotted due to wider variations caused by either injected brine returns or inflow of dilute peripheral waters to the Cl analytical trends. Also, when the equations assuming heat transfer model are applied, they will yield low concentrations of non-volatile components (e.g. SiO_2) in the initial aquifer, especially when discharge enthalpies approach the enthalpy of saturated steam. Consequently, the corresponding aquifer T_{qtz} is low and anomalously differs from $T_{Na/K}$. These were similarly concluded by Arnórsson et al. (2007) and Giroud (2008) when evaluating the "excess enthalpies" of some wet-steam wells in the liquid-dominated fields of Olkaria and Iceland, respectively. In contrast, if calculations are done by the phase segregation model, the resulting $T_{qtz,GA}$ and $T_{Na/K,A}$ are comparable (see Table 6). For these reasons, it is reasonable to account the "excess enthalpy" of Mahanagdong wells by the phase segregation model.

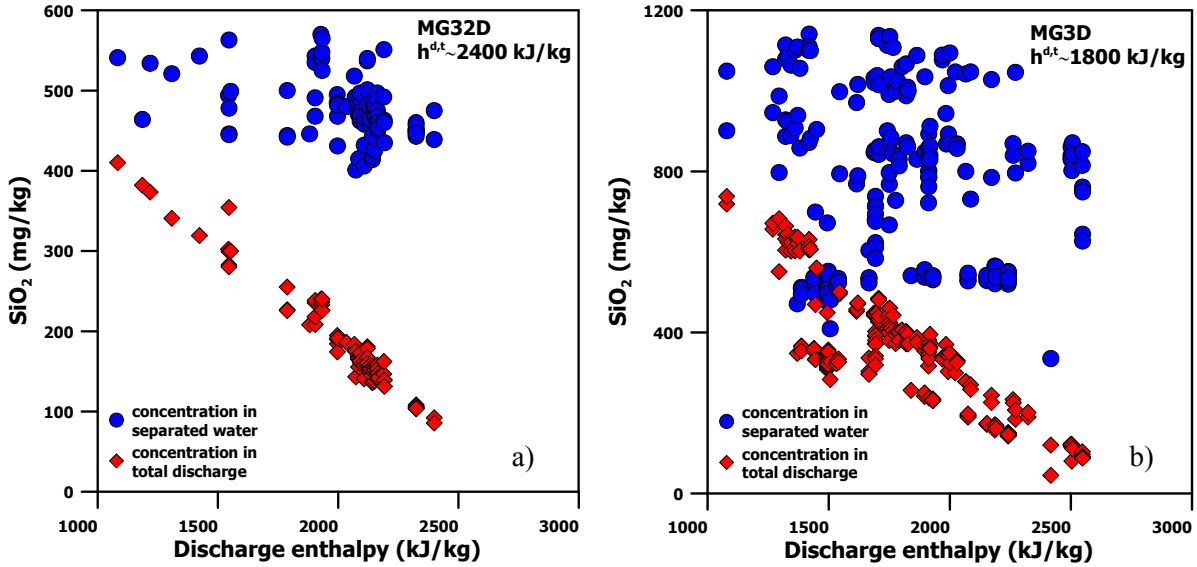

FIGURE 9: Variation in the silica content of Mahanagdong high enthalpy wells a) MG32D and b) MG3D. The total discharge concentration steadily decreases as the discharge enthalpy approaches saturated dry steam. The observed correlation suggests that phase segregation in the producing aquifers is, at least, largely the cause of excess well discharge enthalpy

A two-step method is adopted to reconstruct the initial aquifer conditions of wells with "excess enthalpy" assuming phase segregation model. The 1st step uses both the analytical data obtained in the wellhead and the measured discharge enthalpy to calculate conditions where phase segregation is assumed to occur (P^g). In this work, P^g is chosen at 30°C below the assumed aquifer temperature corresponding to $T_{qtz,GA}$. This is a simplified assumption that will be further elaborated in the discussion section. The selected P^g corresponds to a liquid saturation (i.e. volume fraction of the saturated liquid water) of ~0.2-0.3. Several studies have shown immobility of the liquid phase at such saturation levels (e.g. Horne et al., 2000; Pruess, 2002). The 1st step in the procedure makes use of an equation analogous to equation (2):

$$m_i^{d,t}=m_i^{g,l}(1-X^{g,v})+m_i^{g,v}X^{g,v}=m_i^{d,l}(1-X^{d,v})+m_i^{d,v}X^{d,v} \quad (4)$$

As mentioned, the first superscript, ^{g}, in equation (4) and thereafter indicates the conditions of the fluid immediately after phase segregation. The measured total discharge enthalpy ($h^{d,t}$) corresponds to the total flowing fluid enthalpy after phase segregation ($h^{g,t}$), thus an energy balance at this condition yields:

$$h^{d,t}=h^{g,t}=h^{g,l}(1-X^{g,v})+h^{g,v}X^{g,v} \quad (5)$$

and re-arranging will allow calculation of $X^{g,v}$ analogous to equation (3).

$$X^{g,v}=(h^{d,t}-h^{g,l})/(h^{g,v}-h^{g,l}) \quad (6)$$

Dissolved solids are assumed to partition insignificantly into the vapour phase ($m_r^{g,v}=0$). For a volatile species, its concentration in the vapour phase ($m_s^{g,v}$) is dictated by its distribution coefficient, D_s^g, which is related to its Henry's Law constant (K_s^g) and total pressure (P^g_{tot}) as derived by Arnórsson et al. (2007):

$$D_s{}^g=55.51\ /\ (K_s{}^g\ P_{tot}{}^g)\approx m_s{}^{g,v}/m_s{}^{g,l}\ (for\ dilute\ fluids) \quad (7)$$

Thus equation (4) can be modified for volatile species into:

$$m_s{}^{d,t}=m_s{}^{g,l}(1-X^{g,v})+D_s{}^g m_s{}^{g,l}X^{g,v}=m_s{}^{d,l}(1-X^{d,v})+m_s{}^{d,v}X^{d,v} \quad (8)$$

After the 1st step, the concentrations of all components immediately after phase segregation can be solved ($m_r^{g,l}$, $m_s^{g,l}$ and $m_s^{g,v}$) using the available analytical data at the wellhead, measured discharge enthalpy, specific enthalpies from Steam Tables and equations (3) to (8).

The 2nd step in modelling aquifer fluid compositions for "excess enthalpy" wells involves calculation of individual component concentrations from the concentrations at P^g of non-volatile components in the liquid ($m_r^{g,l}$) and volatile components in both phases ($m_s^{g,l}$ and $m_s^{g,v}$) taking the flowing liquid enthalpy to be that of the initial aquifer fluid. The fraction of steam produced by this step is analogous to equations (3) and (6) and is denoted by $X^{e,v}$ (depressurization boiling from initial aquifer conditions to right before phase segregation). It is to be distinguished from $X^{g,v}$ which represents the steam fraction of the fluid produced right after phase segregation.

$$X^{e,v}=(h^{f,t}-h^{g,l})/(h^{g,v}-h^{g,l}) \quad (9)$$

If the initial aquifer is assumed to be purely liquid, the total fluid enthalpy is equivalent to the liquid enthalpy at the aquifer temperature (i.e. $h^{f,t}=h^{f,l}$). The concentration of any component at segregation point is then related to its total concentration in the initial aquifer by:

$$m_i{}^{f,t}=m_i{}^{f,l}=m_i{}^{g,l}(1-X^{e,v})+m_i{}^{g,v}X^{e,v} \quad (10)$$

In practice, when using WATCH, modelling liquid enthalpy wells is done by inputting the analytical data but not a measured discharge enthalpy, then iterating a reference temperature until the total silica concentration in the liquid aquifer is consistent with $T_{qtz,GA}$, or by choosing arbitrarily a value for aquifer temperature. The 1st step in modelling "excess enthalpy" wells is done by inputting both analytical data and measured discharge enthalpy then choosing a reference temperature equivalent to a selected segregation point. The output of WATCH by this 1st step is picked up to become the input file of the 2nd step. When executing the 2nd step, no enthalpy will be input. It is calculated from the reference temperature. The modelled liquid aquifers feeding the Mahanagdong wells as described by the above procedures are summarized in Table 7.

Arnórsson et al. (2007) and Arnórsson et al. (2010) also proposed methods to derive a vapour fraction of the initial aquifer fluid using the phase segregation model and assuming that the total discharge concentration of the reactive gases H_2 and H_2S are controlled by chemical equilibrium with specific mineral assemblages. The vapour fraction obtained by this procedure is referred to as the equilibrium vapour fraction ($X^{f,v}$) of the initial aquifer fluid beyond the zone of depressurization. In this study, the adopted approach is slightly different from the methods discussed in the above references. If an initial equilibrium vapour fraction is assumed ($X^{f,v}\neq 0$), equation (10) is expanded and equation (7) is used to account the concentrations of a volatile component like H_2 or H_2S in the initial aquifer fluid.

$$m_s{}^{f,t}=m_s{}^{f,l}(1-X^{f,v})+m_s{}^{f,v}X^{f,v}=\ m_s{}^{f,l}(1-X^{f,v})+D_s{}^f m_s{}^{f,l}X^{f,v} \quad (11)$$

$$X^{f,v}=\ [(m_s{}^{f,t}/m_s{}^{f,l})-1][(D_s{}^f-1)]^{-1} \quad (12)$$

TABLE 7: Composition of initial aquifer fluid assuming liquid enthalpy[a]

Well	H[b] (kJ/kg)	Aquifer T (°C)[c]	pH[d]	Dissolved solids, mg/kg											Dissolved gases, mmole/kg							N_2/Ar
				B	SiO_2	Na	K	Mg	Ca	F	Cl	SO_4	Al	Fe	CO_2	H_2S	NH_3	H_2	CH_4	N_2	Ar	
MG9D[e]	1160[i]	265	5.19	22.9	615	1332	253	27.8	22.0	1.02	2101	1512	1.59	589	87.18	5.2	0.32	4.41	0.09	35.22	0.3802	92.6
MG18D[g]	1460	267	5.62	41.0	508	1774	281	0.023	19.3	1.33	2924	49.0	0.302	1.38	39.6	1.45	0.83	0.064	0.052	1.243	0.0122	102.0
MG23D	1212	268	5.66	34.8	513	1479	270	0.018	24.5	1.33	2494	38.2	0.318	0.019	48.3	1.09	0.52	0.064	0.304	0.387	0.005	74.6
MG39D	1195	283	5.89	44.1	562	1855	363	0.018	17.2	1.27	3104	24.4	0.276	0.097	54.3	1.21	0.68	0.005	0.057	0.180	0.002	77.0
MG2D	1208	269	5.33	41.8	515	1725	342	0.026	23.6	1.33	2998	23.0	0.269	0.115	90.4	1.32	0.54	0.035	0.220	0.348	0.004	93.8
MG13D	1327	295	5.91	41.6	599	1653	342	0.012	5.6	1.68	2738	90.3	0.265	0.097	91.8	2.08	0.90	0.055	0.139	0.202	0.002	104.1
MG7D	1177	280	5.59	45.4	554	1877	372	0.022	31.2	1.10	3266	18.4	0.220	0.196	41.0	1.09	0.47	nil	0.011	0.016	0.000	130.9
MG16D[g]	1379	286	5.37	47.0	574	1942	393	0.026	28.9	1.20	3346	16.9	0.270	0.011	109.5	1.45	0.47	0.164	0.198	0.492	0.0047	104.7
MG22D	1163	284	5.58	45.5	567	1876	384	0.021	29.9	1.08	3258	18.2	0.193	0.191	56.2	1.18	0.49	0.020	0.083	0.191	0.002	84.8
MG3D[h]	1840	258	5.41	34.5	476	1787	302	0.193	33.1	0.94	3070	57.8	0.182	0.002	46.5	1.40	1.17	0.119	0.082	0.574	0.0067	85.6
MG14D[g]	1438	275	5.46	42.6	536	2538	533	0.267	74.4	1.04	4453	55.4	0.193	0.005	56.8	2.26	1.74	0.129	0.070	0.172	0.0015	113.9
MG29D[g]	1370	282	5.68	24.6	560	1603	333	0.029	30.3	1.49	2704	42.8	0.143	0.005	44.5	1.37	1.32	0.104	0.077	0.724	0.0103	70.1
MG27D	1084	262	6.03	20.7	495	1028	142	0.027	8.0	1.50	1572	60.5	0.522	0.285	31.1	0.80	0.76	0.020	0.059	2.846	0.042	67.6
MG37D[h]	2229	293	4.28	44.6	579	2635	868	4.911	169.9	2.13	5275	24.9	0.103	8.46	44.2	4.24	3.28	0.084	0.063	0.095	0.0008	113.4
MG35D[h]	2174	307	5.45	51.2	632	1808	350	0.512	13.8	3.74	2874	357	0.221	0.107	161.4	3.63	1.98	0.109	0.412	0.191	0.0010	193.4
MG36D	1193	277	5.82	28.0	544	1344	217	0.010	13.0	1.54	2085	35.7	0.510	0.017	44.2	1.04	0.76	0.050	0.112	2.340	0.036	65.5
MG19	1204	277	5.77	38.7	545	1621	326	0.013	20.4	1.11	2784	25.0	0.305	0.004	69.2	1.00	0.71	0.015	0.146	0.740	0.010	77.6
MG34D[h]	2003	263	5.59	49.4	493	2079	337	0.202	33.7	1.08	3384	89.4	0.155	0.013	46.4	1.19	0.88	0.094	0.123	0.174	0.0012	146.4
MG32D[h]	2399	239	6.10	17.6	405	771	78	0.012	6.5	2.45	524	798	0.688	0.122	69.4	1.39	0.75	0.154	0.158	0.195	0.0014	137.1
MG30D[g]	1253	263	5.50	26.7	495	1687	310	0.028	35.4	1.15	2824	35.9	0.186	0.081	33.5	1.01	1.02	0.045	0.070	0.577	0.0070	81.9
MG31D	1244	277	5.37	33.3	543	1859	348	0.128	31.8	1.14	3162	30.5	0.276	0.047	80.3	1.51	1.10	0.089	0.358	0.456	0.005	90.4
MG26D	1140[i]	261	5.46	23.9	492	1181	185	0.050	26.3	1.30	1938	68.4	0.264	0.018	72.4	1.54	1.03	0.134	0.224	1.161	0.011	107.6
MG28D[h]	2118	262	4.51	32.1	482	1674	324	5.972	19.9	1.30	2805	271	0.129	4.53	53.0	2.24	4.81	0.074	0.143	0.465	0.0042	109.4
MG24D[h]	1796	294	5.36	19.2	595	992	241	0.114	15.2	1.11	1647	68.4	0.174	0.059	150.7	3.24	1.55	0.099	0.358	0.114	0.0008	146.0
MG1	1070	257	6.17	27.3	476	1230	180	0.016	14.6	1.48	1944	72.9	0.440	nil	20.8	0.38	0.32	0.005	0.049	0.213	0.003	82.7
MG9D[f]	1160[i]	265	5.74	27.06	295	1683	294	8.92	10.1	0.963	2732	309	0.130	15.8	33.0	2.01	2.40	0.407	0.068	8.217	0.055	96.8
MG9D[f]	1160[i]	265	5.39	27.33	382	1683	302	11.7	12.4	0.936	2788	264	0.078	5.93	30.3	2.03	1.17	0.035	0.052	5.577	nil	
MG40D[h]	2265	301	4.32	45.7	607	2402	677	11.740	148.8	1.83	4932	50.4	0.531	156	28.2	3.47	7.70	0.179	0.070	0.435	0.0070	62.0

[a] "excess enthalpy" wells assuming phase segregation model, [b] measured total discharge enthalpy ($h^{d,t}$) from tracer flow test, [c] based on T_{qtz} (Gunnarsson and Arnórsson, 2000) except all samples of MG9D (average of $T_{Na/K}$ geothermometers), [d] at aquifer temperature, [e] without caustic soda dosing, [f] with caustic soda dosing, [g] medium "excess enthalpy" well, [h] high "excess enthalpy" well, [i] enthalpy of steam-saturated liquid water, nil- not detectable

All terms in the right hand side of equation (12) can be made available. The total concentration of the volatile in the aquifer, $m_s^{f,t}$, was already obtained by equation (10) when the aquifer was initially assumed to be purely liquid. The partitioning coefficient, D_s^f, is calculated from equation (7) after the Henry's Law coefficient is evaluated at the assumed aquifer temperature using equation (13) or (14) in Table 8. As will be discussed later, the aquifer concentration of the volatiles H_2 and H_2S in the liquid phase ($m_s^{f,l}$) may be potentially fixed by equilibrium with the mineral assemblages grossular-magnetite-epidote-wollastonite or hematite-magnetite and may be computed from the corresponding log K-temperature equation in Table 8 (equation (3) or (5) for $H_2S_{,aq}$; equation (8) or (10) for $H_{2,aq}$).

After deriving an equilibrium vapour fraction, $X^{f,v}$, the total aquifer fluid enthalpy ($h^{f,t}$) is no longer equal to $h^{f,l}$ but can be solved using the relationship:

$$X^{f,v}=(h^{f,t}-h^{f,l})/(h^{f,v}-h^{f,l}) \quad (13)$$

The $h^{f,t}$ value obtained from equation (13) is inserted into WATCH during the 2nd step of the procedure for modelling "excess enthalpy" wells. Consequently, the concentrations of all components will be calculated by WATCH both in the liquid and vapour phases of the initial aquifer at the assumed reference temperature ($T_{qtz,GA}$).

Depending on the analyses of the samples, particularly the H_2S and H_2 gaseous concentrations, it is possible to get a numerical value of the equilibrium steam fraction, $X^{f,v}$, following the procedures described above but with no physical significance. To validate the derived $X^{f,v}$, a balance of the total mass flows (M) can be done assuming the phase segregation model.

$$M^{d,t}=M^{f,t}-M^{e,l} \quad (14)$$

$M^{e,l}$ represents the liquid phase retained in the formation at the chosen segregation point. Dividing all terms in equation (14) by $M^{d,t}$ yields:

$$1=M^{f,t}/M^{d,t}-M^{e,l}/M^{d,t}=V^{f,t}-V^{e,l} \quad (15)$$

$V^{f,t}$ and $V^{e,l}$ represent the masses of aquifer fluid and liquid phase retained in the formation relative to the total discharge of the well, respectively. There are various ways to obtain their values and one way is to account the concentrations of a volatile species. By the phase segregation model, all gases present in the initial aquifer fluid are discharged to the well since the gases retained in the formation are negligible.

$$m_s{}^{d,t}M^{d,t}=m_s{}^{f,t}M^{f,t} \quad (16)$$

$$V^{f,t}=m_s{}^{d,t}/m_s{}^{f,t} \quad (17)$$

$V^{e,l}$ can then be calculated using equation (15). Since "excess enthalpy" is attributed to phase segregation, a derived $X^{f,v}$ is meaningful if the corresponding $V^{e,l}$ value is positive. Modelled initial aquifer fluid compositions considering the derived equilibrium vapour fractions, $X^{f,v}$, are shown in Table 9. Based on their measured discharge enthalpies, five of the wells in Table 9 are termed "medium enthalpy" ($h^{d,t}\approx$ 1200-1500 kJ/kg, "excess enthalpy"$\approx$ 100-300 kJ/kg) and eight are considered "high enthalpy" ($h^{d,t}\approx$ 1800-2400 kJ/kg, "excess enthalpy"$\approx$ 500-900 kJ/kg).

3.3.3 Thermodynamic data

In calculating the distribution of aqueous species and mineral solubility products, WATCH uses the thermodynamic data provided by Arnórsson et al. (1982) except for gas solubility constants which were taken from Arnórsson et al. (1996) and $H_4SiO_4°$ from Gunnarsson and Arnórsson (2000). In addition, dissociational equilibria for Al-hydroxide species are from Arnórsson and Andrésdottir (1999), ferric- and ferrous hydroxide from Diakonov and Tagirov (2002). Finally, the Al-Si dimer of Pokrovski et al. (1998) was incorporated into the speciation calculations.

TABLE 8: Log K-temperature equations of a) mineral assemblages potentially controlling concentrations of H_2S, H_2, CO_2 and b) Henry's Law Constants (valid at 0-350°C at 1 bar for less than 100°C and P_{sat} for higher temperatures, unit activity for all minerals and liquid water)[a]

	Reaction	log K (T in K)
1	**H_2S:** $\frac{1}{3}pyr + \frac{1}{3}pyrr + \frac{2}{3}pre + \frac{2}{3}H_2O_l \leftrightarrow \frac{2}{3}epi + H_2S_{aq}$	$log[H_2S] = 13.608 + \frac{592324}{T^2} - \frac{9346.7}{T} - 0.043552T + 2.9164x10^{-5}T^2 + 5.139logT$
2	**H_2S:** $\frac{2}{3}gro + \frac{1}{3}pyr + \frac{1}{3}pyrr + \frac{2}{3}qtz + \frac{4}{3}H_2O_l \leftrightarrow \frac{2}{3}epi + \frac{2}{3}wol + H_2S_{aq}$	$log[H_2S] = 13.659 + \frac{555082}{T^2} - \frac{9256.6}{T} - 0.04361T + 2.861x10^{-5}T^2 + 5.148logT$
3	**H_2S:** $2gro + \frac{1}{4}pyr + \frac{1}{2}mag + 2qtz + 2H_2O_l \leftrightarrow 2epi + 2wol + H_2S_{aq}$	$log[H_2S] = -0.836 - \frac{216659}{T^2} - \frac{2847.3}{T} + 0.008524T - 2.366x10^{-6}T^2 + 0.152logT$
4	**H_2S:** $\frac{1}{4}pyr + \frac{1}{2}pyrr + H_2O_l \leftrightarrow \frac{1}{4}mag + H_2S_{aq}$	$log[H_2S] = 13.589 + \frac{590215}{T^2} - \frac{9024.5}{T} - 0.044882T + 2.978x10^{-5}T^2 + 5.068logT$
5	**H_2S:** $\frac{1}{2}pyr + \frac{1}{2}mag + H_2O_l \leftrightarrow hem + H_2S_{aq}$	$log[H_2S] = 35.516 - \frac{4156.9}{T} + 0.01267T - 13.914logT$
6	**H_2:** $\frac{4}{3}pyrr + \frac{2}{3}pre + \frac{2}{3}H_2O_l \leftrightarrow \frac{2}{3}epi + \frac{2}{3}pyr + H_{2,aq}$	$log[H_2] = -1.643 - \frac{110535}{T^2} - \frac{802.06}{T} - 4.184x10^{-4}T + 7.574x10^{-6}T^2 - 0.56logT$
7	**H_2:** $\frac{2}{3}gro + \frac{4}{3}pyrr + \frac{2}{3}qtz + \frac{4}{3}H_2O_l \leftrightarrow \frac{2}{3}epi + \frac{2}{3}wol + \frac{2}{3}pyr + H_{2,aq}$	$log[H_2] = -1.546 - \frac{138877}{T^2} - \frac{769.11}{T} - 4.872x10^{-4}T + 6.932x10^{-6}T^2 - 0.528logT$
8	**H_2:** $6gro + 2mag + 6qtz + 4H_2O_l \leftrightarrow 6epi + 6wol + H_{2,aq}$	$log[H_2] = 1.444 - \frac{273812}{T^2} - \frac{3962.1}{T} + 2.401x10^{-3}T + 1.304x10^{-6}T^2 + 0.979logT$
9	**H_2:** $\frac{3}{2}pyrr + H_2O_l \leftrightarrow \frac{3}{4}pyr + \frac{1}{4}mag + H_{2,aq}$	$log[H_2] = -1.572 - \frac{168874}{T^2} - \frac{232.45}{T} - 3.0275x10^{-3}T + 9.517x10^{-6}T^2 - 0.652logT$
10	**H_2:** $2mag + H_2O_l \leftrightarrow 3hem + H_{2,aq}$	$log[H_2] = 824.146 + \frac{3212081}{T^2} - \frac{51505}{T} + 0.11297T - 294.895logT$
11	**CO_2:** $czo + cal + \frac{3}{2}qtz + H_2O_l \leftrightarrow \frac{3}{2}pre + CO_{2,aq}$	$log[CO_2] = -0.89 + \frac{7251.5}{T^2} - \frac{1710.6}{T} + 4.188x10^{-3}T + 2.683x10^{-6}T^2 - 0.064logT$
12	**CO_2:** $\frac{2}{5}czo + cal + \frac{3}{5}qtz \leftrightarrow \frac{3}{5}gro + \frac{1}{5}H_2O_l + CO_{2,aq}$	$log[CO_2] = -1.449 - \frac{40536}{T^2} - \frac{2135.9}{T} + 6.5639x10^{-3}T + 2.725x10^{-6}T^2 - 0.193logT$
13	**K_H:** $H_2S_g \leftrightarrow H_2S_{aq}$	$logK_{H_2S} = 24.229 + \frac{837819}{T^2} - \frac{490.63}{T} - 0.09836T - \frac{900.43}{T^{0.5}} + 5.5x10^{-5}T^2 + 17.61logT$
14	**K_H:** $H_{2,g} \leftrightarrow H_{2,aq}$	$logK_{H_2} = 10.65 + \frac{768091}{T^2} - \frac{7651.7}{T} - 0.0461T + \frac{94.908}{T^{0.5}} + 3.336x10^{-5}T^2 + 3.452logT$
15	**K_H:** $CO_{2,g} \leftrightarrow CO_{2,aq}$	$logK_{CO_2} = 17.135 + \frac{726530}{T^2} + \frac{65.396}{T} - 0.06964T - \frac{731.5}{T^{0.5}} + 3.912x10^{-5}T^2 + 13.19logT$
16	**K_H:** $CH_{4,g} \leftrightarrow CH_{4,aq}$	$logK_{CH_4} = 20.352 + \frac{853894}{T^2} - \frac{444.61}{T} - 0.0814T - \frac{856.26}{T^{0.5}} + 4.581x10^{-5}T^2 + 15.542logT$
17[b]	**K_H:** $N_{2,g} \leftrightarrow N_{2,aq}$	$logK_{N_2} = -55.857 + \frac{2947.41}{T} + 2.68x10^{-6}T^2 + 17.191logT$
18[b]	**K_H:** $Ar_g \leftrightarrow Ar_{aq}$	$logK_{Ar} = -62.606 + \frac{3136.06}{T} - 1.01x10^{-6}T^2 + 19.931logT$

[a] sources of thermodynamic data are mentioned by Karingithi et al. (2010); [a] sources of thermodynamic data are mentioned by Arnórsson (2000); mineral phases: cal-calcite, czo-clinozoisite, epi-epidote, gro-grossular, hem-hematite, mag-magnetite, pre-prehnite, pyr-pyrite, pyrr-pyrrhotite, qtz-quartz, wol-wollastonite

TABLE 9: Composition of the liquid phase of modelled two-phase initial aquifer fluid[a]

Well	H^b (kJ/kg)	Aquifer T (°C)[c]	$\%X^{f,v}$	$V^{e,l}$	pH[d]	Dissolved solids, mg/kg											Dissolved gases, mmole/kg							N_2/Ar
						B	SiO_2	Na	K	Mg	Ca	F	Cl	SO_4	Al	Fe	CO_2	H_2S	NH_3	H_2	CH_4	N_2	Ar	
MG9D[e]	1160[i]	265	212	0	ND[l]																			
MG18D[g]	1460	267	1.79	1.59	5.88	41.0	508	1774	281	0.023	19.3	1.33	2924	49.0	0.302	1.38	16.3	1.08	0.83	0.010	0.005	0.145	0.00696	20.9
MG23D	1212	268	1.74	0.07	5.99	34.8	513	1479	270	0.018	24.5	1.33	2493	38.2	0.318	0.203	18.7	0.77	0.52	0.010	0.027	0.043	0.0030	14.1
MG39D	1195	283	-0.35	-0.36	ND[k]																			
MG2D	1208	269	0.77	0.12	5.50	41.8	515	1725	341	0.026	23.6	1.32	2998	23	0.269	0.115	52.2	1.11	0.54	0.010	0.039	0.075	0.0028	26.5
MG13D	1327	295	0.36	0.03	5.97	41.6	599	1653	342	0.012	5.56	1.68	2738	90.3	0.265	0.097	77.0	1.99	0.89	0.030	0.066	0.110	0.0018	60.9
MG7D	1177	280	ND[j]		ND[k]																			
MG16D[g]	1379	286	3.10	0.33	5.66	47.0	574	1943	393	0.026	28.9	1.20	3348	16.9	0.270	0.011	45.3	1.11	0.48	0.025	0.020	0.064	0.00264	24.1
MG22D	1163	284	-0.03	-0.61	ND[k]																			
MG3D[h]	1840	258	4.45	3.11	5.73	34.5	476	1788	302	0.193	33.1	0.94	3070	57.8	0.182	0.002	10.3	0.74	1.14	0.005	0.003	0.028	0.00198	14.2
MG14D[g]	1438	275	3.17	0.95	5.70	42.6	536	2538	533	0.268	74.5	1.04	4455	55.4	0.193	0.005	19.7	1.57	1.74	0.015	0.005	0.016	0.00073	22.5
MG29D[g]	1370	282	2.05	0.54	5.89	24.6	560	1604	334	0.029	30.3	1.49	2704	42.8	0.143	0.005	20.9	1.10	1.32	0.020	0.009	0.111	0.00654	16.9
MG27D	1084	262	0.45	-0.49	6.17	20.7	495	1028	142	0.027	7.97	1.50	1572	60.5	0.522	0.285	20.9	0.71	0.76	0.005	0.014	0.80	0.0347	22.9
MG37D[h]	2229	293	1.04	5.60	4.29	44.6	579	2636	868	4.912	169.9	2.13	5276	24.9	0.103	8.46	29.8	3.86	3.28	0.030	0.016	0.029	0.00069	42.2
MG35D[h]	2174	307	0.79	4.89	5.48	51.2	632	1808	350	0.512	13.8	3.75	2874	357	0.221	0.107	127.6	3.47	1.99	0.055	0.160	0.087	0.00088	98.4
MG36D	1193	277	0.90	-0.27	6.00	28.0	544	1344	217	0.01	13	1.54	2085	35.7	0.510	0.017	26.1	0.88	0.76	0.015	0.021	0.543	0.0278	19.5
MG19	1204	277	-0.01	-0.12	ND[k]																			
MG34D[h]	2003	263	3.02	4.38	5.95	49.4	493	2080	337	0.202	33.7	1.08	3384	89.4	0.155	0.013	14.0	0.76	0.88	0.010	0.007	0.013	0.0005	25.8
MG32D[h]	2399	239	9.30	4.16	6.96	17.5	405	770	78	0.012	6.5	2.45	524	798	0.688	0.122	10.1	0.60	0.68	0.005	0.002	0.004	0.00015	25.5
MG30D[g]	1253	263	1.29	0.53	5.68	26.7	495	1687	310	0.028	35.4	1.15	2824	35.9	0.186	0.081	15.4	0.79	1.02	0.005	0.007	0.079	0.00441	17.9
MG31D	1244	276	1.97	-0.03	5.60	33.3	543	1858	348	0.128	31.8	1.14	3161	30.5	0.276	0.047	32.1	1.08	1.09	0.015	0.035	0.056	0.0031	18.2
MG26D	1140[i]	261	4.61	-0.32	5.96	23.8	491	1178	184	0.05	26.2	1.30	1933	68.2	0.264	0.018	12.5	0.66	0.93	0.005	0.007	0.045	0.0033	13.5
MG28D[h]	2118	262	2.39	5.41	4.51	32.1	483	1674	324	5.973	19.9	1.30	2805	271	0.129	4.53	17.4	1.49	4.75	0.005	0.009	0.039	0.00199	19.7
MG24D[h]	1796	294	1.27	2.91	5.46	19.2	595	992	241	0.114	15.2	1.11	1647	68.5	0.174	0.059	96.8	2.93	1.56	0.035	0.081	0.032	0.00062	51.3
MG1	1070	257	-0.02	-0.47	ND[k]																			
MG9D[f]	1160[i]	265	14.3	-0.50	6.09	26.8	292	1667	291	8.833	10	0.954	2706	306	0.13	15.67	2.72	0.49	1.94	0.010	0.001	0.142	0.0044	32.5
MG9D[f]	1160[i]	265	0.75	-0.07	5.44	27.3	382	1682	301	11.68	12.4	0.935	2787	264	0.08	5.931	16.9	1.66	1.15	0.010	0.009	1.130	nil	-
MG40D[h]	2265	301	2.26	4.64	4.33	45.8	607	2403	678	11.748	148.9	1.83	4936	50.5	0.531	157	15.8	3.02	7.73	0.045	0.012	0.096	0.00506	18.9

[a] "excess enthalpy" wells modelled assuming phase segregation, [b] measured total discharge enthalpy ($h^{d,t}$) from tracer flow test, [c] based on T_{qtz} (Gunnarsson and Arnórsson, 2000), [d] at aquifer temperature, [e] without acid inhibition, [f] with acid inhibition, [g] medium "excess enthalpy" well, [h] high "excess enthalpy" well, [i] enthalpy of steam-saturated liquid water, [j] very low dissolved H_2 in liquid aquifer, [k] negative $X^{f,v}$, [l] very large $X^{f,v}$ nil- not detectable, ND- not determined

The mineral-gas reactions that potentially could control the concentrations of H_2S, H_2 and CO_2 in the aquifer liquid and temperature equations for their equilibrium constants are listed in Table 9. Henry's Law coefficients, K_s (moles per kg-bar), as a function of temperature for the different gases are also presented in Table 9. These functions calculate the distribution coefficients, D_s, and equilibrium vapour fractions, $X^{f,v}$, in the initial aquifer fluids. The sources of thermodynamic data are noted in Table 9. A few points will be reiterated here. The temperature equations are consistent with the selected thermodynamic data within 0.02 log K units and are valid in the range 0-350°C, at 1 bar below 100°C and at P_{sat} at higher temperatures. The equations in Table 9 assume unit activity of all minerals and liquid water. However, when the log K curves are plotted, the equations are modified to account the activities of end-members of minerals that form solid solutions (epidote, garnet and prehnite). For instance, considering reaction (8) in Table 9:

$$\log K = 6 \log a_{epi} + 6 \log a_{wol} + \log [H_2] - 6 \log a_{gro} - 2 \log a_{mag} - 6 \log a_{qtz} - 4 \log [H_2O] \qquad (18)$$

The minerals wollastonite (wol), magnetite (mag) and quartz (qtz) and liquid water are taken to be pure thereby having unit activities. To determine the equilibrium concentration of aqueous H_2 in the initial aquifer, equation (18) is reduced and re-arranged to:

$$\log [H_2] = \log K - 6 \log a_{epi} + 6 \log a_{gro} \qquad (19)$$

No data are available on mineral compositions from Mahanagdong field in order to estimate the activities of end-members in the epidote (epidote and clinozoisite), garnet (grossular and andradite) and prehnite (Al-prehnite and Fe-prehnite) solid solutions. Scott (2001) calculated the activities of epidote solid solutions from microprobe analyses of cores from the nearby Tongonan wells. On the basis of these analyses, epidote end-members activity is in the range of 0.63-0.99. The average is 0.8. This activity has been selected and thus a value of 0.2 for clinozoisite. The activities selected for the end-members of prehnite (0.8 for Al-prehnite and 0.2 for Fe-prehnite) and garnet (0.3 for grossular and 0.2 for andradite) were taken from Arnórsson et al. (2010) based on analyses of these minerals in the geothermal fields of Iceland and Olkaria, Kenya.

The equilibrium constants for the dissolution reactions listed in Table 10 have been used to evaluate the state of equilibrium of the hydrothermal solutions with respect to individual minerals. Discussions will focus on the individual minerals that comprise the most likely assemblages that buffer the concentrations of the reactive gases CO_2, H_2S and H_2 in Mahanagdong: epidote-clinozoisite, grossular, calcite, wollastonite, pyrrhotite, pyrite and magnetite. The temperature equations of the equilibrium constants of the dissolution reactions in Table 10 were taken from Karingithi et al. (2010).

TABLE 10: Log K-temperature equations of individual minerals dissolution reactions (valid at 0-350°C at P_{sat}, unit activity for all minerals and liquid water)[a]

	Reaction	log K (T in K)
1	$cal + 2H^+ \leftrightarrow Ca^{2+} + H_2O_l + CO_{2,aq}$	$\log K = -68.271 + \frac{4385.24}{T} - 0.007525T + 25.856 logT$
2	$wol + 2H^+ + H_2O_l \leftrightarrow Ca^{2+} + H_4SiO_4^0$	$\log K = -127.096 + \frac{8151.38}{T} - 0.02981T + 49.282 logT$
3	$gro + 4H^+ + 8H_2O_l \leftrightarrow 3Ca^{2+} + 2Al(OH)_4^- + 3H_4SiO_4^0$	$\log K = -517.662 + \frac{17623.7}{T} - 0.14343T + 203.808 logT$
4	$pre + 10H_2O_l \leftrightarrow 2Ca^{2+} + Fe(OH)_4^- + 2Al(OH)_4^- + 3H_4SiO_4^0 + 2OH^-$	$\log K = 833.95 - \frac{25642.8}{T} + 0.5035T - 2.941x10^{-4}T^2 - 369.297 logT$
5	$czo + 12H_2O_l \leftrightarrow 2Ca^{2+} + 3Al(OH)_4^- + 3H_4SiO_4^0 + OH^-$	$\log K = 36.052 - \frac{6854.78}{T} + 0.13236T - 1.3749x10^{-4}T^2 - 33.508 logT$
6	$epi + 12H_2O_l \leftrightarrow 2Ca^{2+} + Fe(OH)_4^- + 2Al(OH)_4^- + 3H_4SiO_4^0 + OH^-$	$\log K = 893.547 - \frac{27077.4}{T} - 0.54124T - 3.022x10^{-4}T^2 - 398.38 logT$
7	$mag + 4H_2O_l \leftrightarrow Fe^{2+} + 2Fe(OH)_4^-$	$\log K = 949.951 - \frac{24258.2}{T} + 0.51474T - 2.402x10^{-4}T^2 - 417.136 logT$
8	$pyr + 2H^+ + H_{2,aq} \leftrightarrow Fe^{2+} + 2H_2S_{aq}$	$\log K = -1.397 - \frac{461.3}{T} - 0.0009128T + 1.626 logT$
9	$pyrr + 2H^+ \leftrightarrow Fe^{2+} + H_2S_{aq}$	$\log K = -3.043 + \frac{1579.06}{T} + 0.001987T + 0.12 logT$
10	$qtz + 2H_2O_l \leftrightarrow H_4SiO_4^0$	$\log K = -34.188 + \frac{197.47}{T} - 5.851x10^{-6}T^2 + 12.245 logT$

[a]- see text for source of thermodynamic data; mineral phases: cal-calcite, czo-clinozoisite, epi-epidote, gro-grossular, mag-magnetite, pyr-pyrite, pyrr-pyrrhotite, qtz-quartz, wol-wollastonite

4. RESULTS AND DISCUSSIONS

It is important to emphasize the underlying assumptions and simplifications before interpreting the results. In reconstructing the initial aquifer fluids, the samples collected in the wellhead are taken to represent the deep aquifers feeding the well; the chemical analyses of the samples are deemed reliable; the aquifer was evaluated at an assumed reference temperature; "excess enthalpy" of well discharge is attributed to segregation of the two-phase fluid in a zone 30°C lower than the selected aquifer temperature; and the fluids travel from the aquifer to the wellhead without precipitating minerals or dissolving the rocks or casing materials they interact with. Aqueous speciation distribution of the aquifer fluid uses thermodynamic database that carries uncertainties. Finally, assuming the concept of local equilibrium within the larger open geothermal system allows the application of thermodynamic principles to assess how closely local equilibrium conditions are approached based on the geochemical data of the modelled aquifers.

The results are initially presented with all mentioned assumptions basically accepted. On opportunity, it will be demonstrated how variable compositions of solid solutions and uncertainties in the thermodynamic data, the choice of segregation point, variations in the reference temperature, or differences in selected analyses like CO_2 and pH will affect the calculated fluid parameters. Behaviour of the minor and trace elements in the water will be integrated to understand some chemical evolution as energy is continuously extracted from the Mahanagdong geothermal field since the middle of 1990's.

4.1 Mineral assemblage-gas equilibria

The equilibrium curves of the mineral assemblages that could potentially fix the concentrations of the reactive gases H_2S, H_2 and CO_2 (reactions 1-12, Table 9) are plotted in Figure 10. Arnórsson et al. (2007) point out that some of the different mineral assemblages shown give very similar aqueous H_2S, H_2 and CO_2 equilibrium concentrations when the endmember activities of the solid solution minerals are properly chosen. In the temperature range 200-300°C and at the selected mineral compositions (a_{epi}=0.8, a_{czo}=0.2, a_{pre}=0.8, a_{gro}=0.3), the two reactions involving CO_2 differ only within 0.28 log K units. H_2S and H_2 are likely to equilibrate with the same mineral assemblages. For H_2S and H_2, reactions that include either prehnite or magnetite are also very similar (reactions 1 and 4 for H_2S; 6 and 9 for H_2 in Table 9) while the log K-temperature curves of assemblages that contain grossular garnet plot lower, especially when magnetite is involved (reactions 3 and 8, Table 9). Mineral assemblages involving only Fe-sulphides and Fe-oxides are also plotted and all take unit activities (reactions 4, 5, 9 and 10, Table 9).

The concentrations of the reactive gases H_2S, H_2 and CO_2 in the aquifer liquid when assuming no vapour to be present is depicted in Figure 10. They show much scatter. As elaborated in later sections, the scatter partly reflects the assumptions in modelling the initial aquifer fluids. Since H_2S and H_2 are likely to equilibrate with the same mineral assemblages, Figure 10 suggests that their aqueous concentration in the total aquifer fluid is potentially buffered by the garnet-bearing (reactions 7 and 8, Table 9) or hematite-magnetite (reaction 10, Table 9) mineral assemblages. At the selected mineral compositions, H_2S data points for liquid enthalpy generally plot above the respective equilibrium curves especially for "high enthalpy" wells MG28D and MG32D. For MG32D, selecting a lower reference temperature (~240°C) also contributed to the large departure from equilibrium. Samples taken at different conditions from the acidic well MG9D are also significantly above equilibrium. Acid wells in Mahanagdong typically have high H_2S levels (e.g., Parilla et al., 1997) and the gases may not have equilibrated with the reservoir rocks (Salonga and Auman, 1997; Siega et al., 1999).

The scatter of data points is most pronounced for H_2 although all plot within the area defined by the hematite-magnetite and garnet-bearing assemblages at the chosen compositions, except for 3 samples. Cathodic reactions from corrosion of well casing probably caused the anomalously high H_2 level of the acidic sample from MG9D (9U in Figure 10). On the other extreme, samples with low H_2 levels

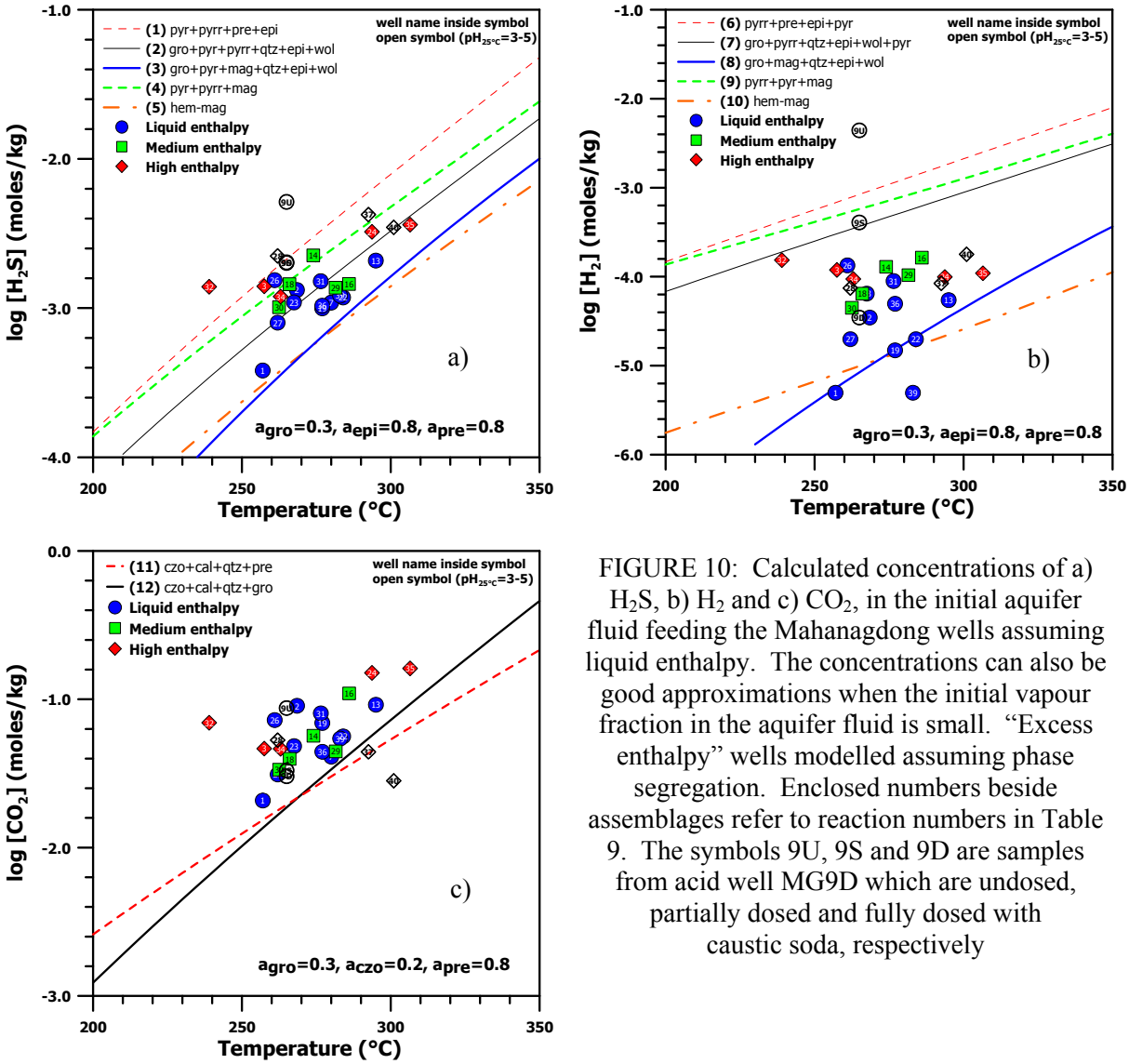

FIGURE 10: Calculated concentrations of a) H_2S, b) H_2 and c) CO_2, in the initial aquifer fluid feeding the Mahanagdong wells assuming liquid enthalpy. The concentrations can also be good approximations when the initial vapour fraction in the aquifer fluid is small. "Excess enthalpy" wells modelled assuming phase segregation. Enclosed numbers beside assemblages refer to reaction numbers in Table 9. The symbols 9U, 9S and 9D are samples from acid well MG9D which are undosed, partially dosed and fully dosed with caustic soda, respectively

reflect the effect of relatively degassed fluids flowing into wells as shown for MG1 and 27D (cooler peripheral waters) and MG7D, 19, 22D and 39D (injected brine) consistent with their corresponding reservoir Cl and CO_2 total discharge trends (unpublished EDC geochemistry reports). Samples from wells MG7D (H_2 level beyond lower scale of graph) and MG39D probably experienced vapour loss as the fluids flow into the well along sub-horizontal aquifers. It may be more appropriate to reconstruct their aquifers by the vapour-loss model proposed by Arnórsson et al. (2010).

The scatter in H_2 aquifer fluid concentrations is probably a reflection of variable fractions of equilibrium steam in the initial aquifer fluid. If considering equilibrium with the assemblage gro+mag+qtz+epi+wol is the cause, the large scatter of the data points can partly be a reflection of the stoichiometry of the reaction. The relatively large stoichiometric coefficients in reaction (8) of Table 9 show that the equilibrium aqueous concentrations of H_2 are strongly affected by the compositions of the grossular garnet and epidote. Figure 11 illustrates how variable compositions of grossular garnet and epidote affect the equilibrium curves of reactions (3), (8) and (12) in Table 9 for H_2S, H_2 and CO_2, respectively. No data are available on mineral compositions from Mahanagdong. Yet even if there is one, Scott (2001) pointed out in Tongonan that the aquifer fluids may have interacted with solid solution minerals of different compositions. Likewise, the stoichiometry will amplify any inherent errors in the calculated log K-temperature equation at any specified composition.

Two minerals (grossular garnet and wollastonite) comprising the assemblage of reactions (3) and (8) were found in both Tongonan and Mahanagdong geothermal fields but are relatively rare compared to the silicate and sulphide alteration minerals mentioned in section 2.2. Both garnet and wollastonite are

indicators of high subsurface temperatures of >300°C (e.g., Reyes, 1990). The appearance of hydrogrossular/grossular garnet may indicate >260°C temperatures together with other geoindicators within the calc-silicate subzone of Philippine geothermal systems. The presence of garnet in lower temperature zones is interpreted as either relict alteration or decreased formation temperature at higher water content. Wollastonite was reported only at the shallow sections of well 501 in Tongonan (Reyes, 1979) and its presence in well AP2D in the more immature Alto Peak geothermal field, southeast of Mahanagdong, was noted in the vicinity of dikes (Reyes et al., 1993). Formation of wollastonite is usually associated with contact metamorphism (e.g. Kristmannsdóttir, 1981) and its hydrothermal formation becomes more improbable at below 300°C and higher CO_2 activity (e.g. Greenwood, 1967). The mineral assemblage hematite-magnetite involved in reactions (5) and (10) in Table 9 are more commonly encountered in Mahanagdong. Hematite usually indicates incursion of cooler fluids and is also more associated with acid alteration assemblages (e.g. Scott, 2001). At the selected mineral compositions and typical Mahanagdong aquifer temperatures (250-300°C), the mineral assemblages gro+mag+qtz+epi+wol and hem+mag have almost similar log K-temperature curves.

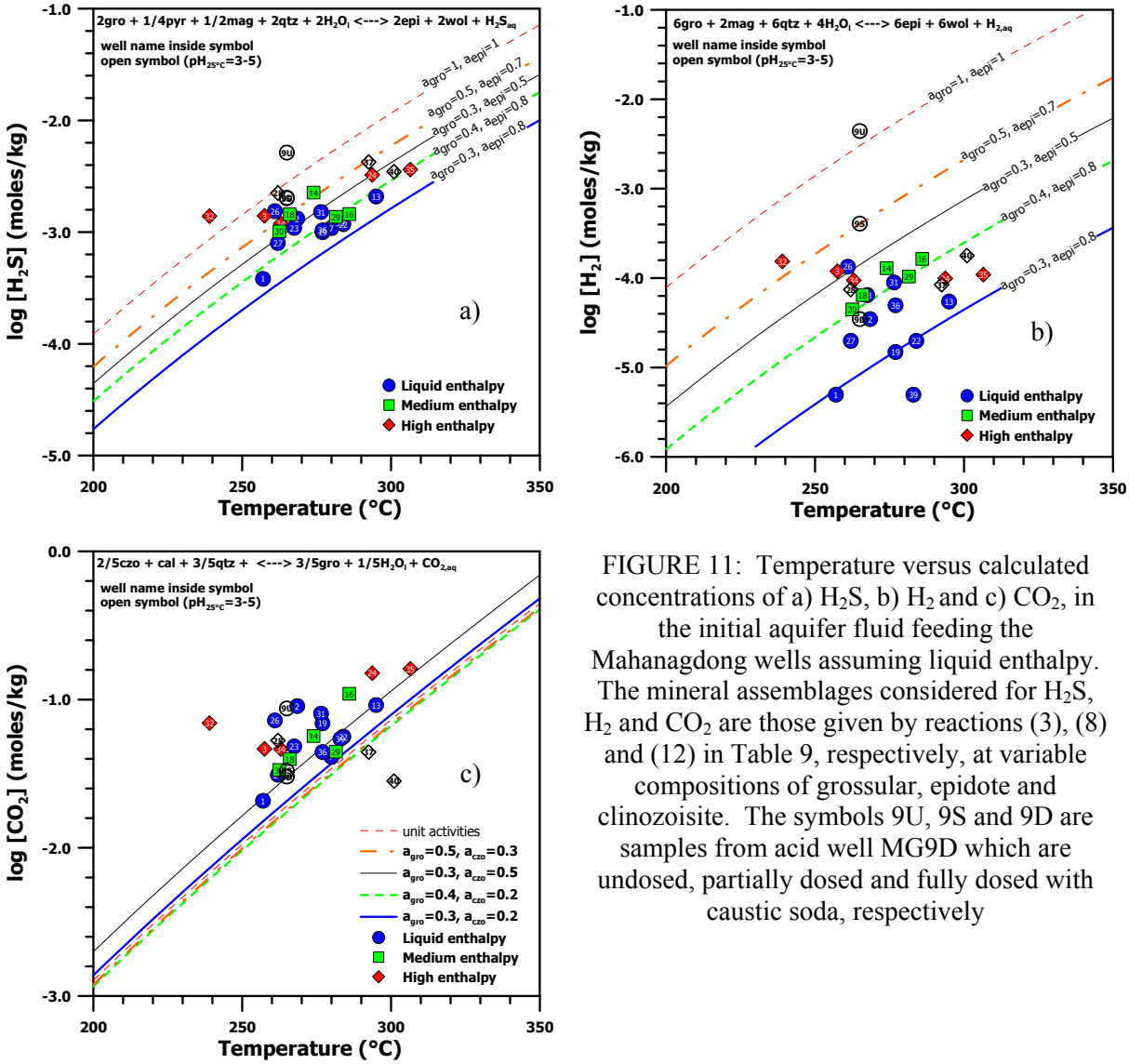

FIGURE 11: Temperature versus calculated concentrations of a) H_2S, b) H_2 and c) CO_2, in the initial aquifer fluid feeding the Mahanagdong wells assuming liquid enthalpy. The mineral assemblages considered for H_2S, H_2 and CO_2 are those given by reactions (3), (8) and (12) in Table 9, respectively, at variable compositions of grossular, epidote and clinozoisite. The symbols 9U, 9S and 9D are samples from acid well MG9D which are undosed, partially dosed and fully dosed with caustic soda, respectively

From the CO_2 data points only, it is difficult to discritize which of the two assemblages control $CO_{2,aq}$ concentrations. The mineral assemblage czo+cal+qtz+gro may be the more probable buffer if considering that the H_2S and H_2 data randomly yet consistently plot around the equilibrium curves involving garnet. Prehnite is also encountered even more rarely than garnet in the wells drilled in both Tongonan and Mahanagdong (Scott, 2001; various EDC well geology reports). Reyes (1990) identifies prehnite, as well as pyrrhotite, pumpyellite, sphene and laumontite, as one of the mineral

indicators of poor permeability in Philippine geothermal systems. On the other hand, Reyes (1990) reports that clinozoisite in neutral-pH alteration suites could indicate >240°C subsurface temperatures and was reported in wells MG9D and MG17D (unpublished EDC well geology reports).

Similar to H_2S, the data points for $CO_{2,aq}$ plot generally above the equilibrium curves. A possible source of additional CO_2 flux into the system is the carbonaceous components within the sedimentary breccia/conglomerate complex (Mahiao Sedimentary Complex) where all Mahanagdong wells produce. The average concentration of $CO_{2,aq}$ in liquid enthalpy wells is higher by 0.45 log units. MG2D and 26D show the highest excess from equilibrium with the mineral assemblages. Salonga et al. (2004) lists MG2D as one of the wells with high supersaturation in calcite resulting to declining mass flows as calcite gradually deposited in the wellbore. MG26D, sampled while on horizontal discharge to commercialize wellhead pressure, is a high enthalpy well (~1800 kJ/kg) tapping from a shallow two-phase zone prior to its wellhead pressure decline. Only the high enthalpy well MG40D plots below the equilibrium curves. Since H_2S_{aq} and $H_{2,aq}$ concentrations of MG40D are considerably above their respective equilibrium values, only $CO_{2,aq}$ is depleted in this well. Samples from MG40D may still be affected by residual drilling fluids as they were taken less than 3 months after completion tests.

4.2 Equilibrium vapour fraction

The calculated aquifer fluid H_2S concentrations are elevated relative to equilibrium with both the hematite-magnetite (reactions 5 and 10, Table 9) and garnet-bearing assemblages at the selected mineral compositions (reactions 3 and 8, Table 9). This is also the case for H_2 and CO_2 with the exception of two liquid and excess enthalpy wells, respectively. These results are taken to indicate that equilibrium vapour is present in the initial aquifer fluid ($X^{f,v}$). The two sets of data points with low H_2 and CO_2 aquifer fluid concentrations, respectively, may represent degassed aquifer fluid. Gaseous vapour was lost from the fluid flowing into the wells.

At 200-300°C, the solubility of H_2S is about 8-18 times more than H_2, the difference decreasing at higher temperatures. For an assumed aquifer temperature, higher H_2S solubility will reflect in lower distribution coefficient, D_s^f, in equation (12) compared to using H_2 analysis. Also, log K-temperature curves of H_2S have steeper positive slopes than the H_2 equilibrium curves. This means that the degree of departure of H_2S levels from equilibrium is more sensitive with the assumed aquifer temperature. As a result, assuming equilibrium of H_2S with mineral assemblages yields variable and unreasonably high $X^{f,v}$ values (3-18%) equivalent to steam-dominated geothermal fields. At 300°C, vapour fractions of 1.8% and 4% by mass correspond to 22% and 40% by volume, respectively. In contrast, H_2 practically partitions to the vapour phase during the first boiling of the initial aquifers due to its much lower solubility compared to H_2S and CO_2. Thus, H_2 concentration is more sensitive to vapour fraction values. H_2 is also very reactive and responds fast according to both temperature and redox conditions (e.g. Giggenbach, 1980). So in this study, $X^{f,v}$ is estimated assuming that H_2 concentration is fixed by the garnet-bearing assemblage (reaction 8, Table 9) at the selected compositions. Choosing the hematite-magnetite assemblage essentially yields the same results because in the temperature range of Mahanagdong wells (about 250-300°C), equilibrium values of H_2 of both assemblages will differ only by at most 0.35 log units.

The equilibrium vapour fractions of aquifers feeding the Mahanagdong wells are summarized in Table 8. As will be discussed later, these $X^{f,v}$ values carry significant error. In liquid enthalpy wells, slightly negative to almost zero $X^{f,v}$ values (-0.01 to -0.4%) are obtained for MG1, 19, 22D and 39D. The $X^{f,v}$ value for MG7D is significantly negative. This well is located within the western to southern periphery of Mahanagdong so likely this well receives a slightly degassed fluid. Degassing can occur during horizontal flow from the upflow zone. The other peripheral wells have positive $X^{f,v}$ values such as MG29D (2%), 27D (0.45%), 23D (1.7%) in the west and MG2D (0.8%) and 16D (3.1%) in the south. The high vapour fraction (39%), calculated from a sample of the acid well MG9D, is an artefact of incomplete neutralization. After ~1.5 months of continuous discharge and with acid inhibition, the sample of MG9D gives a more realistic $X^{f,v}$ of 1.7%. Both liquid (MG9D, 26D, 31D)

and "excess enthalpy" wells (MG3D, 14D, 28D, 30D, 35D) in the vicinity of the inferred upflow zone have equilibrium vapour fractions ranging from 0.8% to 4.6 %. Towards the east, wells (MG24D, 37D, 40D) show $X^{f,v}$ values of 1-2.3%. Going south, wells drilled towards the area bounded by the collapse structure (MG18D, 32D, 34D) register vapour fractions ranging 0.9-3%, excluding the highest value of 9.3% reflected in shallow well MG32D. Both this region and the vicinity of the upflow zone are located within the higher reservoir pressure drawdown in Mahanagdong at 3-4.5 MPa (Sta. Ana et al., 2002).

An equilibrium aquifer fluid vapour fraction lowers the concentrations of H_2S and CO_2 in the liquid phase of the aquifer fluid (Figure 12). Except in the CO_2-depleted MG40D, all samples have come within ~0.3 log units from equilibrium with the czo+cal+qtz+gro assemblage at the selected compositions (reaction 12, Table 9). The aqueous CO_2 concentration of MG9D sample with unreliably large vapour fraction (9S in Figure 12) is too low to be shown in the plot. For H_2S, The average excess of aqueous concentrations from equilibrium values declined from 0.51 (if aquifer fluid is purely liquid) to 0.37 log units. Yet 9 wells still show H_2S levels higher than equilibrium by 0.4-0.7 log units. It is also possible that other reactions, aside from the buffering effect of the garnet-bearing mineral assemblage, contribute in fixing their aqueous concentrations. More importantly, the next section elaborates why the computed degrees of departure from equilibrium should be further qualified due to the large variability that the estimated vapour fractions carry.

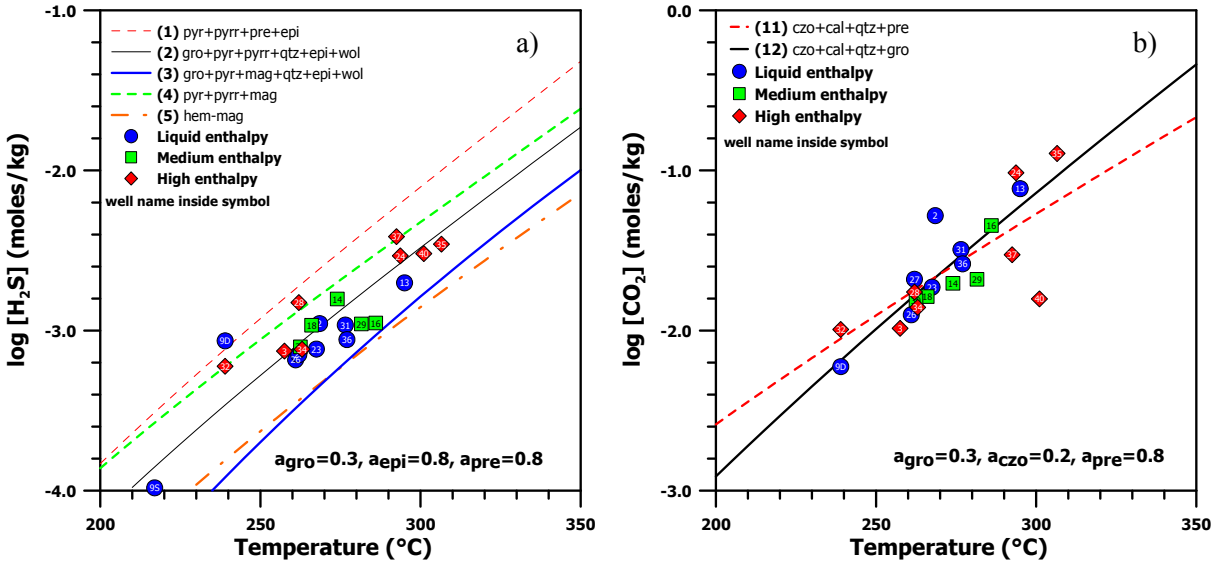

FIGURE 12: Calculated concentrations of a) H_2S and b) CO_2 in the liquid phase of the initial aquifer fluid considering initial vapour fractions, $X^{f,v}$(summarized in Table 8), as calculated from H_2 and assuming equilibrium between $H_{2,aq}$ and the gro+mag+qtz+epi+wol assemblage. Enclosed numbers beside assemblages refer to reactions in Table 9. The symbols 9U, 9S and 9D are samples from acid well MG9D which are undosed, partially dosed and fully dosed with caustic soda, respectively

4.3 Variables in estimating vapour fraction

It was mentioned earlier that the equilibrium curve for the mineral assemblage gro+mag+qtz+epi+wol (reaction 8, Table 9), which potentially could control $H_{2,aq}$, varies widely with the chosen compositions of minerals forming solid solutions (grossular and epidote). The equilibrium curve is more sensitive to the activity of grossular. Increasing the activity of grossular or decreasing the activity of epidote by 0.1 from the previously selected compositions will shift the log K value up by 0.75 and 0.35 units, respectively. No data is available on garnet composition in Mahanagdong. If the a_{gro} is increased, H_2S data points will fit better to the equilibrium curve. Consequently, many of the wells (mostly liquid enthalpy wells) will have negative $X^{f,v}$ values and $CO_{2,aq}$ data points will be too high from equilibrium (see for example Figure 11). The stoichiometry amplifies the cumulative uncertainties in the

thermodynamic data of the components involved in reaction (8) of Table 9. Karingithi (2002) estimates the cumulative error at between -2.45 to -9.75 log K units at 150-350°C.

The next major uncertainty comes from the model adopted to calculate the aquifer compositions. The aquifers of wells discharging "excess enthalpy" were modelled using phase segregation. In reality, phase segregation likely occurs over a wide range of pressures between the aquifer and wellhead conditions depending on the interrelation of several factors that include among others: the effect of pressure gradient, density and viscosity to the liquid and vapour phases; effect of capillary pressure and relative permeability (e.g. Horne et al., 2000; Pruess, 2002). At lower permeability, the effect of capillary pressure is stronger in rocks with smaller pores and fractures. Most of the "excess enthalpy" wells are drilled within the relatively lower transmissivity areas of Mahanagdong as viewed from the contour provided by Sta. Ana et al. (2002). MG32D and 34D are located in the area with highest permeability-thickness values but also with the most pressure drawdown thereby favouring extensive depressurization boiling in the reservoir. The mobility of liquid water is greatly reduced with increasing vapour phase and depending on other conditions may already become immobile when the volume fraction of liquid is reduced to about 0.6. In fracture-dominated geothermal reservoirs like Mahanagdong, studies such as by Chen and Horne (2005) show that partial mobility of liquid can extend up to lower liquid saturation values of 0.2. Therefore, the simplified approach in this study is to choose a segregation point 30°C lower than the assumed aquifer temperature which yields corresponding liquid saturation values approaching ~0.2-0.3. The lower the selected aquifer temperature, the lesser is the temperature drop needed to reach this liquid saturation. For instance, temperature decrease from 300°C to 270°C or from 280°C to 255°C will both attain a liquid saturation of about 0.25.

By the open phase segregation model, Arnórsson et al. (2010) demonstrated the combined effects of variable discharge enthalpy and selection of phase segregation point on the calculated aquifer concentrations of dissolved solids and volatile gases. For the non-volatiles, the phase segregation has little effect at discharge enthalpies below 2000 kJ/kg. At higher discharge enthalpies, for instance at 2600 kJ/kg, the aqueous concentration of dissolved solids can be lower by up to 22% when phase segregation is chosen around 235°C which corresponds to the maximum enthalpy of saturated steam. The "excess enthalpy" wells in Mahanagdong range from 1300 to 2400 kJ/kg. Since all discharge enthalpies were calculated from Tracer Flow Test measurements, the uncertainty is narrow at about ±5% of the values (e.g. Hirtz and Lovekin, 1995). So for high enthalpy wells (2000-2400 kJ/kg) MG28D, 32D, 34D, 37D and 40D, their estimated T_{qtz} are at the most ~2-20% lower when their segregation point is selected around 200-250°C. These points are illustrated in Figure 13 for two representative "excess enthalpy" wells of different measured discharge enthalpies.

On the other hand, the aquifer fluid concentrations of dissolved gases are sensitive functions of the selected phase segregation point at any discharge enthalpy. At 180-250°C, Arnórsson et al. (2010) estimated the maximum variations of the concentrations of gases dissolved in the initial aquifer fluid at different discharge enthalpies as follows: 11% at 1400 kJ/kg, 43% at 1800 kJ/kg, 54% at 2200 kJ/kg and 60% at 2600 kJ/kg. This suggests that the uncertainty in the calculated aqueous concentration of the gas increases proportionally with discharge enthalpy, especially when approaching dry steam since it is difficult to ascertain exactly at which point phase segregation occurs. Figure 14 displays the trends of calculated dissolved H_2 in the initial liquid aquifer of the same representative "excess enthalpy" wells in Figure 12 Lower aquifer fluid gas concentrations are obtained when the phase

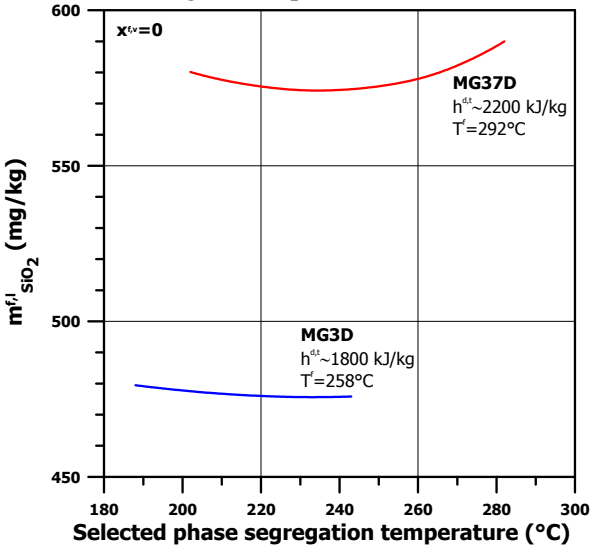

FIGURE 13: Variation in calculated aqueous concentration of a non-volatile component (SiO_2) as a function of selected phase segregation temperature

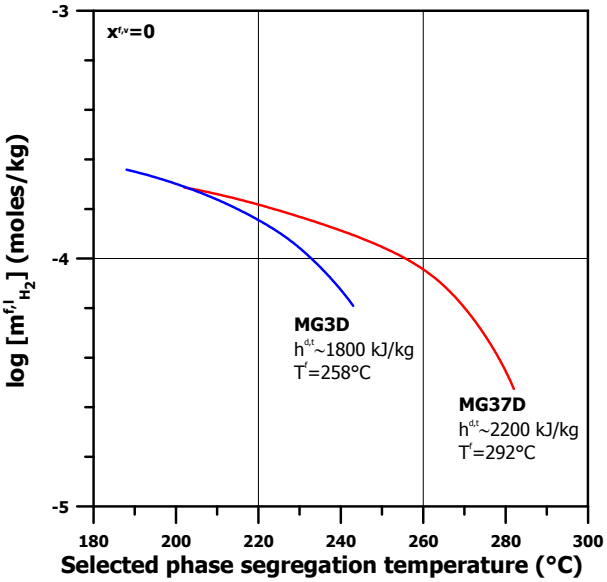

FIGURE 14: Variation in calculated aqueous concentration of a volatile gas (H_2) as a function of selected phase segregation temperature

segregation point is chosen closer to the aquifer and reaches a maximum value as segregation point approaches the operating pressure at the wellhead. Consequently, assuming the data point for aqueous H_2 plots above the log K curve of reaction (8) in Figure 10, higher $X^{f,v}$ values will be obtained if phase segregation is chosen further away from the aquifer temperature. On the representative wells shown and at the selected mineral compositions, the initial vapour fractions of MG3D and 37D can vary from 2.3 to 8.7% and -0.03 and 3.2%, respectively.

The selected aquifer temperature at which all the speciation calculations are carried out is often another contentious issue. Many chemical and isotopic geothermometers are used to estimate the aquifer temperatures beyond the zone of secondary processes like boiling, cooling and mixing on the basic assumptions that the sampled fluids are representative of the undisturbed aquifers and local equilibrium conditions are achieved. Actual downhole measurements may or may not agree with geothermometers. It is not uncommon for many wells to have multiple feed zones at significantly different temperatures. For fields of heterogenous permeability like Mahanagdong, the fluids reaching the surface are inevitably a mixture of different components as deduced from tracer tests and geochemical monitoring. By these scenarios, selecting a representative reference temperature is at best an approximation. To circumvent these complications, the aquifer concentrations are calculated by the same model over a plausible range of temperature for the same representative "excess enthalpy" wells. In Figure 15, the solid symbols represent the aquifer temperatures assuming equilibrium with quartz by the calibrations of Gunnarsson and Arnórsson (2000). If the actual aquifer temperatures deviate within a range, the calculated aquifer fluid H_2 concentration varies as shown by the dashed lines with phase segregation always selected at 30°C below the reference temperature.

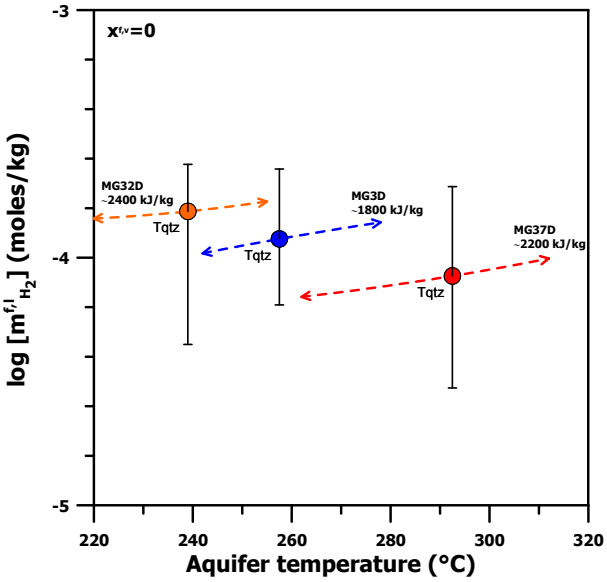

FIGURE 15: Dependence of calculated aqueous concentration of a volatile gas (H_2) in the aquifer fluid on aquifer temperature value. The vertical error bars represent the variation on the calculated $H_{2,aq}$ in the aquifer fluid depending on the selected phase segregation point

Figure 15 indicates that the calculated aqueous gas concentrations differ only by a maximum of about 0.2 log units regardless of the discharge enthalpy. MG32D was specifically included in Figure 15 not only because it has the highest discharge enthalpy (2399 kJ/kg) but also for having the lowest T_{qtz} almost similar to the temperature of saturated steam with maximum enthalpy. The assumed aquifer temperature affects both calculated aquifer fluid component concentrations and activity products and equilibrium constants for all reactions. It also affects the value calculated for $X^{f,v}$. Departure from equilibrium increases with decreasing reference temperature due to the positive slope of the log K-temperature curve of reaction (8) plotted for example in Figure 10. But as with the other wells shown in Figure 15, the calculated aqueous H_2 level in the aquifer of MG32D (and

its $X^{f,v}$) can vary much more from the selection of phase segregation point (the vertical error bar in each symbol) than from the uncertainties in the selected aquifer temperature.

4.4 Gas-gas equilibria

It is also of interest to investigate other competing reactions involving CO_2, H_2S and H_2 to gain insight into constraining derived initial vapour fraction values of the aquifers. The relationships between the gases CO_2, CH_4 and H_2 have been studied in numerous geothermal systems (e.g. Giggenbach, 1980; D'Amore and Truesdell, 1995; Stefánsson and Arnórsson, 2002) including Mahanagdong (Salonga and Auman, 1997; Siega et al., 1999) using the Fischer-Tropsch reaction:

$$CO_{2,aq}+4H_{2,aq}\leftrightarrow CH_{4,aq}+2H_2O_l \qquad (20)$$

The activity product for reaction (20) of all Mahanagdong samples can be calculated and compared with its equilibrium values retrieved from Arnórsson et al. (2010). When assuming liquid enthalpy for the initial aquifer fluid ($X^{f,v}$=0), the activity product for the Fischer-Tropsch reaction display much higher (Figure 16A) and the data points for liquid enthalpy wells (except for 3 samples) are on the average 3.3 log units above equilibrium. The "excess enthalpy" wells show closer approach to equilibrium at 250-290°C but are subject to the uncertainties in the way their aquifers were modelled. In contrast, when the presence of equilibrium vapour is considered, the Q values are systematically above equilibrium by ~4-5 log units (Figure 16B), at comparable levels with the degassed peripheral wells. CH_4 is also very sensitive to both temperature and redox conditions but responds somewhat slower than H_2 (Giggenbach, 1987).

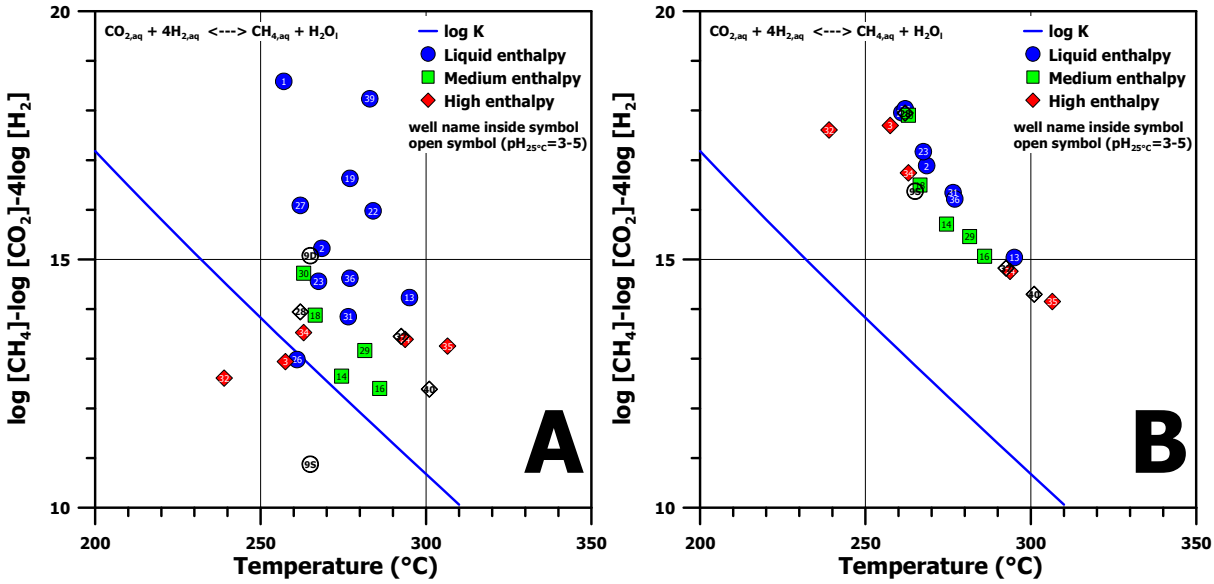

FIGURE 16: Calculated activity products for the Fischer-Tropsch reaction (A) assuming no equilibrium vapour to be present and (B) considering equilibrium vapour fractions of some wells estimated from reaction (8) of Table 9 at the selected mineral compositions. The curves represent equilibrium conditions expressed as aqueous gas concentrations. The symbols 9U, 9S and 9D are samples from acid well MG9D which are undosed, partially dosed and fully dosed with caustic soda, respectively

NH_3 responds like CH_4 to temperature and redox variations but its high solubility in water limits its application as geothermometer or redox indicator. A possible reaction involving NH_3, N_2 and H_2 is the reverse Haber process:

$$2NH_{3(g)}\leftrightarrow N_{2(g)}+3H_{2(g)} \qquad (21)$$

The activity products for reaction (21) using partial pressure data are shown in Figure 17. The equilibrium curves were obtained from Giggenbach (1980). The observed patterns are almost same as those for the Fischer-Tropsch reaction. The Q values show large scatter when total gas concentration

in the aquifer fluid are selected and they are systematically below K, by 0-6 log units. When equilibrium vapour fraction is taken into account, the scatter is much reduced and Q values are some 6 log units more than K. The observations are more or less consistent with the conclusion of Giggenbach (1980) that reactions (20) and (21) seem to come to equilibrium under similar rate and conditions.

It is possible that the disequilibrium of Mahanagdong aquifer fluids with respect to reactions (20) and (21) is partly due to an excess supply of CH_4 or NH_3, respectively. But probably the common species, H_2, highly influences the degree of departure from equilibrium in both reactions. H_2 concentrations in the vapour discharges of Mahanagdong wells range from 0.016 to 3.8 mmoles/kg which are comparable to CH_4 levels and on the average, ~3 times lower than NH_3 and about 1 and 2.5 orders of magnitude lower than H_2S/N_2 and CO_2, respectively. Wells with zero to slightly negative $X^{f,v}$ values have much higher CO_2 to H_2 ratios. H_2 concentration may be swept into a CO_2-rich vapour phase at a much faster rate preventing its level to approach equilibrium with the mineral assemblages. Since H_2 has lower solubility in water, this sweeping effect is more likely to affect it than the more soluble H_2S and NH_3. Other processes by which H_2 in the aquifer fluids can decrease include mixing with a degassed fluid (e.g., injected brine) and when the aquifer fluid loses some vapour during its flow in sub-horizontal aquifers. Therefore, being both reactive and occurring in lower levels, small changes in the concentration of H_2, compared to similar variations in the more abundant gases, dominates the retrieved values.

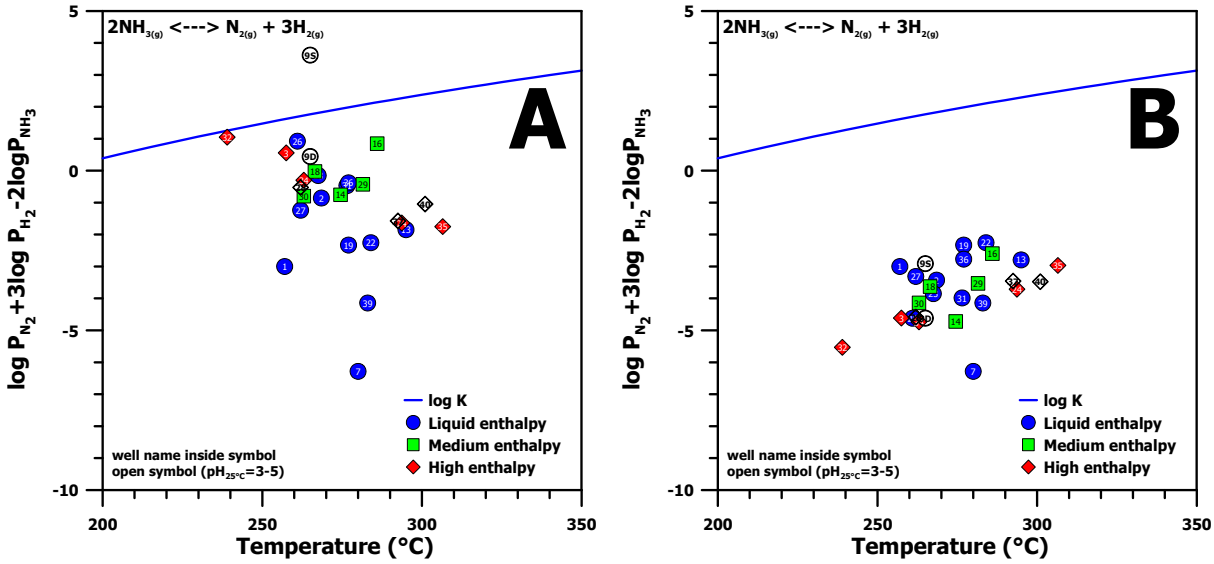

FIGURE 17: Calculated activity products for the Haber reaction (A) assuming no equilibrium vapour to be present and (B) considering equilibrium vapour fractions of some wells estimated from reaction (8) of Table 9 at the selected mineral compositions. The curves represent equilibrium conditions expressed as partial pressure of gases. The symbols 9U, 9S and 9D are samples from acid well MG9D which are undosed, partially dosed and fully dosed with caustic soda, respectively

Figures 16A and 17A show some of the wells closely approach equilibrium with respect to both reactions (20) and (21) when the respective activity products are based on total aquifer fluid gas compositions. When equilibrium vapour fractions in the aquifer are taken into account, the plots suggest that the aqueous H_2 levels considered for Mahanagdong wells are too low to achieve simultaneous equilibrium with the H_2O-CO_2-CH_4-NH_3-N_2-H_2 system. It can be alternatively viewed that higher equilibrium aqueous H_2 levels are required to achieve consistent close approach to equilibrium between the gases via the Fischer-Tropsch and Haber reactions and with the assemblages gro+mag+qtz+epi+wol, czo+cal+qtz+gro (reactions 8 and 12 in Table 9, respectively). For instance, the curve defined in Figure 11 assuming grossular and epidote activities of 0.4 and 0.8, respectively, roughly achieves this purpose. By selecting such mineral compositions, only half of the wells in Mahanagdong would plot above the curve giving positive equilibrium vapour fractions but lower than previously calculated and summarized in Table 8. The other half of the wells would plot below the curve, which is the case for the majority of the liquid enthalpy wells.

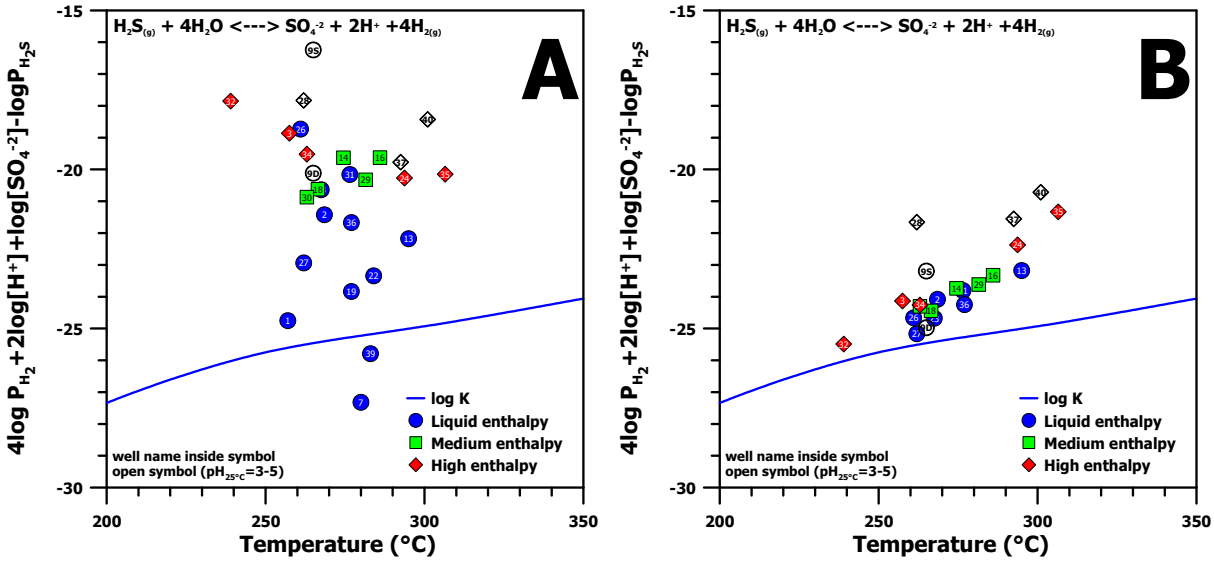

FIGURE 18: Calculated activity products for the redox reaction involving H_2S, SO_4 and H_2 (A) assuming no equilibrium vapour to be present and (B) considering equilibrium vapour fractions of some wells estimated from reaction (8) of Table 3.9 at the selected mineral compositions. The curves represent equilibrium conditions expressed as aqueous gas concentrations. The symbols 9U, 9S and 9D are samples from acid well MG9D which are undosed, partially dosed and fully dosed with caustic soda, respectively

The situation is reversed when considering the reaction below involving H_2S, SO_4 and H_2:

$$H_2S_{(g)}+4H_2O \leftrightarrow SO_4^{2-}+2H^++4H_{2(g)} \quad (22)$$

Equilibrium with respect to reaction (22) may not necessarily be achieved in Mahanagdong fluids due to very slow kinetics below 300°C (Ohmoto and Lasaga, 1982) that is typical of most redox reactions (e.g., Stefánsson and Arnórsson, 2002). Nevertheless, Figure 18A shows that Mahanagdong liquid enthalpy wells with low H_2 concentrations approach closer to equilibrium as similarly observed by Stefánsson and Arnórsson (2002) with saline geothermal fluids in Iceland. The rest of the samples are generally above the log K curve but disequilibrium is reduced if the H_2 levels in the aquifer are fixed by the garnet-bearing assemblage (Figure 18B). Despite such lower H_2 concentrations, large departure still persists in the high enthalpy wells with elevated sulphate levels, of which three are discharging lower pH (MG28D, 37D and 40D). The study of stable sulphur isotope ratios by Bayon and Ferrer (2005) suggests that dissolved sulphate in Mahanagdong wells is largely derived from the disproportionation of SO_2 gas at sub-critical temperatures according to the reaction:

$$4SO_{2,aq}+4H_2O_{(g)} \leftrightarrow 3HSO_4^-+3H^++H_2S_{aq} \quad (23)$$

The H_2S produced from reaction (23) cannot be differentiated from direct magmatic input due to almost similar ^{34}S isotope ratios (~0‰) but the stoichiometry shows that an equivalent 3 moles of SO_4 can be formed to increase the sulphate flux to the system. Some of the dissolved sulphate is partly fixed in the ubiquitous mineral anhydrite as also suggested by its close approach to equilibrium (Figure 19) in both neutral and acid wells.

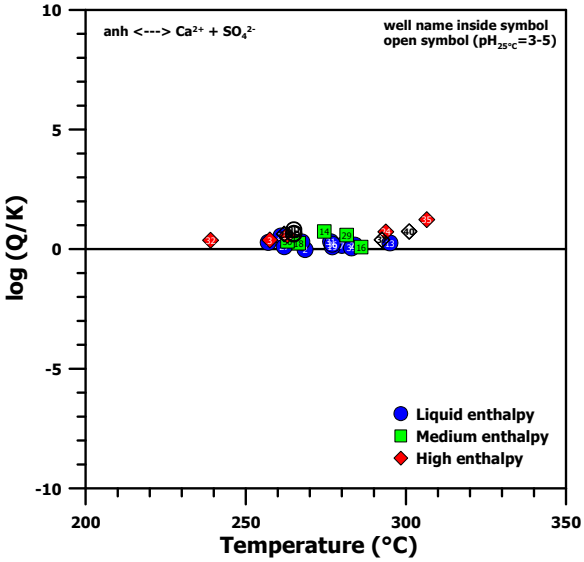

FIGURE 19: Saturation of Mahanagdong fluids with respect to anhydrite. The symbols 9U, 9S and 9D are samples from acid well MG9D which are undosed, partially dosed and fully dosed with caustic soda, respectively

4.5 Mineral-solution equilibria

It is also essential to assess the equilibrium between the hydrothermal solutions and the individual minerals comprising the mineral assemblages that were shown to potentially buffer the reactive gas concentrations of H_2S, H_2 and CO_2. Ideally, a demonstration of close approach to equilibrium must be consistent in both cases. Table 9 lists the dissolution reactions of the hydrothermal minerals considered and their corresponding log K-temperature equations. For each reaction, departure from equilibrium is expressed as saturation index (SI) which relates the reaction quotient/activity product, Q, and equilibrium constant, K, by equation (24):

$$SI = \log (Q/K) \tag{24}$$

The saturation indices are summarized in Figures 20 and 21 with solid symbols assuming liquid aquifers ($X^{f,v}=0$) for all Mahanagdong wells. For clarity, Figures 20 and 21 only show selected wells whose SI values significantly differ when the estimated equilibrium vapour fractions are considered in the aquifers (well numbers without symbols). Endmember activities indicated in Figures 10 and 12 are used.

4.5.1 Calcite and wollastonite

The majority of modelled liquid aquifers have calcite saturation values clustering around equilibrium, yet are systematic undersaturation is observed, by an average of 0.53 SI units (Figure 20A). Undersaturation suggests depleted Ca^{2+} or CO_2 and/or too low pH for the modelled aquifers. Prolonged production from Mahanagdong field inevitably leads to depressurization in the aquifer causing the fluid to boil and potentially degas the system. From Figures 10 and 12, it is unlikely that the system is degassed with respect to CO_2 assuming the mineral assemblage czo+cal+qtz+pre or czo+cal+qtz+gro controls its aquifer concentrations. Referring to the same assemblages, the activity ratio $[Ca^{2+}]/[H^+]^2$ can be fixed from the reactions:

$$3/2\ pre + 2H^+ \leftrightarrow czo + 3/2\ qtz + 2H_2O_l + Ca^{2+} \tag{25}$$

$$3/5\ gro + 2H^+ \leftrightarrow 2/5\ czo + 3/5\ qtz + 4/5\ H_2O_l + Ca^{2+} \tag{26}$$

The corresponding log K equations from Karingithi et al. (2010) modified with the selected activities of the endmembers are shown in Figure 22. The plots suggest that $[Ca^{2+}]/[H^+]^2$ ratios are generally lower than equilibrium conditions consistently leading to negative SI values for calcite. At high temperatures comparable to Mahanagdong aquifers, equilibrium with calcite and solution is rapidly attained (Zhang and Dawe, 1998). This means that beyond the zones of depressurization of the wells, calcite can readily precipitate from initially saturated solutions during extensive boiling and effective degassing. Aqueous Ca is much less abundant than total carbonate carbon (T-CO_2). Therefore the precipitation of calcite in the aquifer will deplete Ca^{2+} more relative to the T-CO_2 content and tends to yield lower SI values. Alternatively, the effective transfer of CO_2 from liquid to vapour phases during boiling will cause the solution pH to increase. If the solution pH re-equilibrates rapidly such as when the OH^- species are taken up by layer silicates, the activity of H^+ will instead increase and lower the activity ratio with respect to Ca^{2+}. All the above points signify that saturation with calcite is closely approached with most of the hydrothermal fluids in Mahanagdong. Low $[Ca^{2+}]/[H^+]^2$ ratios similarly explain the observed undersaturation of the modelled liquid aquifer fluid with respect to wollastonite (Figure 20B). However, it is unlikely that the reservoir processes explained above can sufficiently account for the higher undersaturation by an average of 1.37 SI units (excluding samples from MG9D, 28D, 37D and 40D). This indicates that wollastonite is unstable in the reservoir consistent with the rarity that such mineral is encountered in Mahanagdong.

The calculated SI values for calcite and wollastonite are sensitive to both analytical and thermodynamic parameters but not to the assumed aquifer temperature within about ±15°C (Karingithi

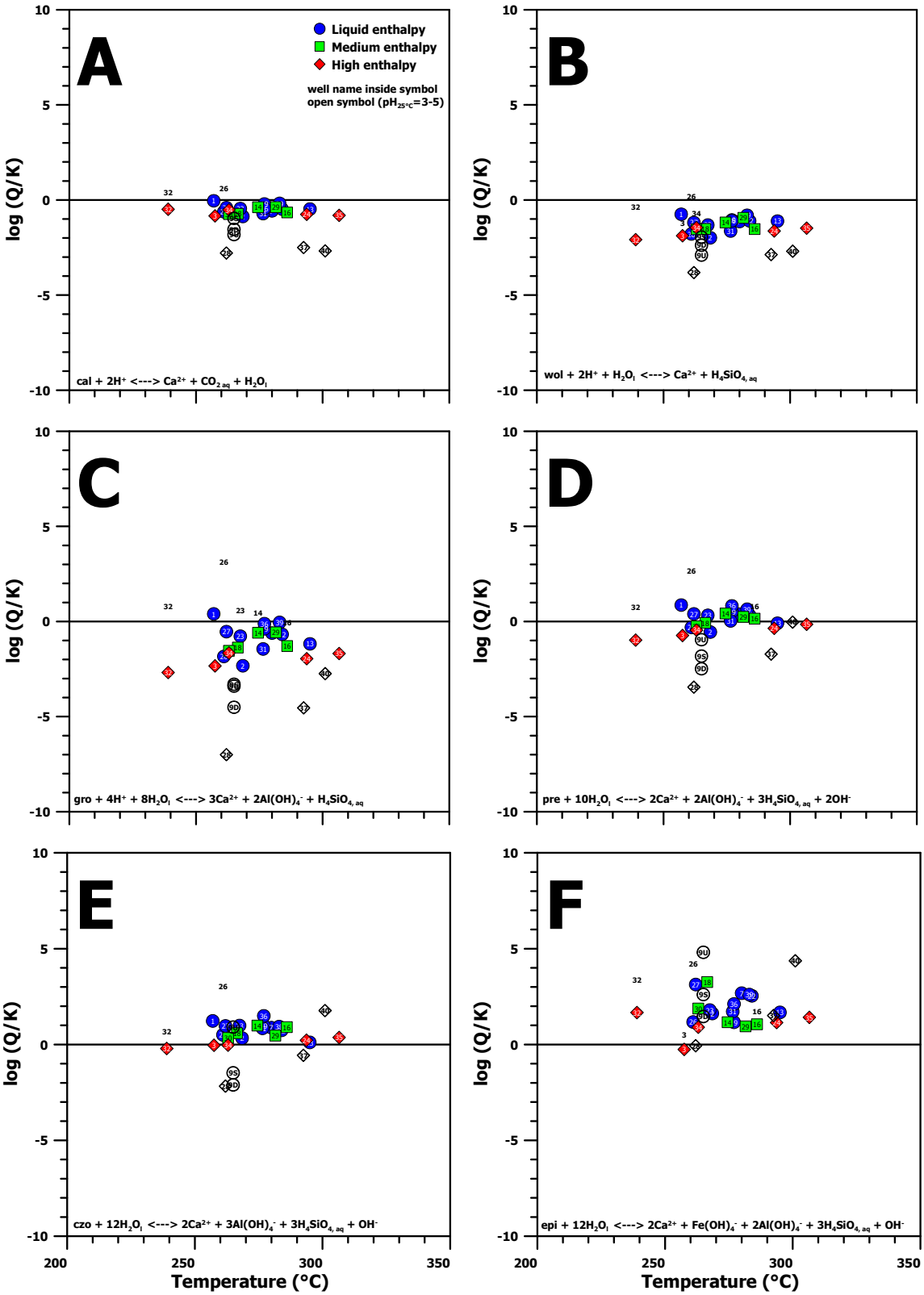

FIGURE 20: Saturation indices of Ca-bearing alteration minerals. Solids symbols represent total aquifer fluid assuming liquid enthalpy. Equilibrium vapour fractions for selected wells are considered in well numbers without symbols. The symbols 9U, 9S and 9D are samples from acid well MG9D which are undosed, partially dosed and fully dosed with caustic soda, respectively. Endmember activities are the same as in Figures 10and 12

et al, 2010). The most important analyses are the measured pH and the total carbonate carbon (T-CO_2). For whatever reasons, including the difference in pH meters, lower pH measurements from the

LRMD EDC laboratory by an average of 0.4 units will shift further the calculated SI to more negative values. When using WATCH for speciation calculations, the measured pH is very important. WATCH initially calculates and sums up the concentrations of all conjugate anions of all acids and OH-bearing species at the temperature at which the pH was measured. This sum (A^-) is takento be constant at all temperatures. The pH at any other temperature is retrieved by iteration until the derived pH satisfies both the value of A^- and all the dissociation constants for the acids and the OH-bearing species. Relatively acidic samples from MG9D, 28D, 37D and 40D as measured on-site produce relatively low aquifer liquid pH. The aquifer fluids of these wells are calcite undersaturated by 1.3-2.8 SI units. Routine titration methods also tend to obtain too low T-CO_2 values for acidic samples since the volatile carbonate species (as H_2CO_3) dominates in such waters. On the other hand, considering the estimated equilibrium vapour fraction in the aquifer feeding the wells and assuming perfect degassing can significantly shift the SI to higher values. In Figures 20 and 21, well numbers without symbols represent the largest shifts in the SI values among all samples when the estimated $X^{f,v}$ summarized in Table 8 are considered.

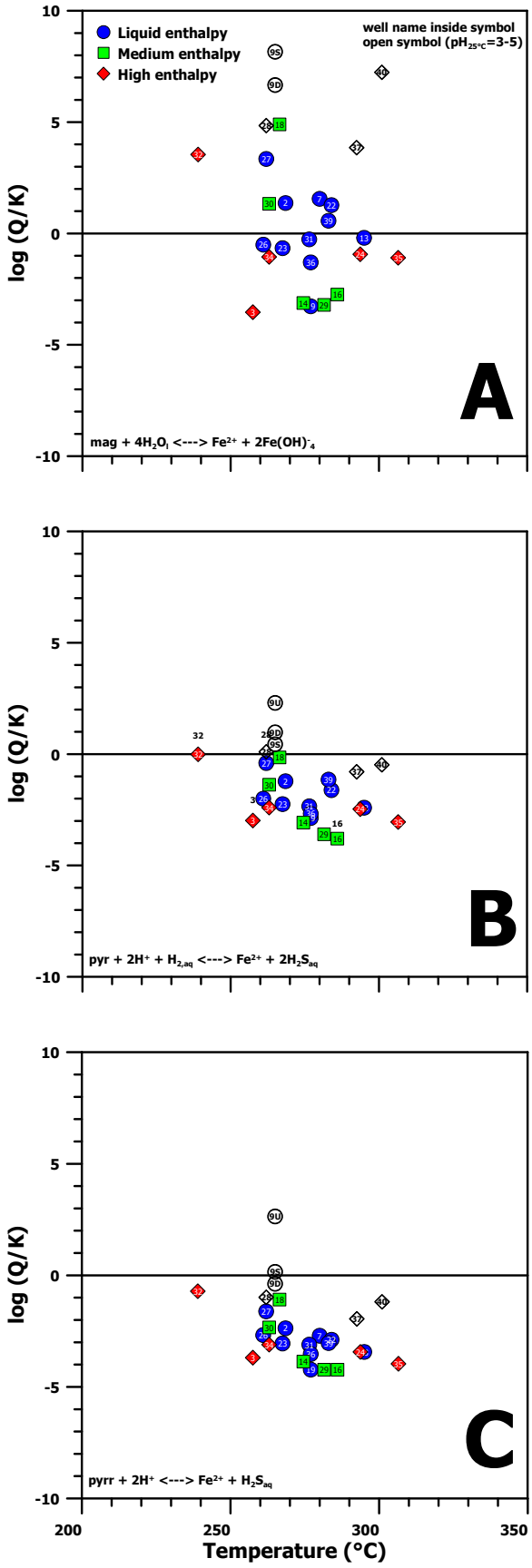

The most important thermodynamic parameter lies in the ion pair $CaHCO_3^+$ species which hosts most of the dissolved calcium. The $CaHCO_3^+$ dissociation constant being used by the speciation program WATCH is based on a low temperature (0-80°C) experimental data and extrapolated to higher temperatures (Arnórsson et al., 1982). Thus there is higher uncertainty in the stability of $CaHCO_3^+$ species at higher temperatures. Consequently, this affects also the calculated activity of the free Ca^{2+} ion. The average undersaturation of 0.53 SI units in the Mahanagdong fluids, exempting the acidic wells, may then partly account the overall uncertainty in obtaining SI value for calcite from sampling, analysis to speciation in addition to the effect of reservoir processes affecting the $[Ca^{2+}]$ /$[H^+]^2$ ratios.

FIGURE 21: Saturation indices of Fe-oxide and Fe-sulphide alteration minerals. Solids symbols represent total aquifer fluid assuming liquid enthalpy. Equilibrium vapour fractions for selected wells are considered in well numbers without symbols. The symbols 9U, 9S and 9D are samples from acid well MG9D which are undosed, partially dosed and fully dosed with caustic soda, respectively. Endmember activities are the same as in Figures 10 and 12

4.5.2 Grossular, prehnite and epidote-clinozoisite

The factors that affect the activity of the free Ca^{2+} ion previously discussed with calcite and wollastonite will also affect SI values of the these aluminium-silicate minerals. But it is more important to note that the solubility reactions shown (Figures 20C, D, E and F) are all dependent on pH and are preferably written in terms of the most dominant Fe-hydroxy, $Fe(OH)_4^-$, and Al-hydroxy, $Al(OH)_4^-$, species. In so doing, the uncertainties on their thermodynamic data are minimized. Confidence is high on the measurements of water samples on-site with calibrated and quick-response pH meters but considerable errors become involved in deriving the pH at the inferred aquifer conditions. For these reasons, it is necessary to assess the plots considering these realities.

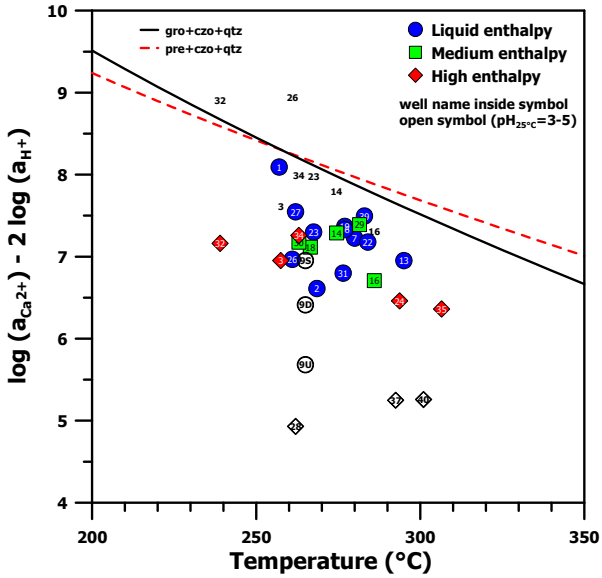

FIGURE 22: $[Ca^{2+}]/[H^+]^2$ activity ratios versus aquifer temperature. Solids symbols represent total aquifer fluid assuming liquid enthalpy. Equilibrium vapour fractions for selected wells are considered in well numbers without symbols. The symbols 9U, 9S and 9D are samples from acid well MG9D which are undosed, partially dosed and fully dosed with caustic soda, respectively. Endmember activities are the same as in Figures 10 and 12

Excluding the wells with relatively acidic discharges (MG9D, 28D, 37D and 40D), data points plot around the equilibrium line. Yet, they are systematically oversaturated by 0.05 and 0.62 SI units for prehnite (20D) and clinozoisite (Figure 20E), respectively. In all the reactions in Figure 20, the aqueous silica activity contributes an insignificant error. Large error comes from the thermodynamic data on Al-species, particularly on the Al-Si dimer, resulting in lower values for the activity of the $Al(OH)_4^-$, species. An even higher general oversaturation in the Fe-bearing mineral epidote by an average of 1.71 SI units for all samples (Figure 20F) is indicative of the overestimated values of the $Fe(OH)_4^-$, species. The hydrolysis constants for both Fe^{2+} and Fe^{3+} iron species used in this study are deemed the most reliable among published data. Yet Arnórsson et al. (2002) demonstrated that the thermodynamic data are in considerable error leading to underestimation of Fe^{2+} activity and corresponding overestimation of $Fe(OH)_4^-$ activity.

The largest scatter but overall undersaturation by 1.15 SI units (excluding acidic wells) is exhibited in the dissolution of grossular (Figure 20C). If the aquifer fluid is initially in equilibrium with grossular, the undersaturating effect of lower pH values is not only magnified by its stoichiometric coefficient of 4 but also affects the dissociation of the $CaHCO_3^+$ that largely determines the free Ca^{2+} species activity. A similar influence of the solution pH to the saturation index is likewise demonstrated when $X^{f,v}$ values in the aquifer are considered (well numbers without symbols). When gases effectively partition to the vapour phase, the solution pH decreases, shifting SI's to higher values. The most noticeable changes are represented by some wells in Figures 20 and 21. These shifts are expectedly observable in wells with higher estimated $X^{f,v}$ ranging 1.7-9.3% (MG32D, 26D, 16D). The variations in the SI's of the same wells are relatively higher in the grossular. Considering all these factors, it is reasonable to conclude that close approach to equilibrium with the considered aluminium-silicates is achieved by most Mahanagdong fluids. If the lower pH values in the modelled aquifers feeding the wells are real, then the same minerals will be unstable in acidic aquifer conditions.

4.5.3 Magnetite, pyrite and pyrrhotite

Figures 16 and 17 indicate that equilibrium for specific redox reactions is not closely approached. In this study, the reduction potential of the H_2S/SO_4 couple (Eh H_2S) calculated by WATCH was used to retrieve speciation distribution between Fe(II) and Fe(III) as H_2S and SO_4 are detected in larger

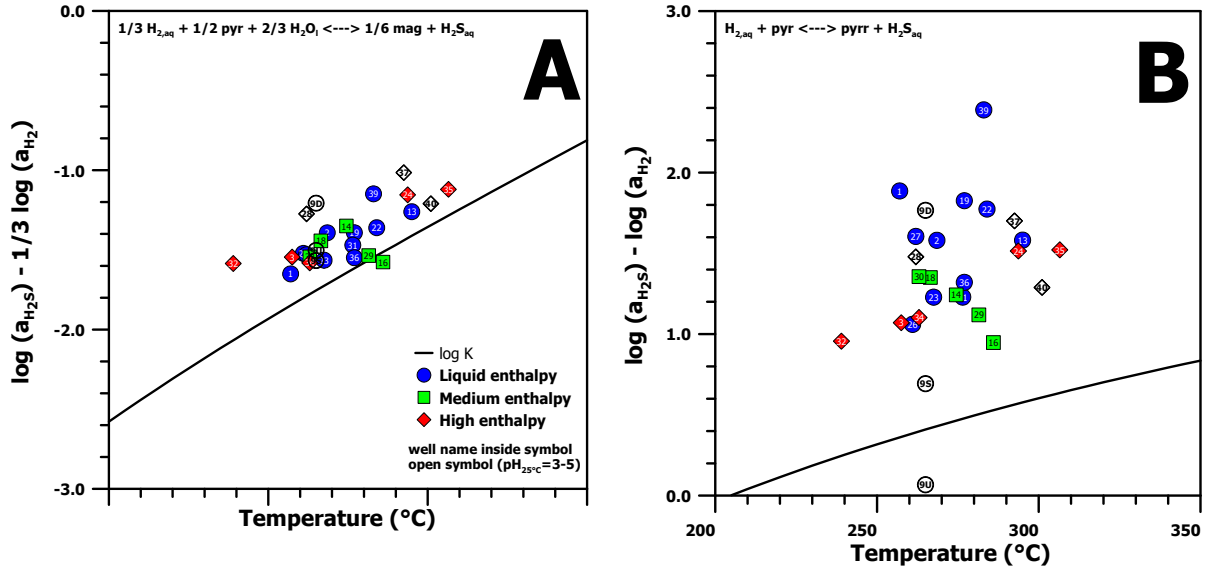

FIGURE 23: Activity ratios of dissolved H_2S and H_2 in the total aquifer fluid assuming liquid enthalpy depicted with the equilibrium curves of (A) pyrite-magnetite and (B) pyrite-pyrrhotite mineral buffer reactions taken from Karingithi et al. (2010). The symbols 9U, 9S and 9D are samples from acid well MG9D which are undosed, partially dosed and fully dosed with caustic soda, respectively

quantities compared to similarly redox sensitive components H_2, NH_3 and CH_4. On average, Eh H_2S values are higher by 0.06 V, 0.08 V and 0.1 V compared to redox pairs H^+/H_2 (Eh H_2), CO_2/CH_4 (Eh CH_4), and N_2/NH_3 (Eh NH_3), respectively, and will therefore give the lowest concentration value for Fe(II), including the Fe^{2+} species, or by about 0.4-0.8 log units.

The limitations in the thermodynamic data on iron hydrolysis are evident in Figure 21. The underestimated activity values for Fe^{2+} species result to overall undersaturation of pyrite and pyrrhotite, by an average of 1.87 and 2.81 SI units, respectively (Figures 21B and C), excluding the samples from MG9D (labelled 9D and 9S) which probably has additional Fe dissolved from casing corrosion. For magnetite (Figure 21A), the uncertainties in both the activities of Fe^{2+} and $Fe(OH)_4^-$ have almost evenly split the data points into two groups with average difference of +2.66 (excluding acidic MG9D and 40D) and -1.68 from the saturation line. When the mineral pair of magnetite and pyrite is considered, equilibrium is closely approached (Figure 23A) by an average departure of only 0.26 log units (excluding acidic MG9D), as neither Fe species are included in the calculations. A different picture is observed with the pyrite and pyrrhotite mineral pair (Figure 23B) reiterating that pyrrhotite is unlikely involved in buffering aqueous H_2S and H_2 in the aquifer.

4.6 Minor and trace elements systematic

The concentrations of minor and trace elements in water samples from Mahanagdong, as presented in Tables 2-3, are generally higher compared to most natural waters but are typical of hydrothermal solutions (e.g., Kristmannsdóttir et al., 2004). Based on published data, the minor and trace elemental levels of Mahanagdong are more enriched compared to primary geothermal waters in the basaltic rocks of Krafla, Iceland (Arnórsson et al., 2007), comparable with fluids associated with andesitic setting in Miravalles, Costa Rica and much lower compared to the hypersaline and mineral-rich geothermal brines in Salton Sea, California and Cheleken Peninsula in Caspian Sea or the oilfield brines of the Mississippi, Salt Dome Basin (Gallup, 1998). Studies of these minor and trace elements are valuable for understanding of their behaviour in magmatic and hydrothermal systems (e.g., Taran et al., 2008), recovery of metals and minerals with economic value (e.g., Gallup, 1998), in dealing with potential scaling problems (e.g., Reyes et al., 2002) and for assessing the environmental effects of toxic constituents in hydrothermal solutions (e.g. Were, 2007).

Great care was taken in handling the samples, yet some of the detected minor and trace elements can originate not only from the deep reservoirs. Additional inputs may come from the impurities in the acid used to treat the samples, from airborne particles during sampling and analyses and leaching of components from the well casing, Webre separator and stainless cooling coil. The elevated levels of Fe, Mn, Cr, Ni and Cu in relatively acidic discharges are most likely affected by corrosion processes and can provide rates approximated from the composition of pipe casing typically used in geothermal wells (Table 11). In-depth understanding of the properties of many trace elements requires more than knowledge of their total dissolved concentrations as it may be more fruitful to determine which species in the solution contain them. This is beyond the scope of this work but is an important matter to consider in the future.

4.6.1 Mobility of the elements

In this work, mobility describes the proportion of the components between the rock and the interacting solution. Mobile elements have higher concentrations in the water relative to the rock and therefore tend to stay more in the solution rather than become fixed by incorporation into secondary minerals. With this property, highly mobile elements act like tracers providing information on the origin of both itself and the fluid (e.g., Arnórsson, 2000). Whole rock analyses and total sulphur analysis of fresh andesites sampled at the surface in Tongonan by Scott (2000) and in Mahanagdong by Salonga et al. (2000), respectively, can be used together with the analyses in Tables 2-3 to calculate an enrichment factor (*EF*) of each element defined as:

$$EF=(m_i^{fluid}/m_{ref}{}^{fluid}) \,/\, (m_i^{rock}/m_{ref}{}^{rock}) \qquad (27)$$

In equation (27), m is a concentration of a component (i relative to any reference component, *ref*). *EF* values do not give the absolute mobility of the elements but estimate their behaviours relative to another component. The reference component selected is silica (SiO_2), which takes an enrichment factor of 1. In Figure 24, three distinct groups are presented. Group I (Cl, As, Na, S, Rb and K) with $EF>1$. The elements of Group I are the most mobile. However, the apparent mobilities of Cl, As and S may be affected by their supply (magmatic, sedimentary, organic etc.). Group II (Ni, Sr, Ca, V and Ba) with $EF\approx1$ has almost congruent dissolution of these components relative to silica. Group III (Mn, Pb, Cu, Zn, Ti, Mg, Al and Fe) with $EF<1$ suggests that these elements are either not easily dissolved by the fluids from the fresh rocks or they are controlled by equilibrium with secondary minerals. Zn and Mg, which have relatively high *EF*'s in acidic discharges, are not major components of the well casing (Table 11) or carbon steel materials. They are probably mobilized from reservoir rocks, enhanced by acidic aquifer fluids. Among Group III elements, Ti and Al still show low mobility even at higher solution acidity.

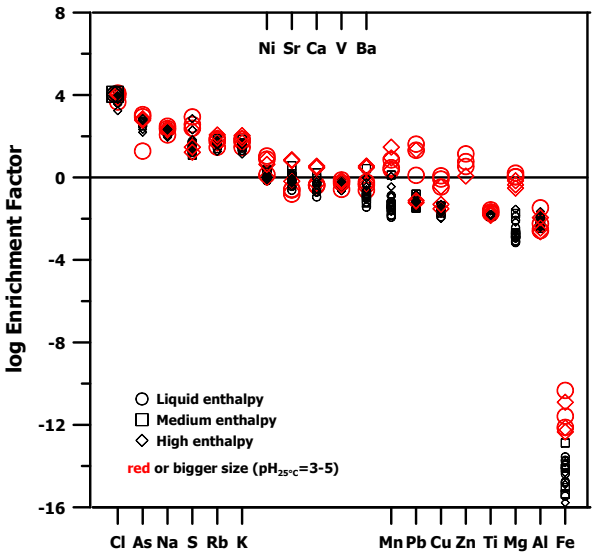

FIGURE 24: Enrichment factors of the different elements normalized to SiO_2 based on the analyses of fresh andesites sampled by Scott (2000) in Tongonan and Salonga et al. (2000) in Mahanagdong

In general, at pH 5-8, only a few metals exist in natural waters as free ions (Were, 2007). Monovalent ions and a few divalent ions of the alkali and alkaline earth metals, respectively, may constitute an appreciable proportion of the total concentration of these metals. Most of the other transition and heavy metals tend to hydrolyze or form ion-pairs and complexes bound to different ligands. The common ligands that may form ion-pairs or complexes with the trace elements are halides (eg., Cl^-, F^-, Br^-), sulphur compounds (e.g., sulphate and sulphide) and carbonates. Table 12 summarizes the linear

TABLE 11: Chemical composition (in addition to iron) of casings commonly used in geothermal wells[a]

Composition (% wt)	Casing Type	
	K55	L80
C	0.36	0.23-0.27
Cr	0.07	≤0.02
Ni	0.01	≤0.02
Mo	0.13	≤0.01
Mn	1.35	0.93-1.34
Si	0.27	0.22-0.27
P	0.014	0.01-0.015
S	0.004	0.003
Ti	0.001	0.001-0.01
Nb	<0.005	<0.005
Cu	0.01	<0.02
V	0.001	≤0.048
Al	0.028	0.044-0.048

[a] From Mack et al. (1999)

correlation coefficients (R^2) of the different minor and trace elements with other analyzed components and the assumed reservoir temperature. For MG9D, only the sample obtained after stable discharge was included to determine the correlation.

Cl and Br only form soluble minerals and their supply is generally insufficient to saturate geothermal fluids minerals thereby making them conservative in such systems (e.g., Arnórsson, 2000). The strong positive correlations of Cl and Br with Li and Rb confirm that these elements are very mobile in the high-temperature field of Mahanagdong. In varying degrees, the trace elements have different partitioning coefficients between crystals and melt. The primary minerals widely encountered in Mahanagdong and in most other Philippine geothermal fields can host the enclosed trace elements (e.g., Best, 2003): hornblende (Ni, Cr, Co, Mn), biotite (Ni, Cr, Co, Rb, Ba), K-feldspar (Ba, Sr), plagioclase (Sr), magnetite and ilmenite (V) and sulphides (Cu, Ni). Many of the trace elements in Mahanagdong generally follow the trend that in aqueous solution, elements with ionic potential (charge/ionic radius in Å) of 3-12 are less soluble and mobile than those outside the range partly explaining high mobility of (ionic potential values retrieved from Best, 2003): Li^{+} (1.1), Rb^{+} (1.66), Sr^{2+} (1.52), Ba^{2+} (1.34) and Cs^{+} (0.55) and intermediate mobility of Ga^{+3} (3.95), As^{+3} (4.17), Be^{2+} (4.44), Mo^{3+} (3.61) and Cr^{3+} (3.97). Conversely, the ability of some trace elements to substitute the major elements with almost similar ionic potential in the mineral crystals may reduce trace element mobility. For instance, Fe or Mg can be substituted by Ni, Cr and Co; Ca by Sr; Ti by V; Al by Ga; Si by Ge; and K by Rb, Ba and Sr. The poor correlation of most elements with reservoir fluid temperature suggests that their mobility is not much affected by temperature-

TABLE: 12 Linear correlation of determination (R^2) of minor and trace elements with other parameters measured in the water samples[a]

	Cl	Br	F	SO_4	H_2S	CO_2	NH_3	T_{qtz} [b]	$pH_{25°C}$
Li	**0.914**	**0.918**	0.053	-0.132	-0.189	-0.130	0.205	**0.202**	-0.281
Rb	**0.902**	**0.931**	0.058	-0.113	-0.118	-0.079	0.241	**0.205**	-0.313
V	0.762	0.770	0.119	-0.005	-0.022	-0.008	0.215	0.104	-0.284
Sr	0.698	0.780	0.070	-0.039	-0.036	-0.030	0.431	0.160	-0.325
Ba	0.655	0.719	0.055	-0.014	-0.020	-0.021	0.418	0.100	-0.299
Cs	0.601	0.521	0.002	-0.190	-0.248	-0.111	0.006	0.055	-0.104
Ga	0.583	0.644	0.052	-0.008	-0.009	-0.007	0.277	0.063	-0.210
As	0.569	0.494	0.013	**-0.223**	**-0.414**	**-0.341**	0.082	0.099	-0.209
Be	0.565	0.500	0.128	0.000	-0.111	-0.056	0.224	0.010	-0.351
Mo	0.534	0.503	0.002	**-0.361**	**-0.327**	-0.188	0.026	0.035	-0.065
Ni	0.479	0.494	0.021	0.001	-0.049	-0.103	0.428	0.023	**-0.372**
Cr	0.428	0.402	0.008	-0.011	-0.063	-0.138	0.254	0.029	-0.293
Mn	0.393	0.435	0.069	-0.022	-0.021	-0.042	**0.618**	0.139	**-0.373**
Co	0.319	0.338	0.023	0.000	-0.020	-0.043	0.503	0.038	-0.335
Cu	0.265	0.257	0.009	0.002	-0.038	-0.094	0.379	0.007	-0.302
Ti	0.195	0.220	**0.590**	0.194	0.045	0.010	0.477	**0.230**	-0.363
Pb	0.190	0.183	0.008	0.006	-0.026	-0.085	0.346	0.004	-0.265
Sb	0.000	-0.002	-0.056	-0.032	-0.069	-0.138	-0.017	-0.012	0.003
U	-0.033	-0.038	-0.017	0.012	0.005	0.010	-0.004	-0.118	0.004
W	-0.091	-0.104	-0.004	-0.105	-0.021	-0.003	-0.152	0.015	**0.264**

[a]- highlighted in each column are correlations with absolute values at upper range, negative sign for inverse linear correlation, [b]- assumed aquifer temperature based on quartz geothermometery (Gunnarsson and Arnórsson, 2000)

dependent mineral-solution equilibria. Nevertheless, higher concentrations of mobile elements Li and Rb as well as Ti in the water samples are generally shown at increasing temperatures.

A few elements exhibit limited mobility in the aqueous solution despite their favourable ionic potentials like Cu^{2+} (2.30) and Pb^{2+} (1.50). Hardardóttir et al. (2009) noted that the levels of Fe, Pb, Cu, Au and Ag in the unboiled liquids in the aquifer are orders of magnitude higher than in the well discharges of the Reykjanes geothermal field because these elements precipitate from the solution likely as sulphides caused by boiling and vapour loss during depressurization. Sulphur also likely affects As and Mo mobility. Arsenic is not totally conservative although Figure 24 suggests that As is more mobile than Na which has the highest mobility among the major aqueous cations. At weaker correlations, the transport of As and Mo is inversely related to the total sulphur content of the fluid (Table 12). Ballantyne and Moore (1988) observed that As is regulated by reactions involving pyrite (FeS_2) in reservoir fluids while Stefánsson and Arnórsson (2005) showed that Mo is controlled by the solubility of molybdenite (MoS_2) in the high-temperature Icelandic geothermal waters. The same study by Stefánsson and Arnórsson (2005) cited the mobility of As, Sb and W to be lower than that of B due to non-stoichiometric dissolution of the rock. In Mahanagdong, Sb and W are highly immobile. W is also the only element which is positively correlated with pH. In Figure 25, As and B in Mahanagdong not only have comparable overall linearity with Cl but also define two linear correlations with almost similar set of wells. A separate line with lower slope seems to characterize wells MG31D, 14D, 37D and 40D indicating relative depletion of As and B in their solutions. B, Sb and As are volatile at higher temperatures with vapour to liquid ratios of 0.02, 0.06 and 0.003, respectively at 200°C (Smith et al., 1987). Some volatile As and B can partition to the vapour phase contributing to their relative depletion in the solutions in addition to any precipitation in the samples of MG31D, 14D, 37D and 40D which have higher aquifer T_{qtz} of >275°C. Their Sb levels in the waters are also depleted. In the other "excess enthalpy" wells, B which partitions into the vapour phase during phase segregation at high temperatures can re-dissolve to the relatively cooler and decreased amount of liquid phase in the depressurization zones thereby increasing the B/Cl ratio of the well discharge (Arnórsson, 2000).

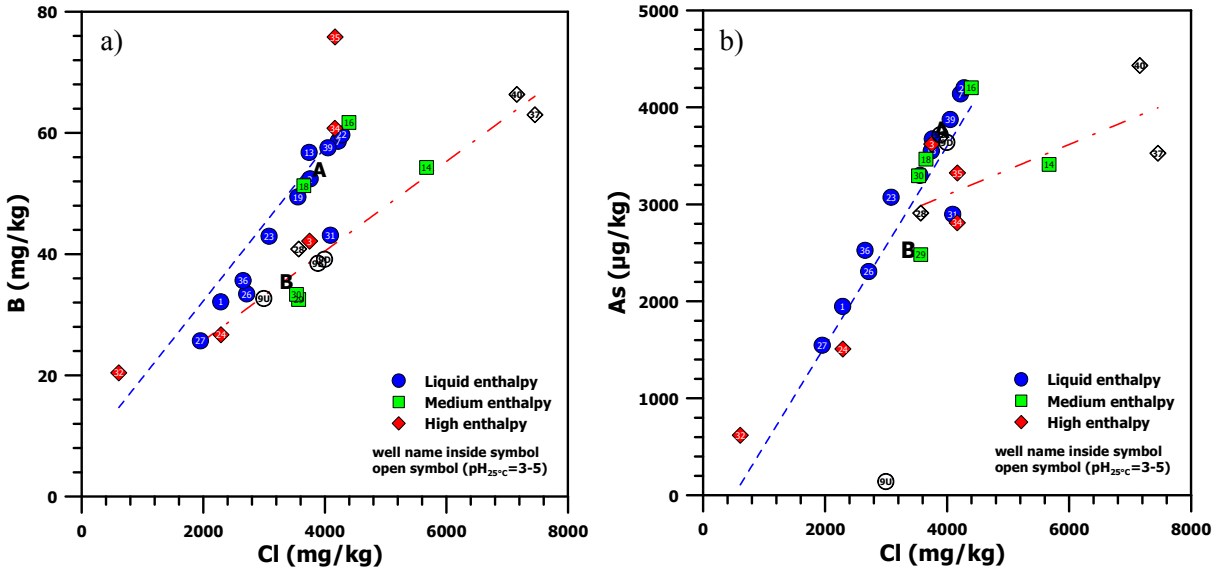

FIGURE 25: a) B and b) As versus Cl concentrations in the sampled waters. Chemistry of separated brine injected in Mahanagdong-A and Mahanagdong-B are marked A and B, respectively. The symbols 9U, 9S and 9D are samples from acid well MG9D which are undosed, partially dosed and fully dosed with caustic soda, respectively

Some of the immobile trace elements in Mahanagdong are consistent with their ionic potentials such as Cr^{3+} (3.97), Ti^{3+} (3.70), Sb^{3+} (3.33), U^{4+} (4.12) or U^{6+} (7.5) and W^{6+} (9.38) but this does not explain the higher than expected mobility of Be^{2+} (4.44) and V^{3+} (3.85). Modelling by Wood (1992) showed that monomeric hydroxide complexes of Be predominate at elevated temperatures ($BeOH^+$, $Be(OH)_2°$ and $Be(OH)^{3-}$) and mixed fluoride-carbonate complexes ($BeCO_3F^-$) substantially increase mobilities at temperatures >200°C, pH 5–7, when both total fluoride and total carbonate exceed 0.01 molal. By studying the host rocks in Tongonan, Scott (2000) reports that both Ti and V are highly immobile.

Thus the observed levels of V in Mahanagdong waters may have external sources, for instance as $VOCl_3$ after exsolution from magma (e.g., Giammanco et al., 1998). Scott (1989) theorized in Tongonan of a magmatic vapour exsolving from a crystallizing magma at 10-15 km depth containing both Cl and neutral-charged metal chloro-complexes eventually condensing and dispersing to the hydrothermal fluids at subcritical temperatures. Obviously, most of the acidity contributed by magmatic components has already evolved or any fresh magmatic inputs are masked by the neutral Cl-type Mahanagdong fluids. Higher pH and more oxidizing conditions can keep Mn, Cr and V in the solution as the formation of insoluble compounds like V_2O_4 and V_2O_3 are less favoured (Giamannco et al., 1998 and 2007). The large difference in the concentrations of sulphate relative to H_2S reflects the oxidizing conditions in the aquifers and may be further enhanced by inflow of cooler peripheral waters and injected brine postulated from geochemical monitoring. However, Reyes et al. (2002) correlated increased concentrations of Ba, Sn, Co, Ti, V and Sc in solution with abundant drill cuttings in the well. Water sampled from the newly-drilled well MG40D coincidentally has the higher levels of Ba, V, Co and Ti than the other wells.

Zn is supposed to be highly mobile in solution not only because of its divalent cationic potential (2.27) but also by its ability to be dominantly present as chloride complexes (e.g., Gallup, 1998). Yet Zn was only detected in the samples of MG9D and 40D. These wells have the most acidic discharges at $pH_{25°C}$ of 3.32 and 3.98, respectively. If the Zn flux to the aquifers is generally limited then the solution may lose Zn, either when deposited as sulphides in boiling zones or incorporated into corrosion products like goethite as observed in Rotokawa, New Zealand (Reyes et al., 2002). It is possible that the detected levels are remnants of higher Zn flux from magmatic input (e.g., Giammanco et al., 2007) in the acid wells. Alternatively, the acidity of the MG9D and 40D reservoir fluids may have the capability to leach Zn from the solid precipitates (e.g., Peralta et al., 1996).

4.6.2 Rare alkalis

The rare alkali metals Li, Rb and Cs are reactive in processes occurring in the deeper and hotter parts of the reservoir and are therefore not totally conservative. But as earlier shown, their highly positive correlations with Cl suggest that once added to the solution, they are considerably mobile. Their concentrations are least affected by shallow processes and carry imprints of their origin. The works of Goguel (1983) indicated that these rare alkali metals were dissolved from rocks well beyond drilled depths and were added to rather than leached from the altered rocks. The relative concentrations of Li, Rb and Cs and the processes that may change them are shown in Figure 26 following the methods of Giggenbach (1991). The data points are far from the composition of the rocks in the crust but still close to its original Li/Cs ratio. The samples cluster in the middle suggesting that they are affected by the secondary processes to almost similar degrees. The eastern and high enthalpy wells MG24D, 37D and 40D show the most extensive depletion of Rb that can start even at elevated temperatures >300°C and the least loss of Cs that likely occurs at lower temperatures <300°C. Thus the positions of wells MG24D, 37D and 40D in Figure 26 towards lower Li/Cs ratio suggest relative proximity to an area characterizing an "upflow" or hotter region.

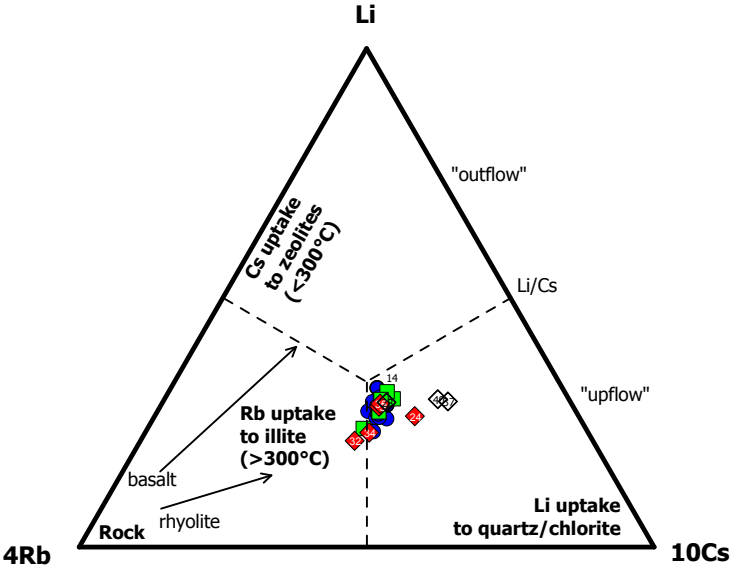

FIGURE 26: Relative Li, Rb and Cs contents in the water samples of Mahanagdong on weight basis. The symbols 9U, 9S and 9D are samples from acid well MG9D which are undosed, partially dosed and fully dosed with acid inhibitor, respectively

At higher temperatures, the very mobile alkalis Li and Rb are abundant in the fluids and tend to be fixed by

secondary minerals at lower temperatures. Figure 27 is a cross plot of molar ratios that involve the other mobile elements: Na/Li and Rb/Cs. The same wells are consistently inclined towards the "upflow" corner, especially MG37D and 40D. The historical values (~1994-1997) of wells MG3D and 14D, which are inferred to be closest to the upflow area based on integrated geoscientific data, are also plotted in Figure 27. The updated rare alkali behaviours of MG3D and 14D show a general shift of the data points towards higher Na/Li and lower Rb/Cs indicating probable loss of Li and Rb, respectively, from the fluid. A similar shift in data points is displayed by acid well MG9D but no recent data can be compared to the previous chemistry of acidic wells MG15D, 20D and 21D which are either currently shut or used as injection well. There are no previous data in MG37D which has been producing since 2005 at the time of sampling whereas MG40D was just newly connected to the system for about a month. The recent rare alkali chemistry of wells MG37D and 40D therefore needs to be validated by more data, including analyses of stable isotopes ^{18}O and ^{2}H. Nevertheless, the recent systematic shown by the rare alkalis gives signatures of higher temperatures in the general vicinity of wells MG37D and 40D. This productive area intersected area by MG40D, however, lies within the contour with corrected gravity values of 0 to -20 µgals implying a net mass loss during the production period 1997-2003 (Apuada and Olivar, 2005).

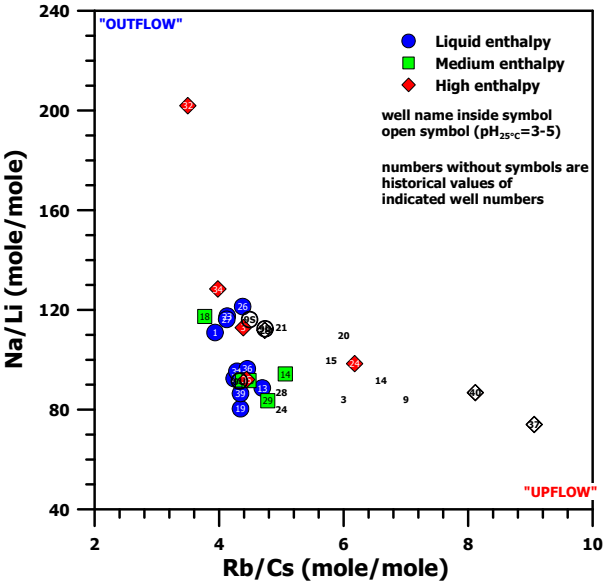

FIGURE 27: Plot of Na and rare alkalis in Mahanagdong waters. The symbols 9U, 9S and 9D are samples from acid well MG9D which are undosed, partially dosed and fully dosed with acid inhibitor, respectively

4.6.3 Halogens

The halogens (F, Cl, Br, I and At) comprise Group VII of the periodic table and are very reactive in elemental form since they only need one electron to complete the octet in their outermost shell. Thus they are rarely found in natural native form but are instead combined as halide ions in salts, solutions and gases (Pyle and Mather, 2009). Interests are increasing in studying halogens as summarized by Aiuppa et al. (2009) considering their role in the genesis of hydrothermal systems and transport of ore-forming metals. For this study, analytical data are only available for F, Cl and Br. For this reason, the discussion below is confined to these elements. They are also the three most abundant halogens in the Earth's major geochemical reservoirs. As volatile components in most magmas, their concentrations are: Cl (800-7,500 ppm), F (10-1,000 ppm but sometimes >5%) and Br (0.06-300 ppm). Compounds of F and Cl are significant in crustal rocks (about 550 ppm and 240 ppm, respectively) while Br is usually <1 ppm. In the oceans, the estimated concentrations of Cl, Br and F are 546 x 10^{-3}, 840 x 10^{-6} and 68 x 10^{-6} mol/kg, respectively (Aiuppa et al., 2009; Pyle and Mather, 2009 and references therein).

Fluorine is the most electronegative of the elements making it very reactive. F also has one of the smallest radii of any anion and very similar to the ionic radius of oxygen. Numerous studies reveal that F substitutes for hydroxyl and for oxygen in silicate crystals and melts. During magma differentiation, ascent and degassing, the tendency of F is to be retained in silicate melts compared to Cl and Br. Furthermore, as the magma evolves, F may be removed to a variable degree from the residual melt not only by fluorite but also by apatite, micas and amphiboles. Thus the formation of these minerals tends to reduce the F in the melt that would otherwise have been available for a gaseous magma phase. The mentioned behaviour of F (see summary of Aiuppa et al., 2009 for corresponding references) partly explains why its concentrations in Mahanagdong geothermal waters only range 1-5 mg/kg with an average of 1.85 mg/kg. For instance, major sinks of F from volatile HF in magma gases include fluorite, CaF_2, and fluorapatite, $Ca_5(PO_4)_3F$ (Symonds et al., 2001). Geothermal fluids are undersaturated with fluorite in basaltic setting but tend to be in equilibrium with this phase in more

felsic volcanic rocks (e.g. Arnórsson et al., 1983a). The modelled liquid aquifers of Mahanagdong are generally undersaturated with fluorite, by 2.4 log units on average (Figure 28). Fluorite is rarely reported from Mahanagdong but was mentioned by Scott (2001) in the shallow and cooler section of a Tongonan well. Fluoride may be consumed by hydroxide-bearing silicates at deeper reservoir levels where it replaces OH^- resulting in insufficient F activity to saturate the solution with fluorite. Figure 29 presents a significant positive correlation between the activities of F^- and OH^- in the modelled aquifer fluids of Mahanagdong.

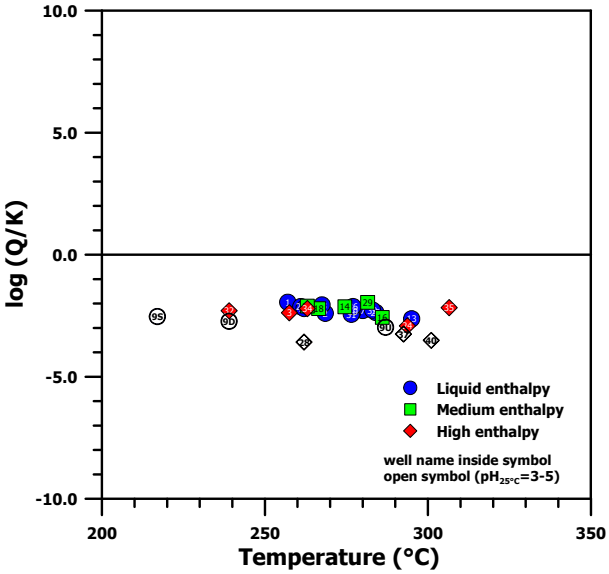

FIGURE 28: Saturation indices of fluorite in modelled total fluid assuming liquid enthalpy in Mahanagdong. The symbols 9U, 9S and 9D are samples from acid well MG9D which are undosed, partially dosed and fully dosed with acid inhibitor, respectivel

Despite its relative scarcity among the halogens, Br concentrations in Mahanagdong waters are on the average one order of magnitude higher than those of F at ~18 mg/kg. Table 12 shows strong positive correlation with Cl indicating similar geochemical behaviour of the two elements. Taran et al. (2008) observed that molar Cl/Br ratios of the acidic hydrothermal waters at El Chíchon volcano, Mexico, plot within the seawater and evapourite region despite evidences of magmatic contributions. The Cl/Br ratios of Mahanagdong waters also display the same signatures (Figure 30).

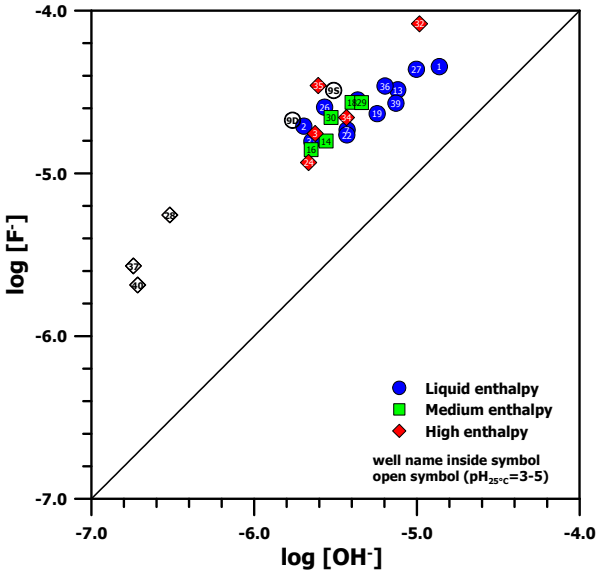

FIGURE 29: Comparison of the activities of F^- and OH^- in the modelled liquid aquifers of Mahanagdong. The symbols 9U, 9S and 9D are samples from acid well MG9D which are undosed, partially dosed and fully dosed with acid inhibitor, respectively

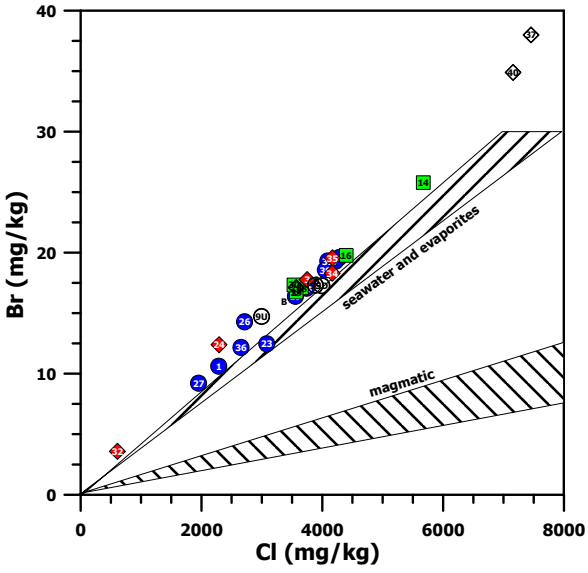

FIGURE 30: Cl vs Br concentrations in the sampled Mahanagdong geothermal waters. All symbols refer to the previous plots

The Cl/Br ratios in Mahanagdong (383-557) approach but are typically lower than seawater value (650). But that does not necessarily disagree with the inferred magmatic contributions established by previous works based on stable ^{18}O and ^{2}H isotopic data (e.g., Alvis-Isidro et al., 1993). The Cl/Br ratios suggest that the magmatic-related sources are derived from seawater or crustal fluids recycled in subduction zones. Halite has been identified in volcanic rocks of Philippine geothermal fields in the

vicinity of intrusive bodies (Reyes, 1990). This process could lower the Cl/Br ratio of the remaining fluid and explain the observed ratios in Mahanagdong. The decreasing Cl/Br ratio relative to seawater may also support the experimental findings of Liebscher et al. (2006). They demonstrated in a H_2O-NaCl-NaBr system, at 380-450°C and about 23-42 MPa, Br is more enriched than Cl in the liquid during phase separation of fluids with initial seawater composition.

4.7 Implications to field utilization

Dynamic changes often occur to producing fields after prolonged extraction of geothermal fluids from the reservoir. The results of this study will be used to gain insights into two important aspects concerning the state of Mahanagdong geothermal field: its sustainability and potential problems in utilization related to fluid acidity.

4.7.1 Reservoir changes

The vapour fraction of the initial aquifer fluids derived from this study represent conditions beyond the zone of depressurization of any discharging well. The vapour fractions can therefore give indirect picture of the deeper sources of the reservoir beyond the depths intersected by wells. They correspond to undisturbed or natural conditions in contrast to the higher steam fractions at lower pressures within the depressurization zone. There are two models to estimate the equilibrium vapour fraction of the initial aquifer fluid (e.g., Arnórsson, 1995). The first model assumes that the total discharge composition of wells is representative of the aquifer fluid (e.g., D'Amore and Truesdell, 1995). Various gas-gas and gas-mineral equilibria are assumed to obtain values for the vapour fraction and aquifer temperature. The second model assumes specific gas-mineral equilibria and takes into account the processes of phase segregation and heat transfer from aquifer rock to aquifer fluid (e.g., Arnórsson et al., 1990).

In the nearby Tongonan geothermal field, Dacillo and Siega (2005) used the first model. They assumed simultaneous equilibrium of components in two reactions: 1) Fischer-Tropsch and 2) a mineral-gas reaction involving H_2, H_2S and the pyrite-hematite mineral assemblage (FT-HSH2). Their approach has advantages. The aquifer fluid vapour fraction can be estimated using only gas chemistry data of wells that ceased to discharge liquid phases. The results are also graphically presented on a grid where changes in the reservoir parameters (temperature and vapour fraction) can be distinguished. If the FT-HSH2 method is applied using total discharge concentrations of gases in Mahanagdong, lower vapour fractions are obtained (Figure 31) compared to the results in

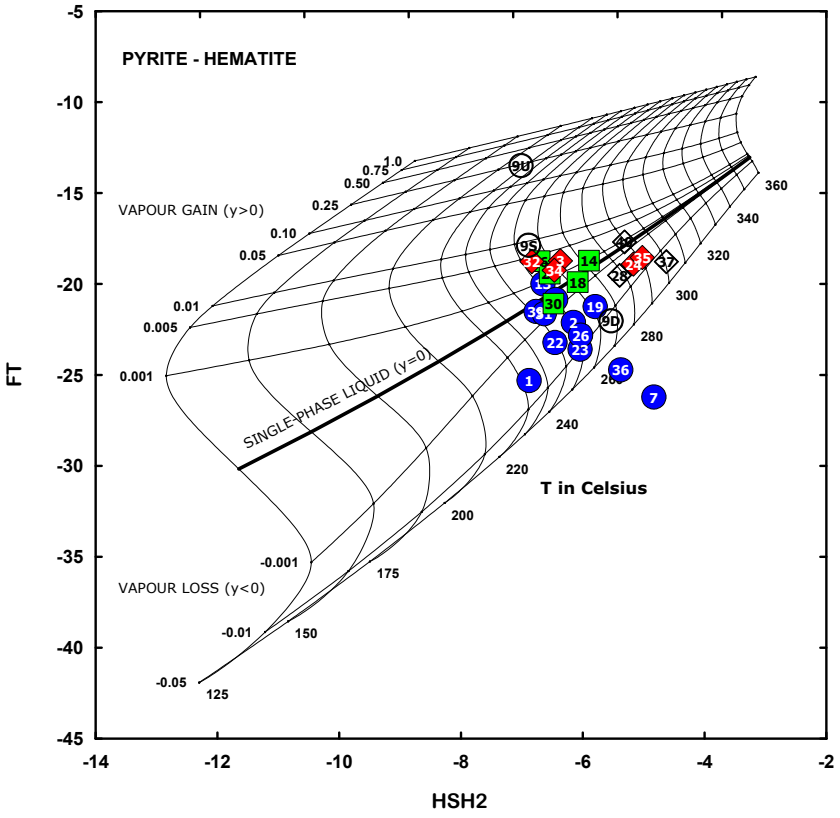

FIGURE 31: FT-HSH2 grid diagram using total discharge concentration of gases from Mahanagdong wells calculated from gas chemistry data in Table 4. Symbols of data points are similar to Figure 10.

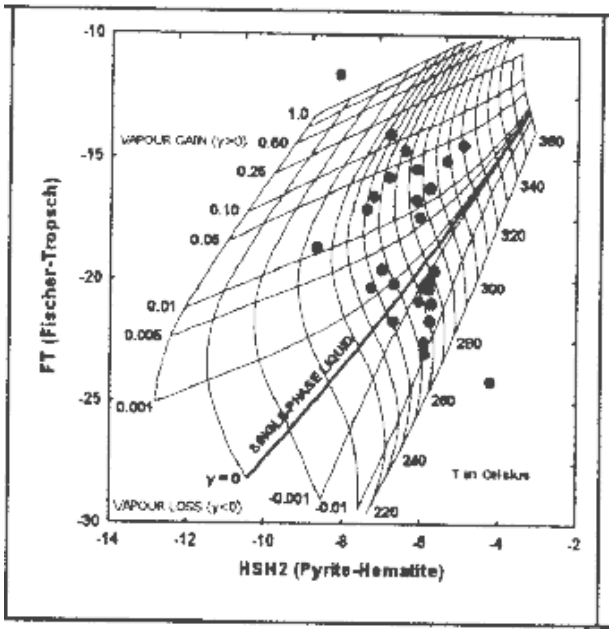

FIGURE 32: FT-HSH2 grid diagram using total discharge concentration of gases from Mahanagdong wells during early production stage (pre-1999) as assessed by Siega et al. (1999).

this study. Except for 2 samples of the acid well MG9D (9U and 9S), aquifer fluids of wells with higher vapour fractions are below 0.5% and the simultaneous equilibria temperatures ($T_{FT\text{-}HSH2}$) are lower than $T_{qtz,GA}$ by an average of about 30°C in liquid enthalpy wells. Siega et al. (1999) present an FT-HSH2 grid diagram of Mahanagdong during the early production years (Figure 32). The data points in Figure 32 have generally shifted towards lower temperatures and vapour loss if compared with Figure 31. A well to well comparison is not possible since the sources of analytical data were not indicated by Siega et al. (1999). In Mahanagdong, the aquifer fluids of liquid enthalpy wells significantly depart from equilibrium conditions of the redox Fischer-Tropsch reaction (Figure 16). Also, as the discharge enthalpy of the well approaches saturated steam, the difference between the concentrations of dissolved gases in the initial aquifer fluid and in the total discharge at the wellhead increases. These are the main considerations when validating the derived aquifer fluid vapour fractions by such procedure (see for example Arnórsson et al., 2007).

The modelling of initial aquifer fluids, assuming phase segregation to account "excess enthalpy", is supported by geochemical trends, reservoir engineering basis and reasonable agreement between T_{qtz} and $T_{Na/K}$ geothermometry. As discussed earlier, the second method, adopted in this study to estimate the initial aquifer vapour fraction based on the assumption of close approach to equilibrium of $H_{2,aq}$ in the initial aquifer fluids with the gro+mag+epi+qtz+wol mineral assemblage also has its limitations. The equilibrium values of the considered reaction (reaction 8 in Table 9) are strongly affected by mineral compositions of grossular and epidote. At the selected mineral compositions, the resulting initial aquifer vapour fractions shown in Table 8 are higher than those obtained by the FT-HSH2 method. Data presented in this contribution and earlier data collected by EDC have been used to evaluate if and how initial vapour fractions have changed with time in different sectors of Mahanagdong. The comparative results of the different parameters for each well (aquifer temperature, aquifer fluid initial vapour fraction and well discharge enthalpy) are shown in Figure 33. The spatial distribution of the same results across the Mahanagdong field is presented in Figure 34.

An assessment of each well is outside the scope of this study. In Figure 34, either the derived values for selected wells (from Figure 33) or a range of these values in a particular area were displayed. As depicted in Figure 34, the results generally correlate well with reservoir processes inferred from geochemical and reservoir engineering monitoring studies (Figure 5). The inferred upflow region within the area where MG3D and 14D were drilled has high $X^{f,v}$ values (3-5%) and that have increased with time ($\Delta X^{f,v}$ of +1.5 to +2.5%) over about 15 years of production despite decreases in $T_{qtz,GA}$ and $h^{d,t}$ likely caused by recharge of brine injected into the northern part of the reservoir. Herras et al. (2005) observed that although the estimated rates of brine returns are relatively fast (40-100 m/day) only 0.3-2% of the tracer injected in MG21D were recovered and maximum cooling of about 2°C can occur within 6-8 years from 2003. The data from the two studies may imply that considerable supply from deeper sources still feed the upflow area. East of the postulated upflow region (i.e., MG24D, 35D, 37D), the reservoir temperatures remains unchanged but equilibrium vapour fractions have declined ($\Delta X^{f,v}$ of -1 to -2%). By contrast, in south-southwest from the upflow area (i.e., MG28D, 29D, 27D, 30D, 31D), both $T_{qtz,GA}$ and vapour fractions have declined, for example, in MG27D by about 17°C and 2.5%, respectively.

Towards the major outflow region of Mahanagdong-A and within the collapse structure (i.e., MG18D, 32D, 34D, 36D), equilibrium vapour fractions are generally positive and stable. Yet, some wells display a decline in $X^{f,v}$ (e.g., MG36D) but others show an increase (e.g., MG32D) by a similar degree of about 4%. The general picture presented is intensive boiling in an area experiencing reservoir pressure drawdown but is prone to encroaching cooler peripheral waters probably through the aquifer tapped by MG27D. The encroaching cooler peripheral waters from the western front are also reflected in MG22D, 39D and 7D which has the most depleted level in H_2. According to tracer tests carried out by Herras et al. (2005), MG7D and 16D are the two most affected wells by brine returns from the southern injection sink (i.e., MG5RD) followed by MG2D, 22D and 23D. The scheme to inject further south of the production area has led to an increase in the equilibrium vapour fraction of MG16D and 23D ($\Delta X^{f,v}$ of +2.7% and +1.3%, respectively) but allowed cooler peripheral waters to increasingly dominate in MG7D.

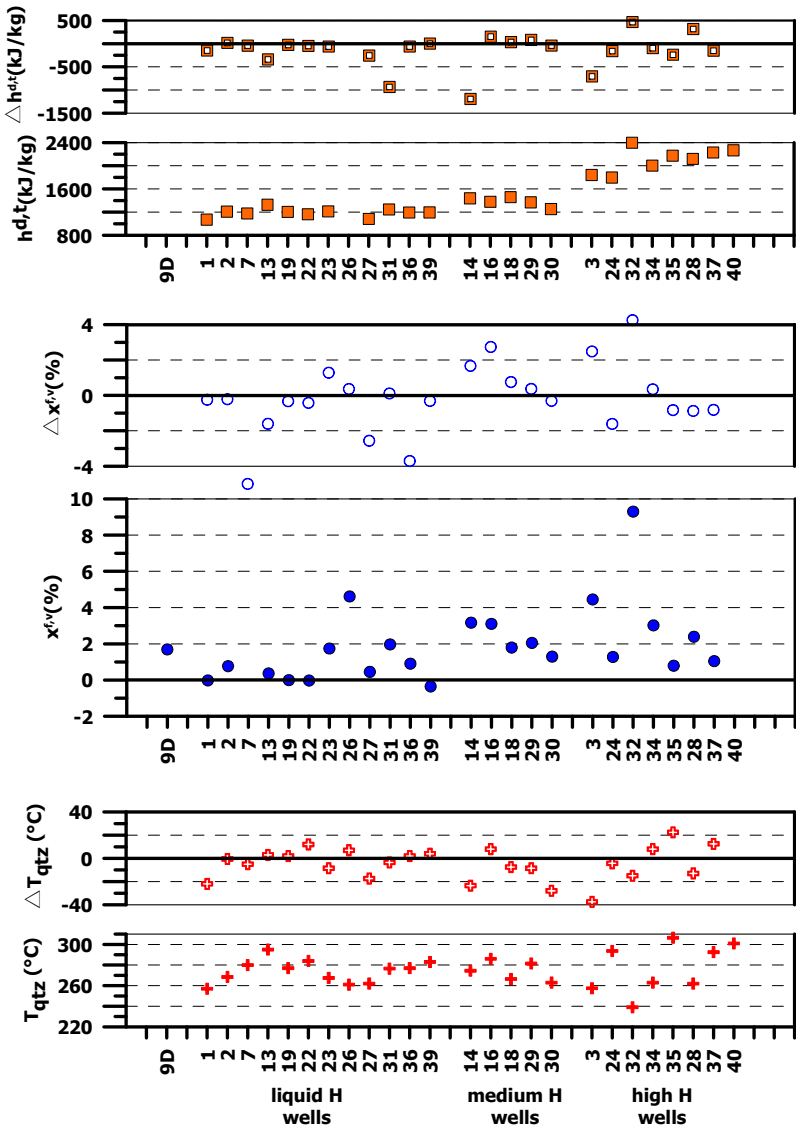

FIGURE 33: Summary of discharge enthalpy and initial aquifer temperature and equilibrium vapour fraction of Mahanagdong wells assuming the phase segregation model derived from data used in this study (filled symbols). Open symbols represent relative changes when using historical geochemical data of wells in 1997-1998 except in wells MG26D (2001) and MG34D, 35D, 36D, 37D, 39D (2005-2007). Due to depleted level of H_2 in the recent discharge of well MG7D, no initial aquifer fluid vapour fraction can be computed. The change in initial aquifer fluid vapour fraction for MG7D is shown outside the lower range limit to represent the highest vapour loss among the wells. No enthalpy data are shown for wells on discharge to silencers during the time of sampling (MG9D and 26D).

4.7.2 Fluid acidity

Several studies have greatly improved the understanding of the nature of deep acidic fluids at Mahanagdong. Such fluids have been accounted north of Mamban Fault (e.g., Dulce et al., 1995; Parilla et al., 1997; Martinez, 1998; Salonga et al., 2000; Bayon and Ferrer, 2005). The use of stable isotopes of hydrogen, oxygen and sulphur indicate that the acidic waters, which are of the Cl-SO_4 type, discharged by wells MG9D, 15D, 20D and 21D, significantly depart from primary magmatic composition (e.g., Salonga et al., 2000). The results suggest that both neutral and acidic fluids originate from a dominantly hydrothermal setting that has already evolved from previous magmatic environments. Poorly connected structures in the area may have led to inefficient water-rock interaction. The results yielded by speciation programs show that the dissociation of HSO_4^- as the fluid rises from the aquifer to the wellhead is the primary mechanism that buffers the acidity of the fluid.

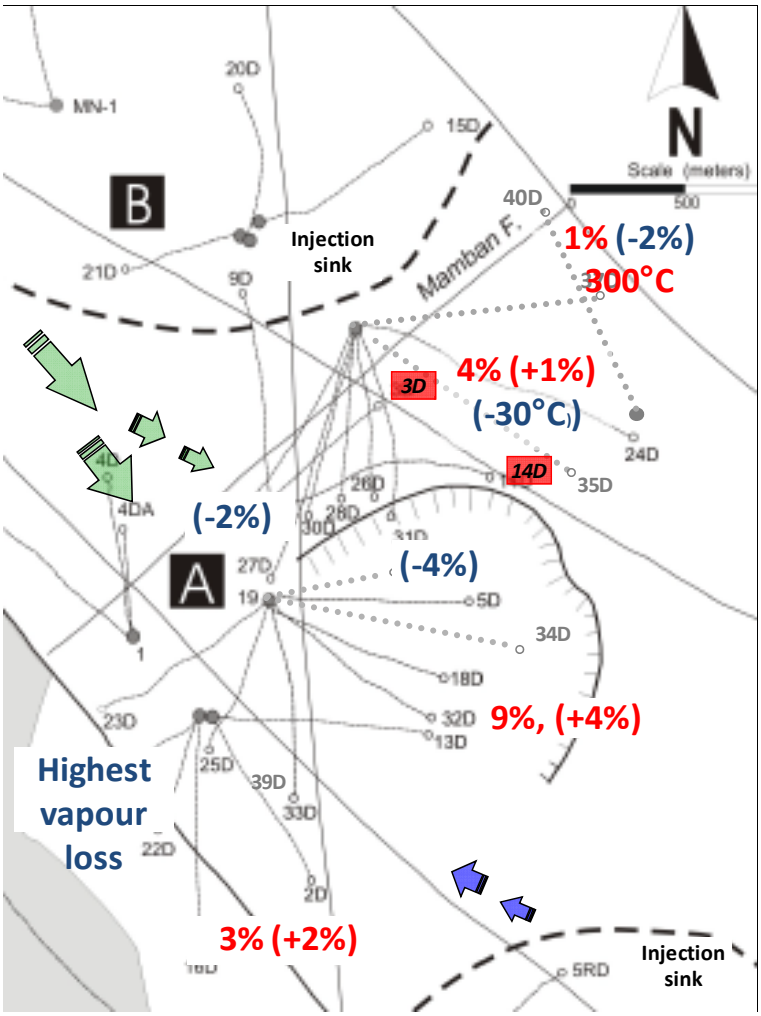

FIGURE 34: Spatial distribution across the Mahanagdong geothermal field of the different parameters summarized in Figure 4.24. Values placed at the bottom of a welltrack apply to the indicated well. Otherwise, the values represent that of the area. Wells inferred to tap the "upflow" area (3D, 14D) are emphasized. Initial vapour fractions shown in % are those derived in this study (see text). Aquifer temperatures shown are based on $T_{qtz,GA}$. Changes in initial vapour fractions and $T_{qtz,GA}$ after ~15 years of field utilization are enclosed in parentheses. Large letters A and B refer to location of 120 MWe and 60 MWe power plants, respectively

During the course of this study, the opportunity to sample acidic fluids was initially offered during the acid inhibition tests of MG9D. Relatively acidic samples were additionally obtained from online wells MG28D, 37D and 40D. Acidity poses corrosion problems to geothermal facilities. Moreover, the acidic samples from the producing and online wells raised concerns whether an acidic reservoir has either began to encroach the drawndown neutral production zones or have been tapped by new well MG40D. As discussed in section 4.6, the acidic fluids have higher levels of trace elements in the water samples compared to the neutral fluids (i.e., Zn, Fe, Mn, Pb, Cu, Ni and Co). Figure 35 presents the different element ratios based on major component concentrations in the modelled aquifer fluids that feed the Mahanagdong wells (Table 7). The only chemical differences between acidic and neutral pH waters, apart from pH and the mentioned trace elements, are higher levels of SO_4 and Mg in the former. The modelled aquifer pH (~4.5) of two acidic samples is lower by about 1 unit compared to the other aquifer fluids (i.e., MG37D and 40D).

The results of previous work and also of this study evidently assume that well fluid acidity is caused by bisulphate dissociation. It was pointed out earlier that the aquifer fluids at Mahanagdong are anhydrite saturated (Figure 19). The formation of anhydrite will thus control aqueous concentrations of SO_4^{2-} together with Ca^{2+}. There are three possible reactions in the formation of sulphuric acid in thermal solutions (e.g., IAEA, 2005 and references therein):

1. Oxidation of H_2S similar to that producing acidic hot springs and ponds at the surface (H_2S/SO_4=1);
2. Hydrolysis of magmatic SO_2 gas (H_2S/SO_4=1/3);
3. Hydrolysis of native sulphur at shallow depth (H_2S/SO_4=3).

Thus the molar ratios of SO_4 and H_2S in the modelled initial aquifer fluids in Mahanagdong can give initial estimates to discriminate the sources of sulphate. This is presented in Figure 36. The historical chemistry of acidic wells MG15D (shut), 20D (shut) and 21D (brine injection), retrieved from Parilla et al. (1997), were also included in Figure 36 for comparison. The acid wells are clustered into 2

general groups based on the reactions that produce H_2SO_4: a) MG9D, 20D, 21D and 28D- between oxidation of H_2S and hydrolysis of magmatic SO_2 gas and b) MG15D, 37D and 40D- hydrolysis of native sulphur. Such grouping is consistent with the spatial distribution of the wells across the field. Thus, the source of recent acidity observed in MG28D probably originates from the same reservoir fluids tapped by MG9D but is uncertain whether the fluids enter the well via the main feed zone or via shallower depths through any breaks in the casing. If by the former route, then such indicates a gradual encroachment of the acidic reservoir into the production zone. The acidity in wells MG37D and 40D may partly come from hydrolysis of native sulphur, which is also reported in rare to moderate amounts from cuttings retrieved during the drilling of wells in the area of MG24D, 35D and 37D (unpublished EDC well geology reports). They may also partly draw from the same reservoir tapped by acid well MG15D. Other mechanisms related to the high enthalpy discharges and aquifer temperatures (measured and $T_{qtz,GA}$) of wells MG37D and 40D are also possible but are yet to be investigated. The systematic of rare alkalis showed that the upflow region may extend towards the east of the presently accepted area. Data are however still lacking whether the observed acidity in wells MG37D and 40D indirectly indicates the existence of a less mature hydrothermal system.

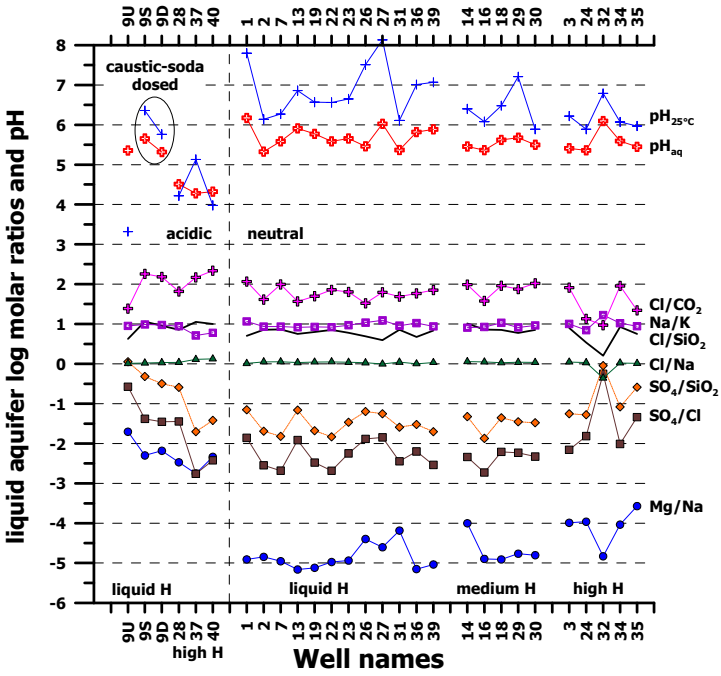

FIGURE 35: Major element ratios from concentrations in the modelled initial aquifer fluids feeding the Mahanagdong wells

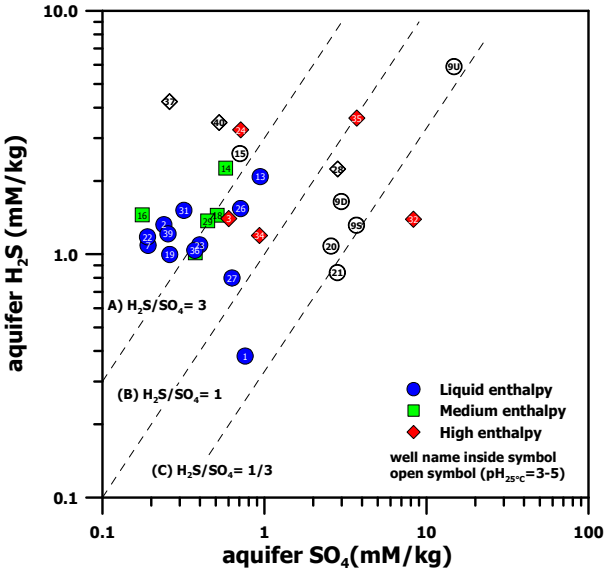

FIGURE 36: H_2S and SO_4 concentrations in the modelled initial aquifer fluids feeding the Mahanagdong wells. Data from acidic wells MG15D, 20D and 21D were retrieved from Parilla et al. (1997). The dashed lines represent the molar ratios for the reactions involving native S hydrolysis (A), H_2S oxidation (B) and SO_2 disproportionation (C).

Stable sulphur isotope studies by Salonga et al. (2000) and Bayon and Ferrer (2005) show that dissolved sulphate of Mahanagdong fluids are of the "heavy group", i.e. $\delta^{34}S$>15‰ CDT, indicating that they are directly derived from SO_2 disproportionation at greater depths. Figure 36 suggests that reactions in the aquifer either led to enrichment of H_2S or depletion of SO_4 in the fluids that effectively shifted the data points towards the signatures of H_2S oxidation and S hydrolysis. From the same study of the mentioned authors, H_2S of the Mahanagdong fluids originating from SO_2 hydrolysis cannot be differentiated from magmatic source as both have similar isotope ratios close to 0‰ CDT. Data from this study shows that dissolved H_2S of modelled aquifer fluids Mahanagdong are generally above equilibrium conditions with respect to assemblages involving grossular and magnetite (Figures 10 and 12). An apparent excess flux of H_2S supplies the system but its specific origin is still undetermined.

5. SUMMARY AND CONCLUSIONS

The high-temperature, liquid-dominated Mahanagdong geothermal field has supplied steam since 1996 to power plants with total capacity of 180 MWe. For evaluation of the geochemical structure of the field after ~15 years of production, fluid samples were obtained from 26 wet-steam wells in 2009. A double-cyclone Webre separator was used for separate sampling of the vapour and liquid phases at the wellheads. Both types of samples were collected at the same pressure. The pH of most water samples were measured on-site. The LRMD EDC laboratory analyzed both the gas and water samples for major components. Analyses of major elements in the water samples were also carried out at the Institute of Earth Sciences, University of Iceland using ICP-AES and IC and were selected for subsequent data processing. In addition, trace element concentrations were determined in the water samples at Merced, University of California using a quadrupole ICP-MS. The analytical results from the laboratories of LRMD EDC and the Institute of Earth Sciences, University of Iceland compare generally well for most major components (%Mean Difference within 10%). Larger differences are observed in elements occurring at lower concentrations (e.g., Mg and Fe) and in pH, H_2S and T-CO_2. The difference in analyses of components determined by both ICP-AES and ICP-MS increases either when the levels in the samples approach the instrument detection limit or are significantly above the standard concentrations.

Using the analytical data of the wellhead samples, the initial aquifer fluids feeding the Mahanagdong wells were modelled with the aid of the speciation programs WATCH and also by SOLVEQ, in the case of one acidic sample. Some of the wells at Mahanagdong have liquid enthalpy, i.e. the enthalpy of well discharges is similar to that of steam-saturated water at the aquifer temperature. Other wells have "excess enthalpy", meaning that the enthalpy of well discharges is higher than that of liquid water at the aquifer temperature. Since the Mahanagdong reservoir is liquid-dominated, the excess enthalpy reflects a change in the enthalpy of the flowing fluid between initial aquifer fluid conditions and the wellhead. Various processes can cause such an increase in the enthalpy of the flowing fluid. Quartz and Na/K geothermometer temperatures compare well when it is assumed that the excess enthalpy is caused by phase segregation in the depressurization zone around wells. Such phase segregation involves partial or complete retention of liquid water in the aquifer due to its adhesion onto mineral grain surfaces by capillary pressure whereas all the vapour flows in the wells. Aquifer fluid component concentrations were thus calculated on the basis of phase segregation model taking the phase segregation to occur at a temperature of 30°C below the aquifer temperature. At these conditions, liquid saturation is about 0.2 that seems a reasonable number for fracture-dominated reservoir rock.

Sensitivity analyses show that modelling results are slightly affected when the reference temperature is varied within ±20°C but are quite dependent to the selected phase segregation point and the discharge enthalpy in the case of volatile components, but insignificantly for non-volatile components. For non-volatile components, significant variation in their calculated concentrations (up to ~20% lower) can only occur if discharge enthalpy is >2000 kJ/kg and phase segregation is selected within the temperature range that gives maximum enthalpy of steam (200-250°C). On the other hand, the calculated concentration of gases in the aquifer fluids can vary widely depending on the choice of phase segregation temperature. This variation involving the volatile components increases proportionally with the discharge enthalpy of the well thus considerable uncertainty is involved when discharge enthalpy approaches that of dry steam.

Having obtained component concentration in the initial aquifer fluid, the WATCH speciation program was used simultaneously to calculate individual species activities, by assuming that (1) the aquifer fluid is represented by liquid alone and (2) that it is two-phase. For the latter case, the vapour fraction was calculated from the H_2 content of the aquifer fluid assuming that its concentration in the liquid was fixed by equilibrium with specific mineral assemblage. The modelled aquifer fluids composed purely of liquid were assessed how closely they have approached equilibrium conditions with respect to various mineral-gas, gas-gas and mineral-solution reactions that may occur in the aquifer. The concentrations of the reactive gases H_2S, H_2 and CO_2 show much scatter when depicted against possible mineral-gas reactions. But with few exceptions, the data points for both H_2S and H_2 lie

somewhat above equilibrium conditions with mineral assemblages involving 1) grossular, pyrite, and magnetite and 2) pyrite, magnetite and hematite. The scattered data points partly reflect the uncertainties involved in modelling the initial aquifer fluids which include, among others, 1) the assumption of a single reservoir fluid with a certain temperature to represent what may actually be a mixture of different fluid sources and 2) the variables involved in adopting the phase segregation model to explain the "excess enthalpy" of wells. If equilibrium of the gases with the considered mineral assemblage is accepted, then the data points may also indicate that the fluids in the aquifer have interacted with solid-solutions of different compositions. The activities of grossular and epidote were selected as 0.3 and 0.8, respectively, but data of their composition in Mahanagdong is lacking. At the selected compositions of grossular and epidote, data points for CO_2 were generally above the equilibrium curve for mineral assemblages including clinozoisite+calcite+quartz and grossular or prehnite. Different redox reactions that involve gases generally show significant departure from equilibrium conditions largely influenced by the H_2 levels in the fluid. Considering the uncertainties involved in analysis, modelling and thermodynamic data, the initial aquifer fluids display close saturation with various calcium-bearing, Fe-sulphide and Fe-oxide secondary minerals but are significantly undersaturated with fluorite, grossular and wollastonite which are rarely reported in Mahanagdong.

The high concentrations of the reactive gases (CO_2, H_2S and H_2) in the modelled total aquifer fluid, in relation to equilibrium curves involving their aqueous concentrations, may be due to the presence of vapour in this fluid. Equilibrium vapour fractions were derived by selecting the phase segregation point at 30°C below the aquifer temperature and by assuming that equilibrium prevailed between H_2 in the aquifer liquid with the gro+mag+qtz+epi+wol assemblage. At inferred Mahanagdong aquifer temperatures (about 250-300°C), about the same equilibrium vapour fraction values would be obtained if the magnetite-hematite assemblage had been selected instead of the garnet-bearing assemblage. The derived equilibrium vapour fraction values generally would have been lower had the aquifer fluid compositions been modelled by assuming that 1) total discharge gas concentrations represented gas concentrations in the initial aquifer fluid and 2) equilibria according to the Fischer-Tropsch and pyrite-hematite reactions been assumed. The calculated vapour fraction values correlate reasonably well with inferred reservoir processes characterizing the Mahanagdong field. In the postulated upflow area, initial vapour fraction values are ~4%. A high-temperature, two-phase reservoir located east of the upflow region is characterized by vapour loss of up to 2%. A possible extension of upflow towards the east is suggested by systematics of the rare alkali analyses. Highest change in equilibrium vapour fraction value (+4%) occurs in shallow well MG32D reflecting intense boiling within the collapse structure. Indications of encroaching peripheral waters from the northwest towards the drawndown area cause negative equilibrium vapour fraction values in MG27D and 36D. Injection scheme to the south of the field have led to 1-2% increase in equilibrium vapour fraction values in wells MG16D and 23D. The same injection scheme may be responsible for an increased inflow of colder peripheral waters from the west as manifested by the maximum vapour loss in MG7D.

Based on available analyses of fresh rocks, the most mobile elements in the Mahanagdong fluids are Cl, As, Na, S, Rb, K, Li and Br. Ti and Al have the lowest mobility, both in neutral pH and acidic fluids. The acidic discharges have high metal content. Zn and Mg are probably mobilized from the reservoir rocks whereas Fe, Mn, Pb, Cu, Ni and Co in acidic waters are likely to come, at least partly, from well casing material. The only chemical differences between acidic and neutral pH waters, apart from pH and the mentioned metals, are higher levels of SO_4 in the former. The modelled aquifer pH (~4.5) of two acidic samples is lower by about 1 unit compared to the other aquifer fluids. The acidity at the surface of the Cl-SO_4-type waters is mainly caused by the dissociation of HSO_4^- as the fluids cool by depressurization boiling when they flow from the aquifer to the wellhead. The molar ratios of H_2S and SO_4 in the aquifer fluids, if they still retain the signal of their magmatic sources, suggest that the disproportionation of SO_2 at subcritical conditions (MG9D and 28D) and hydrolysis of native sulphur (MG37D and 40D) contribute to acidic fluids discharged by the indicated wells.

REFERENCES

Aiuppa, A., Baker, D.R., and Webster, J.D., 2009: Halogens in volcanic systems. *Chemical Geology, 263*, 1-18.

Akaku, K., Reed, M.H., Yagi, M., Kai, K., and Yasuda, Y., 1991: Chemical and physical processes occurring in the Fushime geothermal system, Kyushu, Japan. *Geochemical Journal, 25,* 315–333.

Alcober, E.H., Saw, V.S., Herras, E.B., Dacillo, D.B., Angcoy Jr., E.C., Colo, M.H.B., Abapo, R.N., Parayno, G.E., and Belas-Dacillo, K.A., 2008: Sustaining the Leyte Geothermal Production Field: 10 years of BOT operation and future direction. *Proceedings 29th PNOC-EDC Geothermal Conference*, Makati City, Philippines, 181-193.

Alvis-Isidro, R.R.A., Solana, R.R., D'Amore, F., Nuti, S., and Gonfiantini, R., 1993: Hydrology of the Greater Tongonan geothermal system, Philippines, as deduced from geochemical and isotopic data. *Geothermics, 22,* 435–450.

Angcoy Jr., E.C., Alcober, E.H., Sta. Ana., F.X.M., Cabel Jr., A.C., Bayrante, L.F., Malate, R.C.M., and Ogena, M.S., 2008: Conquering the challenges in geothermal utilization---the EDC experience. *30th Anniversary Workshop,* UNU-GTP, Iceland, http://www.unugtp.is.

Apuada, N.A., and Olivar, R.E.R., 2005: Repeat microgravity and levelling surveys at Leyte Geothermal Production Field, North Central Leyte, Philippines. *Proceedings World Geothermal Congress 2005*, Antalya, Turkey, CD, 9 pp., paper no. 0711.

Arnórsson, S., 1995: Estimation of initial steam fraction in boiling geothermal reservoirs. *Proceedings World Geothermal Congress 1995*, Firenze, Italy, 1653-1657.

Arnórsson, S. (ed.), 2000: *Isotopic and chemical techniques in geothermal exploration, development and use. Sampling methods, data handling and interpretation*. International Atomic Energy Agency, Vienna, 351 pp.

Arnórsson, S., 2003: Arsenic in surface- and up to 90°C ground waters in a basalt area, N-Iceland: processes controlling its mobility. *Appl. Geochem., 18,* 1297-1312.

Arnórsson, S., Angcoy, Jr., E.C., Bjarnason, J.Ö., Giroud, N., Gunnarsson, I., Kaasalainen, H., Karingithi, C., and Stefánsson, A., 2010: Gas chemistry of volcanic geothermal systems. *Proceedings World Geothermal Congress 2010*, Bali, Indonesia, (in press).

Arnórsson, S., and Andrésdóttir, A., 1999: The dissociation constants of Al-hydroxy complexes at 0-350°C and P_{sat}. In: Ármansson (ed.) *5th International symposium on Geochemistry of the Earth's Surface,* Rotterdam, Balkema, 425-428.

Arnórsson, S., Bjarnason, J.Ö., Giroud, N., Gunnarsson, I., and Stefánsson, A., 2006: Sampling and analysis of geothermal fluids, *Geofluids*, *6,* 203-216.

Arnórsson, S., Björnsson, S., Muna, Z.W., and Ojiambo, S.B., 1990: The use of gas chemistry to evaluate boiling processes and initial steam fractions in geothermal reservoirs with an example from the Olkaria field, Kenya. *Geothermics, 19,* 497-514.

Arnórsson, S., Geirsson, K., Andrésdóttir, A., and Sigurdsson, S., 1996: *Compilation and evaluation of thermodynamic data on aqueous species and dissociational equilibria in aqueous solution I. The solubility of CO_2, H_2S, H_2, CH_4, N_2, O_2 and Ar in pure water.* Science Institute Report RH-17-96, University of Iceland, 20 pp.

Arnórsson, S., Gunnarsson, I., Stefánsson, A., Andrésdóttir, A., and Sveinbjörnsdóttir, A.E., 2002:

Major element chemistry of surface- and ground waters in basaltic terrain, N-Iceland. I. Primary mineral saturation. *Geochim. Cosmochim. Acta, 66,* 4015-4046.

Arnórsson, S., and Gunnlaugsson, E., 1983a: The chemistry of geothermal waters in Iceland II. Mineral equilibria and independent variables controlling water compositions. *Geochim. Cosmochim. Acta, 47*, 547-566.

Arnórsson, S., Gunnlaugsson, E., and Svavarsson, H., 1983b: The chemistry of geothermal waters in Iceland III. Chemical geothermometry in geothermal investigations. *Geochim. Cosmochim. Acta, 47*, 567-577.

Arnórsson, S., Sigurdsson, S., and Svavarsson, H., 1982: The chemistry of geothermal waters in Iceland. I. Calculations of aqueous speciation from 0° to 370°C. *Geochim. Cosmochim.Acta, 46,* 1513-1532.

Arnórsson, S., Stefánsson, A., and Bjarnason, J.Ö., 2007: Fluid-fluid interaction in geothermal systems. *Reviews in Mineralogy & Geochemistry*, *65,* 229-312.

Aurelio, M.A., Huchon, P., Barrier, E., and Gaulon, R., 1994: Displacement rates along the Philippine Faults estimated from slip-vectors and regional kinematics. *J. Geol. Soc. Phil., 29,* 65–78.

Ballantyne, J.M., and Moore, J.N., 1988: Arsenic geochemistry in geothermal systems. *Geochim. Cosmochim. Acta, 52*, 475-483.

Balmes, C.P., 1994: The geochemistry of the Mahanagdong sector, Tongonan Geothermal Field, Philippines. Report 2 in: *Geothermal training in Iceland 1994.* UNU-GTP, Iceland, 31-52.

Bayon, F.E.B., and Ferrer, H., 2005: Sulphur isotope ratios in Philippine geothermal systems. In: D'Amore, F. (coordinator), *Use of isotope techniques to trace the origin of acidic fluids in geothermal systems*, IAEA, Austria, 111-132.

Best, M.G., 2003: *Igneous and metamorphic petrology 2nd edition*. Blackwell Science Ltd., Turin, 758 pp.

Bjarnason, J.Ö., 1994: *The speciation program WATCH, version 2.1.* Orkustofnun, Reykjavík, 7 pp.

Caranto, J.A, and Jara, M.P., 2006: Factors controlling reservoir permeability at the Leyte Geothermal Production Field, Tongonan, Philippines. *Proceedings 27th PNOC-EDC Geothermal Conference*, Makati City, Philippines, 107-112.

Chen, C., and Horne, R.N., 2005: Multiphase flow properties of fractured geothermal rocks. *Proceedings World Geothermal Congress 2005*, Antalya, Turkey, CD, 9 pp., paper no. 1101.

Dacillo, D.B., and Salonga, N.D., 2004: *Conceptual flow patterns from stable isotope systematics of the Mahanagdong Geothermal Field, Philippines*. PNOC-EDC internal report (unpublished).

Dacillo, D.B., and Siega, F.L., 2005: Geochemical assessment on the sustainability of the deep geothermal resource of Tongonan Geothermal Field (Leyte, Philippines). *Proceedings World Geothermal Congress 2005*, Antalya, Turkey, CD, 7 pp., paper no. 0869.

D'Amore, F., 1991: Gas geochemistry as a link between geothermal exploration and exploitation. In: D'Amore, F. (coordinator), *Application of geochemistry in geothermal reservoir development*. UNITAR/UNDP publication, Rome, 93-117.

D'Amore, F., and Truesdell, A.H., 1995: Correlation between liquid saturation and physical phenomena in vapour-dominated geothermal reservoirs. *Proceedings World Geothermal Congress*

1995, Firenze, Italy, 1927-1932.

Department of Energy, 2009: *DoE,* website: *http://www.doe.gov.ph*.

Diakonov, I., and Tagirov, B.R., 2002: *Iron (III) speciation in aqueous solutions: Part 2. Thermodynamic properties of $Fe(OH)^{+2}$, $Fe(OH)^{+}_{2}$ and $Fe(OH)_3°$ species and solubility of iron (III) oxides, and hydroxides*. In preparation.

Druschel, G.K., Schoonen, M.A.A., Nordstrom, D.K., Ball, J.W., Yong, X., and Cohn, C.A., 2003: Sulfur geochemistry of hydrothermal waters in Yellowstone National Park, Wyoming, USA. III. An anion-exchange resin technique for sampling and preservation of sulfoxyanions in natural waters. *Geochem. Trans., 4(3)*, 12-19.

Dulce, R.G., Rosell, J.B., and Zaide-Delfin, M.C., 1995: Sulfide minerals as indicators of acid Cl-SO_4 fluids. *Proceedings 17th PNOC-EDC Geothermal Conference*, Makati City, Philippines, 137-149.

Energy Development Corporation, 2009: *EDC,* website: *http://www.energy.com.ph*.

Fournier, R.O., and Potter, R.W. II, 1982: A revised and expanded silica (quartz) geothermometer. *Geoth. Res. Council Bull.,11-10*, 3-12.

Gallup, D.L., 1998: Geochemistry of geothermal fluids and well scales, and potential for mineral recovery. *Ore Geology Reviews, 12*, 225-236.

Giammanco, S., Ottaviani, M., Valenza, M., Veschetti, E., Principio, E., Giammanco, G., and Pignato, S., 1998: Major and trace elements geochemistry in the ground waters of a volcanic area: Mt. Etna (Sicily, Italy). *Wat. Res., 32*, 19-30.

Giammanco, S., Ottaviani, M., and Veschetti, E., 2007: Temporal variability of major and trace element concentrations in the groundwaters of Mt. Etna (Italy): Effects of transient input of magmatic fluids highlighted by means of cluster analysis. *Pure Appl. Geophys., 164,* 2523-2547.

Giggenbach, W.F., 1980: Geothermal gas equilibria. *Geochim. Cosmochim. Acta, 44*, 2021-2032.

Giggenbach, W.F., 1987: Redox processes governing the chemistry of fumarolic gas discharges from White Island, New Zealand. *Appl. Geochem., 2*, 143-161.

Giggenbach, W.F., 1991: Chemical techniques in geothermal exploration. In: D'Amore, F. (coordinator), *Application of geochemistry in geothermal reservoir development*, UNITAR/UNDP publication, Rome, 119-144.

Giroud, N., 2008: *A chemical study of arsenic, boron and gases in high-temperature geothermal fluids in Iceland.* PhD dissertation, Faculty of Science, University of Iceland, 110 pp.

Glover, R.B., Lovelock, B., and Ruaya, J.R., 1981: A novel way of using gas and enthalpy. *New Zealand Geothermal Workshop*, Auckland, New Zealand, 163-169.

Goguel, R., 1983: The rare alkalies in hydrothermal alteration at Wairakei and Broadlands, geothermal fields, N.Z. *Geochim. Cosmochim. Acta, 47*, 429-437.

Gonzalez, R.C., Alcober, E.H., Siega, F.L., Saw, V.S., Maxino, D.A., Ogena, M.S., Sarmiento, Z.F., and Guillen, H.V., 2005: Field management strategies for the 700 MW Greater Tongonan Geothermal Field, Leyte, Philippines. *Proceedings World Geothermal Congress 2005*, Antalya, Turkey, CD, 7 pp., paper no. 2412.

Greenwood, H.J., 1967: Mineral equilibria in the system MgO-SiO_2-H_2O-CO_2. In: Abelson, P.H.

(e.), *Researches in Geochemistry*, *2*, 542-567.

Gunnarsson, I., and Arnórsson S., 2000: Amorphous silica solubility and the thermodynamic properties of $H_4SiO_4°$ in the range of 0°to 350°C at P_{sat}. *Geochim. Cosmochim. Acta, 64*, 2295-2307.

Gunnarsson, I., and Arnórsson S., 2005: Impact of silica scaling on the efficiency of heat extraction from high-temperature geothermal fluids. *Geothermics, 34*, 320-329.

Hardardóttir, V., Brown, K.L., Fridriksson, Th., Hedenquist, J.W., Hannington, M.D., Thorhallsson, S., 2009: Metals in deep liquid of the Reykjanes geothermal system, southwest Iceland: Implications for the composition of seafloor black smoker fluids. *Geology, 37/12*, 1103-1106.

Herras, E.B., Licup, A.C., Vicedo, R.O., Parilla, E.V., and Jordan, O.T., 1996: The hydrological model of the Mahanagdong sector, Greater Tongonan Geothermal Field, Philippines. *Geothermal Resources Council, Transactions, 20*, 681-688.

Herras, E.B., Siega, F.L., and Magdadaro, M.C., 2005: Naphthalene disulfonate tracer test data in the Mahanagdong Geothermal Field, Leyte, Philippines. *Proceedings World Geothermal Congress 2005*, Antalya, Turkey, CD, 7 pp., paper no. 1212.

Hirtz, P., and Lovekin, J., 1995: Tracer dilution measurements for two-phase geothermal production: comparative testing and operating experience. *Proceedings World Geothermal Congress 1995*, Firenze, Italy, 1881-1886.

Horne, R.N., Satik, C., Mahiya, G., Li., K., Ambuso, W., Tovar, R., Wang, C., and Nassori, N., 2000: Steam-water relative permeability. *Proceedings World Geothermal Congress 2000*, Kyushu-Tohoku, Japan, 2609-2615.

IAEA, 2005: *Use of isotope techniques to trace the origin of acidic fluids in geothermal systems*. IAEA, Vienna, 204 pp.

Iler, R.K., 1979: *The chemistry of silica: solubility, polymerization, colloid and surface properties, and biochemistry*. John Wiley and Sons, New York, 866 pp.

International Geothermal Association, 2009: *IGA*, website: http://www.geothermal-energy.org

Johnson, J.W., Oelkers, E.H., and Helgeson, H.C., 1992: SUPCRT92- A software package for calculating the standard molal thermodynamic properties of minerals, gases, aqueous species, and reactions from 1-bar to 5000-bar and 0-degrees-C to 1000-degrees-C. *Computers and Geosciences, 18*, 899-947.

Karingithi, C.W., 2002: *Hydrothermal mineral buffers controlling reactive gases concentration in the Greater Olkaria geothermal system, Kenya.* University of Iceland, MSc thesis, UNU-GTP, Iceland, report 2, 51 pp.

Karingithi, C.W., Arnórsson, S., and Grönvold, K., 2010: Processes controlling aquifer fluid compositions in the Olkaria geothermal system, Kenya. *J. Volc. Geothermal Res. (submitted).*

Kristmannsdóttir, H., 1981: Wollastonite from hydrothermal altered basaltic rocks in Iceland. *Min. Mag., 44*, 95-99.

Kristmannsdóttir, H., Arnórsson, S., Sveinbjörnsdóttir, A.E., and Ármannsson, H., 2004: The project Icelandic water resources (in Icelandic). *Proceedings of the spring conference of the Icelandic Geological Society,* 33-34.

Liebscher, A., Lüders, V., Heinrich, W., and Schettler, G., 2006: Br/Cl signature of hydrothermal fluids: liquid-vapour fractionation of bromine revisited, *Geofluids*, *6,* 113-121.

Los Baños, C.F., and Maneja, F.C., 2005: The resistivity structure of the Mahanagdong Geothermal Field, Leyte, Philippines. *Proceedings World Geothermal Congress 2005*, Antalya, Turkey, CD, 7 pp., paper no. 0723.

Mack, R.D., McCoy, T., and Ring, L., 1999: How in situ expansion affects casing and tubing properties---statistical data included. *World Oil, http://www.worldoil.com*.

Martinez, M.V.M., 1998: Mineral alteration in acid and neutral-pH hydrothermal reservoir: the case of Mahanagdong Geothermal Field, Leyte. *Proceedings 19th PNOC-EDC Geothermal Conference*, Makati City, Philippines, 299-309.

Molina, P.O., Tanaka, T., Itoi, R., Siega, F.L., and Ogena, M.S., 2005: Analysis and interpretation of naphthalene disulfonate tracer tests at the Mahanagdong Geothermal Field, Philippines. *Proceedings World Geothermal Congress 2005*, Antalya, Turkey, CD, 9 pp., paper no. 1157.

Ohmoto, H., and Lasaga, A.C., 1982: Kinetics of reactions between aqueous sulphates and sulphides in hydrothermal systems. *Geochim. Cosmochim. Acta, 46,* 1727-1745.

Pang Z., and, Ármansson, H. (eds.), 2006: *Analytical procedures and quality assurance for geothermal water chemistry*. UNU-GTP, Reykjavik, Iceland, report 1, 172 pp.

Parilla, E.V., Martinez, M.V.M., and Salonga, N.D., 1997: Assessment of fluid acidity in Alto Peak and Mahanagdong geothermal fields, Leyte, Philippines. *Proceedings 18th PNOC-EDC Geothermal Conference*, Makati City, Philippines, 182-188.

Pokrovski, G.S., Schott, J., Salvi, G., Gout, R., and Kubicki, J.D., 1998: Structure and stability of aluminium-silica complexes in neutral to basic solutions. Experimental study and molecular orbital calculations. *Min. Mag., 62A,* 1194-1195.

Pruess, K., 2002: *Mathematical modeling of fluid flow and heat transfer in geothermal systems – an introduction in five lectures.* UNU-GTP, Iceland, report 3, 84 pp.

Pyle, D.M., and Mather, T.A., 2009: Halogens in igneous processes and their fluxes to the atmospher and oceans from volcanic activity: a review. *Chemical Geology, 263*, 110-121.

Reed, M.H., and Spycher, N.F., 1989: *SOLVEQ: A computer program for computing aqueous-mineral-gas equilibria. A manual.* Department of Geological Sciences, University of Oregon, Eugene, Oregon, 37 pp.

Reyes, A.G., 1979: *The borehole geology and alteration mineralogy of Malitbog-1, Tongonan, Leyte, Philippines*. UNU-GTP, Iceland, report 1, 84 pp.

Reyes, A.G., 1990: Petrology of Philippine geothermal systems and the application of alteration mineralogy to their assessment. *J. Volc. Geothermal Res., 43*, 279-309.

Reyes, A.G., Giggenbach, W.F., Saleras, J.R.M., Salonga, N.D., and Vergara, M.C., 1993: Petrology and geochemistry of Alto Peak, a vapour-cored hydrothermal system, Leyte province, Philippines. *Geothermics, 22, 5/6*, 479-519.

Reyes, A.G., Trompetter, W.J., Britten, K., and Searle, J., 2002: Mineral deposits in the Rotokawa geothermal pipelines, New Zealand. *J. Volc. Geothermal Res., 119*, 215-239.

Salonga, N.D., and Siega, F.L., 1996: *Preliminary report on the stable isotope geochemistry of Mahanagdong geothermal field, Leyte.* PNOC-EDC internal report (unpublished).

Salonga, N.D., and Auman, R.O., 1997: Gas equilibria in Tongonan, Mahanagdong and Alto Peak geothermal fields, Leyte, Philippines. *Proceedings 18th PNOC-EDC Geothermal Conference*, Makati City, Philippines, 156-165.

Salonga, N.D., Bayon, F.E.B., and Martinez, M.V.M., 2000: The implication of stable 34S and 18O isotope systematics on the sulfur cycle in Mahanagdong hydrothermal system (Philippines). *Proceedings World Geothermal Congress 2000*, Kyushu-Tohoku, Japan, 2845-2850.

Salonga, N.D., Dacillo, D.B., and Siega, F.L., 2004: Providing solutions to the rapid changes induced by stressed production in Mahanagdong geothermal field, Philippines. *Geothermics, 33*, 181-212.

Scott, G.L., 1989: Magmatic chloride and metals in fluids, Tongonan geothermal field, Philippines. *J. Volc. Geothermal Res., 38*, 355-360.

Scott, G.L., 2000: Heat source for Tongonan geothermal field. *The Island Arc, 9*, 513-526.

Scott, G.L., 2001: Hydrothermal alteration and fluid geochemistry of the Tongonan geothermal field, Philippines. *Resource Geology, 51/2*, 117-134.

Seastres, Jr., J.S., Salonga, N.D., Saw, V.S., and Maxino, D.A., 2000: Reservoir management strategies to sustain the full exploitation of Greater Tongonan Geothermal Field, Philippines. *Proceedings World Geothermal Congress 2000*, Kyushu-Tohoku, Japan, 2863-2868.

Siega, F.L., Salonga, N.D., and D'Amore, F., 1999: Gas equilibria controlling H_2S in different Philippine geothermal fields. *Proceedings 20th PNOC-EDC Geothermal Conference*, Makati City, Philippines, 29-35.

Sta. Ana., F.X.M., Hingoyon-Siega, C.S., and Andrino, R.P., 2002: Mahanagdong geothermal sector, Greater Tongonan Geothermal Field, Philippines: reservoir evaluation and modelling update. *Proceedings of the 27th Workshop on Geothermal Reservoir Engineering, Stanford University, California*, 7 pp.

Stefánsson, A., and Arnórsson, S., 2002: Gas pressures and redox reactions in geothermal fluids in Iceland. *Chemical Geology, 190*, 251-271.

Stefánsson, A., and Arnórsson, S., 2005: The geochemistry of As, Mo, Sb and W in natural geothermal waters, Iceland. *Proceedings World Geothermal Congress 2005*, Antalya, Turkey, CD, 6 pp, paper no. 0890.

Stefánsson, A., Gunnarsson, I., and Giroud, N., 2007: New methods for the direct determination of dissolved inorganic, organic and total carbon in natural waters by Reagent-Free™ Ion Chromatography and inductively coupled plasma atomic emission spectrometry. *Analytical Chimica Acta, 582*, 69-72.

Symonds, R.B., Gerlach, T.M., and Reed, M.H., 2001: Magmatic gas scrubbing: implications for volcano monitoring. *J. Volc. Geothermal Res., 108*, 303-341.

Taran, Y., Rouwet, D., Inguaggiato, S., and Aiuppa, A., 2008: Major and trace element geochemistry of neutral and acidic thermal springs at El Chichón volcano, Mexico, implications for monitoring of the volcanic activity. *J. Volc. Geothermal Res., 178*, 224-236.

Urbino, G.A., and Pang Z., 2006: 2003 Inter-laboratory comparison of geothermal water chemistry. In: Pang Z., and, Ármannsson, H. (eds.), *Analytical procedures and quality assurance for geothermal*

water chemistry. UNU-GTP, Reykjavik, Iceland, 131-172.

Urmeneta, N.N.A., 1993: *Natural state simulation of the Mahanagdong geothermal sector, Leyte, Philippines*. UNU-GTP, Iceland, report 15, 30 pp.

Vasquez, N.Z., and Tolentino, B.S., 1972: The geology of the Tongonan geothermal field. *The ComVol Letter, 6 (nos. 3 and 4)*, 1-20.

Were, J., 2007: The *speciation of trace elements in spent geothermal fluids and implications for environmental health around Olkaria, Kenya.* University of Iceland, MSc thesis, UNU-GTP, Iceland, report 1, 73 pp.

White, D.E., Muffler, L.J., and Truesdell, A., 1971: Vapour-dominated hydrothermal system compared with hot-water systems. *Economic Geology, 66,* 75-97.

Zaide-Delfin, M.C., and Dulce, R.G., 1996: Hydrothermal petrology and fluid flows in the Mahanagdong Geothermal Field, Leyte, Philippines. *PNOC-EDC internal report (unpublished).*

Zhang, Y., and Dawhe, R., 1998: The kinetics of calcite precipitation from a high salinity water. *Applied Geochemistry, 13/2*, 177-184.

APPENDIX A: WATER ANALYSES BY DIFFERENT ANALYTICAL METHODS

TABLE 1: pH measurements

Sampling date	Well	pH meter calibration		On-site		During T-CO_2 titration[a]						EDC pH meter[b]	
						Trial 1		Trial 2		Ave.	pH Difference		
		°C	%slope	pH	°C	pH	°C	pH	°C	pH	Trial 1-Trial 2	pH	°C
11Dec08	MG9D[c]			3.32	23.5	ND		ND				3.35	22.7
18Dec08	MN3RD[d]	23.3	95.59	6.67	27.8	6.77	25.1	6.67	24.7	6.72	0.10	ND	
19Dec08	MG9RD[d]	22.4	97.6	8.07	26.2	8.04	23.1	7.97	22.9	8.01	0.07	ND	
26Dec08	MG18D	24.1	102.73	6.48	23.6	6.47	23.2	6.49	21.9	6.48	-0.02	6.18	20.8
	MG23D			6.65	22.8	6.70	21.9	6.71	21.2	6.71	-0.01	6.56	20.8
	MG39D			7.07	24.4	6.94	23.0	6.91	22.9	6.93	0.03	6.83	20.5
07Jan09	MG2D	23.3	98.58	6.14	24.4	6.27	24.6	6.26	24.4	6.27	0.01	5.52	21.4
	MG13D			6.86	24.8	6.84	24.8	6.84	23.9	6.84	0.00	6.18	21.8
	MG7D			6.27	24.1	6.30	23.1	6.33	23.6	6.32	-0.03	5.30	21.5
	MG16D			6.08	24.3	6.22	22.9	6.20	23.1	6.21	0.02	5.95	21.5
	MG22D			6.56	23.8	6.56	23.0	6.59	23.3	6.58	-0.03	6.01	20.6
09Jan09	MG3D	22.4	98.28	6.22	23.7	6.07	23.4	6.11	23.2	6.09	-0.04	5.99	20.8
	MG14D			6.40	24.1	6.46	22.9	6.48	23.0	6.47	-0.02	6.39	20.9
10Jan09	MG29D	23.1	98.72	7.21	22.9	7.14	22.9	7.13	23.1	7.14	0.01	6.96	21.6
	MG27D			8.13	23.0	8.13	23.3	8.11	23.4	8.12	0.02	8.03	20.3
	MG37D			5.13	24.2	5.31	23.3	5.30	23.3	5.31	0.01	4.70	20.9
	MG35D			5.97	23.8	6.08	23.0	6.08	23.4	6.08	0.00	5.94	20.9
13Jan09	MG36D	22.5	98.61	7.01	21.1	6.82	22.5	6.91	22.8	6.87	-0.09	6.86	22.4
	MG19			6.57	21.4	6.42	22.3	6.57	22.9	6.50	-0.15	6.24	22.6
	MG34D			6.07	21.3	5.90	22.1	6.02	23.1	5.96	-0.12	6.05	22.6
	MG32D			6.79	20.7	6.58	20.6	6.63	21.6	6.61	-0.05	6.90	22.0
17Jan09	MG30D	23	98.78	5.89	23.2	6.26	22.1	6.26	22.3	6.26	0.00	6.38	24.0
	MG31D			6.11	21.8	6.25	22.2	6.28	22.3	6.27	-0.03	6.47	24.9
	MG26D			7.51	21.9	7.32	22.2	7.33	22.3	7.33	-0.01	6.60	24.3
	MG28D			4.22	22.6	4.18	21.9	4.18	21.9	4.18	0.00	3.96	25.1
19Jan09	MG24D	23	98.41	5.89	21.9	6.50	26.8	6.51	26.3	6.51	-0.01	5.90	24.2
	MG1			7.80	24.9	7.61	25.8	7.61	25.4	7.61	0.00	7.80	24.0
07Jun09	MG9D[e]			ND	ND	6.33[f]	23.5	6.39[f]	23.4	6.36	-0.06	6.48	27.5
01Jul09	MG9D[e]			ND	ND	5.80[f]	24.2	5.72[f]	24.2	5.76	0.08	5.65	25.0
27Jul09	MG40D			ND	ND	3.97[f]	22.3	3.98[f]	23.7	3.98	-0.01	3.94	24.3
Ave. of Absolute Differences =											0.04		
Standard Deviation of Absolute Differences =											0.04		

[a]-measured shortly after sampling, [b]-measured within 3 days from sampling, [c]-without acid inhibition, [d]-injection wells for separated brine,[e]-with acid inhibition, [f]-using EDC pH meter, ND- not determined

TABLE 2: Sulphide sulphur (H_2S) determination

Sampling date	Well	Titration on-site ($HgAc_2$) with dithizone indicator				EDC[a]	Titration vs EDC
		Trial 1	Trial 2	Ave.	% Mean Difference	mg/kg	% Mean Difference
		mg/kg	mg/kg	mg/kg			
11Dec08	MG9D[b]	16.32	14.62	15.5[c]	11.0	ND	
18Dec08	MN3RD[d]	4.57	4.22	4.40	8.0	ND	
19Dec08	MG9RD[d]	0.77	0.78	0.78	-1.3	ND	
26Dec08	MG18D	2.86	2.7	2.78	5.8	2.26	-21
	MG23D	1.63	1.62	1.63	0.6	1.88	15
	MG39D	2.73	2.52	2.63	8.0	1.98	-28
07Jan09	MG2D	0.34	0.31	0.33	9.2	0.4	21
	MG13D	2.84	2.83	2.84	0.4	2.68	-5.6
	MG7D	0.42	0.42	0.42	0.0	NIL	
	MG16D	0.92	0.96	0.94	-4.3	1.45	43
	MG22D	0.61	0.63	0.62	-3.2	1.22	65
09Jan09	MG3D	3.1	3.08	3.09	0.6	1.83	-51
	MG14D	4.53	4.62	4.58	-2.0	2.05	-76
10Jan09	MG29D	2.86	2.79	2.83	2.5	2.21	-24
	MG27D	2.21	2.23	2.22	-0.9	0.87	-87
	MG37D	0.82	0.82	0.82	0.0	1.32	47
	MG35D	1.28	1.4	1.34	-9.0	2.93	74
13Jan09	MG36D	2.18	4.23	3.21	-64.0	0.61	-136
	MG19	1.06	0.94	1.00	12.0	0.35	-96
	MG34D	2.19	2.12	2.16	3.2	1.87	-14
	MG32D	2.58	2.18	2.38	16.8	13	138
17Jan09	MG30D	0.52	0.53	0.53	-1.9	0.76	37
	MG31D	1.17	1.63	1.40	-32.9	0.03	-192
	MG26D	0.82	0.74	0.78	10.3	NIL	
	MG28D	1.81	1.8	1.81	0.6	ND	
19Jan09	MG24D	4.15	4.13	4.14	0.5	7.61	59
	MG1	1.70	1.72	1.71	-1.2	1.33	-25
07Jun09	MG9D[e]	0.27	0.23	0.25	15.2	1.46	142
01Jul09	MG9D[e]	0.13	0.12	0.13	5.4	0.84	148
27Jul09	MG40D	0.34	0.34	0.34	0.0	ND	
Ave. of Absolute % Mean Differences)=					7.6		67.2
Standard Deviation (σ) of Absolute % Mean Differences =					12.9		52.2

[a] Iodometry, [b] without acid inhibition, [c] excluded in Mean, may be over-titrated due to coloured precipitates, [d] injection wells for separated brine, [e] with acid inhibition, ND- not determined, NIL- not detected

TABLE 3: Total carbonate carbon (T-CO_2) determination

Sampling Date	Well	Titration[a]				ICP-AES (Unfiltered)				ICP-AES (Filtered)				EDC[b]
		Trial 1	Trial 2	Ave.	% Ave. Difference	Trial 1	Trial 2	Ave.	% Mean Difference	Trial 1	Trial 2	Ave.	% Mean Difference	mg/kg
		mg/kg	mg/kg	mg/kg		mg/kg	mg/kg	mg/kg		mg/kg	mg/kg	mg/kg		
11Dec08	MG9D[e]	ND	ND			11.6	11.5	11.5	1.0	5.1	4.7	4.9	8.2	ND
18Dec08	MN3RD[d]	54.8	56.1	55.5	-2.3	39.0	42.3	40.7	-8.0	23.7	24.6	24.1	-4.0	ND
19Dec08	MG9RD[d]	3.5	4.5	4.0	-25.0	6.4	6.8	6.6	-5.9	6.7	5.9	6.3	11.8	ND
26Dec08	MG18D	40.2	39.9	40.1	0.7	34.4	34.1	34.2	1.1	25.6	26.3	26.0	-2.9	43.5
	MG23D	43	43.8	43.4	-1.8	32.0	32.2	32.1	-0.5	28.2	29.8	29.0	-5.5	39.3
	MG39D	45.8	50.2	48.0	-9.2	39.8	30.5	35.2	26.5	31.2	31.6	31.4	-1.2	49.7
07Jan09	MG2D	50.3	55.3	52.8	-9.5	46.2	52.9	49.5	-13.6	21.8	21.2	21.5	2.7	72.5
	MG13D	62.8	60.8	61.8	3.2	52.6	53.7	53.1	-2.0	45.0	47.0	46.0	-4.4	55.9
	MG7D	40.6	35.9	38.3	12.3	32.2	37.3	34.7	-14.8	17.4	17.0	17.2	2.1	108
	MG16D	58.4	64.5	61.5	-9.9	53.0	53.4	53.2	-0.8	31.7	32.4	32.0	-2.2	72.3
	MG22D	39.3	30.9	35.1	23.9	27.0	26.6	26.8	1.3	18.2	18.1	18.2	0.3	40.4
09Jan09	MG3D	60.4	50.4	55.4	18.1	47.1	52.6	49.8	-10.9	21.6	21.8	21.7	-1.2	38.1
	MG14D	44.1	59.4	51.8	-29.6	37.0	35.7	36.4	3.5	25.9	26.9	26.4	-3.9	40.6
10Jan09	MG29D	18.5	34.1	26.3	-59.3	30.5	28.0	29.3	8.8	24.9	26.5	25.7	-6.3	39
	MG27D	28.4	28.7	28.6	-1.1	30.3	30.0	30.2	1.2	37.0	40.0	38.5	-7.6	37.4
	MG37D	60.6	43.6	52.1	32.6	33.2	27.3	30.3	19.5	10.4	9.6	10.0	7.3	36.1
	MG35D	70.6	71.3	71.0	-1.0	63.6	49.6	56.6	24.8	25.9	25.5	25.7	1.8	66
13Jan09	MG36D	39.1	36.8	38.0	6.1	32.7	27.9	30.3	15.8	26.3	26.6	26.5	-1.0	32.9
	MG19	83.9	64.5	74.2	26.1	49.7	48.7	49.2	2.0	41.0	42.9	42.0	-4.5	58.6
	MG34D	103.8	81	92.4	24.7	63.2	55.2	59.2	13.5	22.6	22.2	22.4	1.7	33.1
	MG32D	231.8	217.6	224.7	6.3	212	210	210.5	0.9	157.8	172.6	165.2	-8.9	181
17Jan09	MG30D	54.9	49	52.0	11.4	46.5	45.9	46.2	1.2	29.2	29.1	29.2	0.6	26
	MG31D	56.1	44.3	50.2	23.5	42.8	39.6	41.2	7.8	23.6	24.4	24.0	-3.4	38.8
	MG26D	23.3	19.2	21.3	19.3	ND	ND			ND	ND			25.9
	MG28D	37.8	31.8	34.8	17.2	26.3	24.2	25.3	8.2	8.5	8.7	8.6	-2.4	ND
19Jan09	MG24D	115.3	117.1	116.2	-1.5	ND	ND			ND	ND			208
	MG1	42.2	47	44.6	-10.8	ND	ND			ND	ND			41.6
07Jun09	MG9D[e]	8.5	22.6	15.5	-90.9	ND	ND			ND	ND			2.83
01Jul09	MG9D[e]	7.7	4.7	6.2	47.3	7.5	6.9	7.2	7.6	ND	ND			0.64
27Jul09	MG40D	ND	ND			17.5	16.5	17.0	5.6	ND	ND			ND
Ave. of Absolute % Mean Differences =					18.1				8.0				4.0	
SD (σ) of Absolute % Mean Differences =					20.1				7.6				3.0	

[a] measured shortly after sampling, [b] titration, measured within 3 days from sampling, [c] without acid inhibition, [d] injection wells for separated brine, [e] with acid inhibition, ND- not determined

TABLE 4: B determination

Date	Well	ICP-AES				ICP-MS[a]				EDC[b]	ICP-AES vs EDC
		Trial 1	Trial 2	Ave.	% Mean Difference	Trial 1	Trial 2	Ave.	% Mean Difference	mg/kg	% Mean Difference
		mg/kg	mg/kg	mg/kg		mg/kg	mg/kg	mg/kg			
11Dec08	MG9D[c]	32.5	32.8	32.7	-1.0	24.983	20.309	22.646	20.6	32.3	1.2
18Dec08	MN3R[d]	35.3	36.0	35.6	-1.7	32.529	26.198	29.364	21.6	29.2	19.9
19Dec08	MG9R[d]	53.5	54.5	54.0	-1.8	48.722	37.869	43.295	25.1	ND	
26Dec08	MG18D	50.9	51.6	51.3	-1.3	46.748	36.839	41.794	23.7	47.5	7.6
	MG23D	42.6	43.3	42.9	-1.5	40.961	32.460	36.711	23.2	44.9	-4.4
	MG39D	57.5	57.5	57.5	0.0	51.643	44.530	48.087	14.8	54.6	5.2
07Jan09	MG2D	52.1	52.7	52.4	-1.2	49.662	39.977	44.820	21.6	55.3	-5.3
	MG13D	57.1	56.4	56.8	1.2	51.651	41.938	46.794	20.8	43.4	26.7
	MG7D	58.3	58.9	58.6	-0.9	53.640	42.706	48.173	22.7	59.3	-1.1
	MG16D	60.8	62.6	61.7	-2.9	57.199	45.570	51.384	22.6	62.1	-0.6
	MG22D	59.5	59.9	59.7	-0.6	53.720	45.159	49.440	17.3	54.0	10.0
09Jan09	MG3D	41.8	42.5	42.1	-1.7	40.262	36.733	38.498	9.2	38.9	8.0
	MG14D	53.6	55.0	54.3	-2.7	51.468	39.943	45.706	25.2	51.0	6.2
10Jan09	MG29D	32.9	32.1	32.5	2.6	30.394	24.857	27.626	20.0	29.0	11.4
	MG27D	25.6	25.8	25.7	-0.5	25.360	20.337	22.849	22.0	25.9	-0.8
	MG37D	62.9	63.1	63.0	-0.2	57.858	45.614	51.736	23.7	59.0	6.5
	MG35D	73.9	74.6	74.3	-0.9	68.962	55.288	62.125	22.0	72.2	2.8
13Jan09	MG36D	36.1	35.2	35.6	2.7	33.429	26.847	30.138	21.8	29.1	20.2
	MG19	49.2	49.7	49.4	-0.9	46.482	37.608	42.045	21.1	45.2	9.0
	MG34D	61.0	60.5	60.8	0.9	58.479	46.253	52.366	23.3	56.7	6.9
	MG32D	20.3	20.6	20.4	-1.5	21.031	16.367	18.699	24.9	18.5	9.8
17Jan09	MG30D	33.2	33.6	33.4	-1.2	32.429	27.647	30.038	15.9	39.5	-16.8
	MG31D	43.0	43.2	43.1	-0.4	41.019	33.170	37.095	21.2	39.1	9.8
	MG26D	33.2	33.7	33.4	-1.4	30.833	27.935	29.384	9.9	29.3	13.2
	MG28D	40.7	41.0	40.8	-0.9	39.910	31.699	35.804	22.9	37.2	9.3
19Jan09	MG24D	26.5	26.9	26.7	-1.4	24.188	20.635	22.412	15.9	24.0	10.6
	MG1	31.9	32.3	32.1	-1.3	31.940	26.936	29.438	17.0	31.9	0.7
07Jun09	MG9D[e]	38.4	38.5	38.5	-0.2	42.497	32.146	37.322	27.7	41.6	-7.8
01Jul09	MG9D[e]	39.0	39.3	39.2	-0.5	40.208	32.782	36.495	20.3	41.0	-4.6
27Jul09	MG40D	66.2	66.5	66.4	-0.5	59.633	47.009	53.321	23.7	81.6	-20.6
Ave. of Absolute % Mean Differences =					1.2				20.7		8.9
SD (σ) of Absolute % Mean Differences =					0.8				4.2		6.7

[a] readings mostly above standard values, [b] titrimetry (mannitol), [c] without acid inhibition, [d] injection wells for separated brine,[e] with acid inhibition, ND- not determined

TABLE 5: Total silica (as SiO2) determination

Date	Well	ICP-AES				EDC[a]	ICP-AES vs EDC
		Trial 1	Trial 2	Ave.	% Mean Difference	mg/kg	% Mean Difference
		mg/kg	mg/kg	mg/kg			
11Dec08	MG9D[b]	849	903	876	-6.2	1036	-16.7
18Dec08	MN3RD[c]	671	714	692	-6.2	654	5.7
19Dec08	MG9RD[c]	680	722	701	-6.0	687	2.0
26Dec08	MG18D	617	654	635	-5.8	607	4.5
	MG23D	616	651	634	-5.4	598	5.8
	MG39D	715	754	734	-5.3	698	5.1
07Jan09	MG2D	628	664	646	-5.6	651	-0.8
	MG13D	795	842	819	-5.7	755	8.1
	MG7D	696	737	716	-5.8	683	4.8
	MG16D	737	771	754	-4.5	712	5.7
	MG22D	724	764	744	-5.4	679.0	9.1
09Jan09	MG3D	564	599	581	-6.0	549	5.7
	MG14D	671	695	683	-3.5	643.0	6.0
10Jan09	MG29D	723	754	739	-4.2	692.0	6.5
	MG27D	600	631	615	-5.0	573	7.1
	MG37D	797	838	818	-5.0	802.0	1.9
	MG35D	885	948	916	-6.8	877	4.4
13Jan09	MG36D	676	709	693	-4.8	642	7.6
	MG19	679	713	696	-5.0	644	7.8
	MG34D	593	621	607	-4.6	572	6.0
	MG32D	458	483	471	-5.2	447	5.1
17Jan09	MG30D	603	635	619	-5.3	591	4.6
	MG31D	686	720	703	-4.8	661	6.2
	MG26D	671	706	689	-5.0	640	7.3
	MG28D	599	630	614	-5.1	579	5.9
19Jan09	MG24D	806	849	828	-5.2	772.0	6.9
	MG1	544	577	560	-5.9	540	3.7
07Jun09	MG9D[d]	418	419	419	-0.2	557	-28.3
01Jul09	MG9D[d]	547	547	547	0.0	587.0	-7.0
27Jul09	MG40D	874	888	881	-1.5	895	-1.6
Ave. of Absolute % Mean Differences =					4.8		6.6
SD (σ) of Absolute % Mean Differences =					1.6		5.0

[a] spectrophotometry (heteropoly blue), [b] without acid inhibition, [c] injection wells for separated brine,[d] with acid inhibition, ND- not determined

TABLE 6: Cl determination

Date	Well	ICP-AES				IC				EDC[a]	ICP-AES vs EDC
		Trial 1	Trial 2	Ave.	% Mean	Trial 1	Trial 2	Ave.	% Mean	mg/kg	% Mean
		mg/kg	mg/kg	mg/kg	Difference	mg/kg	mg/kg	mg/kg	Difference		Difference
11Dec08	MG9D[b]	3003	2987	2995	0.6	2886	2978	2932	-3.1	3189	-6.3
18Dec08	MN3R[c]	3386	3348	3367	1.1	3397	3461	3429	-1.9	3478	-3.2
19Dec08	MG9R[c]	3948	3878	3913	1.8	4335	4396	4365	-1.4	4045	-3.3
26Dec08	MG18D	3627	3679	3653	-1.4	3731	3819	3775	-2.3	3725	-2.0
	MG23D	3087	3075	3081	0.4	3142	3229	3185	-2.7	3116	-1.1
	MG39D	3643	4051	3847	-10.6	4217	4323	4270	-2.5	4181	-8.3
07Jan09	MG2D	3795	3719	3757	2.0	3989	4049	4019	-1.5	4157	-10.1
	MG13D	3751	3731	3741	0.5	3751	3838	3794	-2.3	3786	-1.2
	MG7D	4219	3655	3937	14.3	4174	4268	4221	-2.2	4216	-6.8
	MG16D	4408	4385	4396	0.5	4386	4494	4440	-2.4	4512	-2.6
	MG22D	4278	4279	4278	0.0	4243	4223	4233	0.5	4263	0.4
09Jan09	MG3D	3770	3729	3749	1.1	3716	3781	3748	-1.7	3736	0.4
	MG14D	5672	5028	5350	12.0	5668	5786	5727	-2.1	5797	-8.0
10Jan09	MG29D	3581	3555	3568	0.7	3595	3726	3661	-3.6	3514	1.5
	MG27D	1967	1937	1952	1.5	1945	2007	1976	-3.1	2037	-4.3
	MG37D	7511	7400	7455	1.5	7983	8132	8058	-1.8	7492	-0.5
	MG35D	4183	4152	4168	0.8	4183	4167	4175	0.4	4216	-1.2
13Jan09	MG36D	2685	2623	2654	2.3	2659	2751	2705	-3.4	2668	-0.5
	MG19	3554	3557	3556	-0.1	3583	3658	3621	-2.1	3475	2.3
	MG34D	4197	4134	4166	1.5	4287	4404	4346	-2.7	4216	-1.2
	MG32D	613	606	609	1.3	582	586	584	-0.6	562	8.1
17Jan09	MG30D	3158	3532	3345	-11.2	3605	3710	3658	-2.9	3567	-6.4
	MG31D	4133	4050	4091	2.0	4157	4295	4226	-3.3	4202	-2.7
	MG26D	2714	2282	2498	17.3	2765	2830	2798	-2.3	2671	-6.7
	MG28D	3562	3575	3569	-0.4	3557	3670	3613	-3.1	3587	-0.5
19Jan09	MG24D	2129	2291	2210	-7.3	2325	2398	2361	-3.1	2348	-6.1
	MG1	2312	2261	2286	2.3	2272	2309	2291	-1.6	2389	-4.4
07Jun09	MG9D[d]	3891	3880	3885	0.3	3991	3978	3984	0.3	4256	-9.1
01Jul09	MG9D[d]	3993	3996	3994	-0.1	4194	4196	4195	0.0	4324	-7.9
27Jul09	MG40D	7156	7162	7159	-0.1	5999	5983	5991	0.3	6228	13.9
Ave. of Absolute % Mean Differences =					3.2				2.0		4.4
SD (σ) of Absolute % Mean Differences =					4.8				1.0		3.6

[a] Argentometric-Potentiometric, [b] without acid inhibition, [c] injection wells for separated brine, [d] with acid inhibition, ND- not determined

TABLE 7: Na determination

Date	Well	ICP-AES				EDC[a]	ICP-AES vs EDC
		Trial 1	Trial 2	Ave.	% Mean	mg/kg	% Mean Difference
		mg/kg	mg/kg	mg/kg	Difference		
11Dec08	MG9D[b]	1902	1893	1898	0.5	2013	-5.9
18Dec08	MN3RD[c]	1987	1975	1981	0.6	2103	-6.0
19Dec08	MG9RD[c]	2286	2290	2288	-0.1	2381	-4.0
26Dec08	MG18D	2217	2215	2216	0.1	2289	-3.2
	MG23D	1837	1817	1827	1.1	1822	0.3
	MG39D	2445	2397	2421	2.0	2498	-3.1
07Jan09	MG2D	2163	2161	2162	0.1	2400	-10.4
	MG13D	2304	2214	2259	4.0	2260	0.0
	MG7D	2437	2412	2424	1.1	2472	-1.9
	MG16D	2500	2602	2551	-4.0	2597	-1.8
	MG22D	2477	2452	2464	1.0	2423	1.7
09Jan09	MG3D	2185	2181	2183	0.2	2215	-1.4
	MG14D	3190	3274	3232	-2.6	3228	0.1
10Jan09	MG29D	2170	2062	2116	5.1	2054	3.0
	MG27D	1286	1267	1276	1.5	1189	7.1
	MG37D	3780	3668	3724	3.0	3711	0.4
	MG35D	2646	2599	2622	1.8	2645	-0.9
13Jan09	MG36D	1775	1647	1711	7.5	1591	7.3
	MG19	2086	2057	2071	1.4	2036	1.7
	MG34D	2607	2514	2560	3.7	2590	-1.1
	MG32D	900	891	896	1.0	791	12.4
17Jan09	MG30D	2125	2094	2110	1.5	2084	1.2
	MG31D	2425	2384	2405	1.7	2405	0.0
	MG26D	1658	1650	1654	0.5	1597	3.5
	MG28D	2140	2120	2130	0.9	2172	-2.0
19Jan09	MG24D	1382	1377	1380	0.4	1318	4.6
	MG1	1455	1437	1446	1.2	1452	-0.4
07Jun09	MG9D[d]	2378	2408	2393	-1.3	2561	-6.8
01Jul09	MG9D[d]	2405	2415	2410	-0.4	2816	-15.5
27Jul09	MG40D	3480	3492	3486	-0.3	3087	12.1
Ave. of Absolute % Mean Differences =					1.7		4.0
SD (σ) of Absolute % Mean Differences =					1.7		4.1

[a] AAS, [b] without acid inhibition, [c] injection wells for separated brine, [d] with acid inhibition, ND- not determined

TABLE 8: K determination

Date	Well	ICP-AES				EDC[a]	ICP-AES vs EDC
		Trial 1	Trial 2	Ave.	% Mean Difference	mg/kg	% Mean Difference
		mg/kg	mg/kg	mg/kg			
11Dec08	MG9D[b]	358	361	360	-0.7	372	-3.4
18Dec08	MN3RD[c]	369	369	369	-0.1	372	-0.8
19Dec08	MG9RD[c]	434	435	434	-0.2	429	1.3
26Dec08	MG18D	351	352	351	-0.3	348	0.9
	MG23D	332	334	333	-0.5	312	6.6
	MG39D	476	472	474	0.7	455	4.1
07Jan09	MG2D	428	428	428	0.1	433	-1.1
	MG13D	473	460	467	2.8	425	9.4
	MG7D	480	480	480	0.0	470	2.1
	MG16D	507	525	516	-3.5	493	4.5
	MG22D	505	503	504	0.5	463	8.5
09Jan09	MG3D	368	370	369	-0.5	355	3.8
	MG14D	663	694	679	-4.6	647	4.8
10Jan09	MG29D	450	430	440	4.4	410	7.1
	MG27D	177	175	176	0.7	164	7.0
	MG37D	1228	1224	1226	0.4	1174	4.3
	MG35D	506	508	507	-0.3	447	12.6
13Jan09	MG36D	283	270	276	4.7	256	7.6
	MG19	417	415	416	0.4	399	4.2
	MG34D	419	412	415	1.8	398	4.3
	MG32D	90.9	90.7	90.8	0.2	85	6.6
17Jan09	MG30D	388	388	388	0.1	367	5.6
	MG31D	449	450	450	-0.2	419	7.1
	MG26D	258	259	259	-0.3	246	5.0
	MG28D	412	411	412	0.2	413	-0.3
19Jan09	MG24D	335	336	335	-0.1	324	3.5
	MG1	213	212	212	0.3	214	-0.8
07Jun09	MG9D[d]	418	418	418	-0.1	421	-0.7
01Jul09	MG9D[d]	431	433	432	-0.6	453	-4.8
27Jul09	MG40D	981	986	983	-0.5	847	14.9
Ave. of Absolute % Mean Differences =					1.0		4.9
SD (σ) of Absolute % Mean Differences =					1.4		3.5

[a] AAS, [b] without acid inhibition, [c] injection wells for separated brine, [d] with acid inhibition, ND- not determined

TABLE 9: Ca determination

Date	Well	ICP-AES				EDC[a]	ICP-AES vs EDC
		Trial 1	Trial 2	Ave.	% Mean Difference	mg/kg	% Mean Difference
		mg/kg	mg/kg	mg/kg			
11Dec08	MG9D[b]	31.2	31.6	31.4	-1.2	26.2	18.0
18Dec08	MN3RD[c]	35.7	35.8	35.8	-0.2	ND	
19Dec08	MG9RD[c]	31.7	31.6	31.7	0.3	ND	
26Dec08	MG18D	24.0	24.1	24.1	-0.3	23.8	1.1
	MG23D	30.3	30.4	30.3	-0.2	30.1	0.7
	MG39D	22.5	22.4	22.5	0.5	22.1	1.7
07Jan09	MG2D	29.7	29.5	29.6	0.6	32.7	-9.9
	MG13D	7.70	7.50	7.60	2.6	6.9	9.7
	MG7D	40.4	40.2	40.3	0.5	39.8	1.1
	MG16D	37.0	38.9	38.0	-4.9	38.5	-1.4
	MG22D	39.5	39.2	39.3	0.8	37.1	5.9
09Jan09	MG3D	40.3	40.6	40.4	-0.7	40.8	-1.0
	MG14D	93.0	96.6	94.8	-3.8	98.4	-3.8
10Jan09	MG29D	41.0	39.0	40.0	4.9	40.0	0.0
	MG27D	9.90	9.87	9.88	0.3	9.6	2.9
	MG37D	240	240	240	0.01	268	-11.0
	MG35D	19.9	20.0	20.0	-0.5	18.4	8.2
13Jan09	MG36D	16.9	16.0	16.5	5.8	14.1	15.5
	MG19	26.1	26.1	26.1	0.1	25.2	3.5
	MG34D	41.9	41.1	41.5	1.7	46.0	-10.3
	MG32D	7.47	7.56	7.52	-1.1	17.5	-79.8
17Jan09	MG30D	44.2	44.4	44.3	-0.4	45.2	-2.0
	MG31D	41.3	41.2	41.2	0.3	41.4	-0.4
	MG26D	36.8	36.8	36.8	-0.04	36.6	0.5
	MG28D	25.3	25.3	25.3	-0.3	26.1	-3.1
19Jan09	MG24D	21.1	21.2	21.2	-0.2	25.8	-19.8
	MG1	17.0	17.2	17.1	-1.1	35.6	-70.4
07Jun09	MG9D[d]	14.3	14.6	14.4	-2.5	17.0	-16.3
01Jul09	MG9D[d]	17.7	17.8	17.8	-0.6	19.0	-6.6
27Jul09	MG40D	216	217	216	-0.4	162	28.7
Ave. of Absolute % Mean Differences =					1.2		11.9
SD (σ) of Absolute % Mean Differences =					1.6		19.3

[a] AAS, [b] without acid inhibition, [c] injection wells for separated brine, [d] with acid inhibition, ND- not determined

TABLE 10: Mg determination

Date	Well	ICP-AES				EDC[a]	ICP-AES vs EDC
		Trial 1	Trial 2	Ave.	% Mean Difference	mg/kg	% Mean Difference
		mg/kg	mg/kg	mg/kg			
11Dec08	MG9D[b]	39.3	39.8	39.6	-1.2	31.1	23.9
18Dec08	MN3RD[c]	0.347	0.359	0.353	-3.5	ND	
19Dec08	MG9RD[c]	0.037	0.040	0.038	-6.6	ND	
26Dec08	MG18D	0.028	0.030	0.029	-6.4	0.12	-121.5
	MG23D	0.021	0.023	0.022	-8.6	<0.05	
	MG39D	0.023	0.025	0.024	-6.3	<0.05	
07Jan09	MG2D	0.028	0.037	0.033	-26.3	<0.05	
	MG13D	0.016	0.019	0.017	-21.5	<0.05	
	MG7D	0.027	0.030	0.028	-10.6	<0.05	
	MG16D	0.032	0.033	0.033	-3.6	<0.05	
	MG22D	0.027	0.028	0.027	-5.4	<0.05	
09Jan09	MG3D	0.233	0.239	0.236	-2.5	0.13	58.1
	MG14D	0.345	0.337	0.341	2.2	0.3	26.9
10Jan09	MG29D	0.036	0.040	0.038	-9.2	<0.05	
	MG27D	0.033	0.035	0.034	-7.0	<0.05	
	MG37D	6.87	7.01	6.94	-1.9	5.9	16.0
	MG35D	0.733	0.750	0.742	-2.3	0.6	21.1
13Jan09	MG36D	0.013	0.014	0.013	-5.4	<0.05	
	MG19	0.016	0.017	0.016	-7.8	<0.05	
	MG34D	0.246	0.250	0.248	-1.6	0.16	43.2
	MG32D	0.014	0.015	0.014	-7.1	<0.05	
17Jan09	MG30D	0.035	0.036	0.035	-4.6	<0.05	
	MG31D	0.164	0.166	0.165	-1.6	0.1	49.0
	MG26D	0.069	0.071	0.070	-2.5	<0.05	
	MG28D	7.54	7.65	7.60	-1.4	7.4	2.6
19Jan09	MG24D	0.153	0.162	0.158	-5.5	<0.05	
	MG1	0.018	0.021	0.019	-14.4	<0.05	
07Jun09	MG9D[d]	12.7	12.7	12.7	0.0	14.3	-12.0
01Jul09	MG9D[d]	16.7	16.7	16.7	0.3	18.2	-8.4
27Jul09	MG40D	17.0	17.1	17.0	-0.2	ND	
Ave. of Absolute % Mean Differences =					5.9		34.8
SD (σ) of Absolute % Mean Differences =					6.0		33.6

[a] AAS, [b] without acid inhibition, [c] injection wells for separated brine, [d] with acid inhibition, ND- not determined

TABLE 11: F determination

Date	Well	IC			
		Trial 1	Trial 2	Ave.	% Mean Difference
		mg/kg	mg/kg	mg/kg	
11Dec08	MG9D[a]	1.51	1.41	1.46	6.7
18Dec08	MN3RD[b]	1.83	1.70	1.77	7.1
19Dec08	MG9RD[b]	1.74	1.63	1.69	6.7
26Dec08	MG18D	1.71	1.61	1.66	5.9
	MG23D	1.71	1.56	1.64	8.9
	MG39D	1.70	1.63	1.66	4.6
07Jan09	MG2D	1.71	1.61	1.66	5.7
	MG13D	2.39	2.21	2.30	7.9
	MG7D	1.46	1.38	1.42	5.3
	MG16D	1.62	1.53	1.57	6.0
	MG22D	1.46	1.37	1.42	6.2
09Jan09	MG3D	1.18	1.12	1.15	5.3
	MG14D	1.36	1.28	1.32	6.5
10Jan09	MG29D	1.98	1.93	1.96	2.8
	MG27D	1.93	1.79	1.86	7.5
	MG37D	3.10	2.92	3.01	5.7
	MG35D	5.56	5.30	5.43	4.9
13Jan09	MG36D	2.01	1.91	1.96	4.8
	MG19	1.47	1.38	1.42	6.0
	MG34D	1.36	1.31	1.33	3.5
	MG32D	2.93	2.77	2.85	5.5
17Jan09	MG30D	1.48	1.40	1.44	5.8
	MG31D	1.52	1.44	1.48	5.4
	MG26D	1.87	1.77	1.82	5.5
	MG28D	1.69	1.61	1.65	5.1
19Jan09	MG24D	1.59	1.49	1.54	6.5
	MG1	1.78	1.69	1.74	5.3
07Jun09	MG9D[c]	1.38	1.37	1.37	0.6
01Jul09	MG9D[c]	1.35	1.34	1.34	0.6
27Jul09	MG40D	2.65	2.66	2.66	-0.2
Ave. of Absolute % Mean Differences =					5.3
SD (σ) of Absolute % Mean Differences =					2.0

[a] without acid inhibition, [b] injection wells for separated brine, [c] with acid inhibition

TABLE 12: Total sulphur (as SO4) determination

Date	Well	ICP-AES				IC				EDC[a]	ICP-AES vs EDC
		Trial 1	Trial 2	Ave.	% Mean	Trial 1	Trial 2	Ave.	% Mean	mg/kg	% Mean Difference
		mg/kg	mg/kg	mg/kg	Difference	mg/kg	mg/kg	mg/kg	Difference		
11Dec08	MG9D[b]	2125	2186	2155	-2.8	2113	2047	2080	3.2	113	180.1
18Dec08	MN3R[c]	65.0	66.0	65.5	-1.6	72.5	67.6	70.0	6.9	ND	
19Dec08	MG9R[c]	49.7	51.2	50.4	-3.1	48.3	45.4	46.8	6.2	ND	
26Dec08	MG18D	60.9	61.5	61.2	-1.0	56.7	54.3	55.5	4.3	43.7	33.3
	MG23D	47.2	47.2	47.2	0.0	40.4	38.7	39.5	4.4	46.0	2.5
	MG39D	32.2	31.3	31.8	2.9	30.4	29.6	30.0	2.4	25.2	23.1
07Jan09	MG2D	28.6	29.0	28.8	-1.4	31.5	29.8	30.7	5.7	40.0	-32.6
	MG13D	122	125	123	-2.2	129	121	125	5.7	125	-1.3
	MG7D	23.3	24.0	23.7	-2.9	17.2	16.5	16.9	4.2	24.9	-5.1
	MG16D	24.9	22.2	23.6	11.1	24.0	22.7	23.4	5.4	20.5	13.9
	MG22D	23.8	24.0	23.9	-0.8	19.1	18.0	18.6	5.6	27.4	-13.7
09Jan09	MG3D	71.4	69.9	70.6	2.2	73.6	69.4	71.5	5.9	91.8	-26.0
	MG14D	77.5	70.5	74.0	9.5	79.3	74.9	77.1	5.7	66.4	10.9
10Jan09	MG29D	56.2	56.8	56.5	-0.9	47.0	45.0	46.0	4.2	48.3	15.7
	MG27D	74.9	75.3	75.1	-0.6	65.7	63.0	64.4	4.1	75.0	0.1
	MG37D	34.7	35.7	35.2	-2.8	28.5	28.0	28.3	1.8	27.4	25.0
	MG35D	513	522	517	-1.9	441	438	440	0.6	550	-6.1
13Jan09	MG36D	44.7	46.1	45.4	-3.0	38.5	38.3	38.4	0.7	45.2	0.5
	MG19	31.8	32.0	31.9	-0.5	24.3	22.9	23.6	6.1	33.5	-4.9
	MG34D	110	110	110	-0.5	113	110	111	2.8	118	-7.0
	MG32D	921	935	928	-1.4	809	813	811	-0.5	912	1.7
17Jan09	MG30D	45.2	44.7	44.9	1.1	32.8	32.0	32.4	2.3	38.7	14.9
	MG31D	40.1	38.9	39.5	3.1	39.3	38.4	38.8	2.5	43.0	-8.5
	MG26D	95.0	96.4	95.7	-1.4	89.6	86.3	87.9	3.8	95.0	0.7
	MG28D	342	349	345	-1.9	361	350	355	3.1	344	0.4
19Jan09	MG24D	95.7	94.7	95.2	1.1	113	108	111	4.5	91.7	3.8
	MG1	84.9	86.6	85.7	-1.9	83.0	78.1	80.5	6.2	89.0	-3.7
07Jun09	MG9D[d]	437	441	439	-0.7	533	537	535	-0.9	536	-19.9
01Jul09	MG9D[d]	377	380	378	-0.6	429	432	431	-0.5	405	-6.8
27Jul09	MG40D	73.2	73.3	73.2	-0.2	82.5	81.6	82.1	1.1	ND	
Ave. of Absolute % Mean Differences =					2.2				3.7		17.1
SD (σ) of Absolute % Mean Differences =					2.4				2.0		34.1

[a] colorimetry (barium chromate/bromophenol blue), [b] without acid inhibition, [c] injection wells for separated brine, [d] with acid inhibition, ND- not determined

TABLE 13: Al determination

Date	Well	ICP-AES				ICP-MS	ICP-AES vs ICP-MS
		Trial 1	Trial 2	Ave.	% Mean Difference	mg/kg	% Mean Difference
		mg/kg	mg/kg	mg/kg			
11Dec08	MG9D[a]	2.19	2.34	2.26	-6.8	0.3054	152.4
18Dec08	MN3RD[b]	0.215	0.222	0.218	-3.1	0.2216	-1.6
19Dec08	MG9RD[b]	0.222	0.233	0.227	-4.7	0.2251	0.9
26Dec08	MG18D	0.355	0.361	0.358	-1.8	0.3766	-5.0
	MG23D	0.373	0.384	0.379	-3.1	0.3931	-3.8
	MG39D	0.331	0.342	0.336	-3.2	0.3598	-6.7
07Jan09	MG2D	0.325	0.330	0.327	-1.7	0.3370	-2.9
	MG13D	0.339	0.356	0.348	-4.9	0.3623	-4.2
	MG7D	0.273	0.280	0.277	-2.4	0.2843	-2.7
	MG16D	0.311	0.303	0.307	2.7	0.3540	-14.2
	MG22D	0.251	0.252	0.252	-0.1	0.2537	-0.8
09Jan09	MG3D	0.210	0.214	0.212	-1.8	0.2220	-4.8
	MG14D	0.227	0.210	0.219	7.6	0.2456	-11.7
10Jan09	MG29D	0.179	0.182	0.180	-1.8	0.1894	-4.9
	MG27D	0.618	0.632	0.625	-2.2	0.6485	-3.7
	MG37D	0.145	0.147	0.146	-1.4	0.1362	6.7
	MG35D	0.276	0.284	0.280	-2.8	0.3198	-13.3
13Jan09	MG36D	0.487	0.514	0.500	-5.3	0.6492	-25.9
	MG19	0.341	0.356	0.349	-4.3	0.3890	-10.9
	MG34D	0.182	0.186	0.184	-2.1	0.1906	-3.6
	MG32D	0.741	0.756	0.749	-2.0	0.7996	-6.6
17Jan09	MG30D	0.230	0.233	0.232	-1.1	0.2165	6.7
	MG31D	0.325	0.333	0.329	-2.6	0.3569	-8.2
	MG26D	0.365	0.376	0.370	-2.9	0.3681	0.6
	MG28D	0.164	0.163	0.164	0.7	0.1343	19.8
19Jan09	MG24D	0.241	0.243	0.242	-1.1	0.2377	1.7
	MG1	0.470	0.492	0.481	-4.6	0.5170	-7.3
07Jun09	MG9D[c]	0.187	0.183	0.185	2.2	0.1288	35.6
01Jul09	MG9D[c]	0.111	0.112	0.111	-1.4	0.0736	40.9
27Jul09	MG40D	0.765	0.775	0.770	-1.3	0.1268	143.4
Ave. of Absolute % Mean Differences =					2.8		18.4
SD (σ) of Absolute % Mean Differences =					1.8		36.6

[a] without acid inhibition, [b] injection wells for separated brine, [c] with acid inhibition

TABLE 14: Total Fe determination

Date	Well	ICP-AES				ICP-MS	ICP-AES vs ICP-MS	EDC[a]	ICP-AES vs EDC
		Trial 1	Trial 2	Ave.	% Mean	mg/kg	% Mean Difference	mg/kg	% Mean Difference
		mg/kg	mg/kg	mg/kg	Difference				
11Dec08	MG9D[b]	829	851	840	-2.7	743.0772	12.3	47.8	178
18Dec08	MN3RD[c]	0.08	0.09	0.09	-5.7	0.5484	-146	0.34	-120
19Dec08	MG9RD[c]	0.48	0.48	0.48	0.4	1.4232	-98.6	0.21	79
26Dec08	MG18D	0.08	0.09	0.08	-12.9	1.7223	-182	0.22	-92.3
	MG23D	0.19	0.34	0.26	-57.3	0.2509	4.3	0.28	-6.7
	MG39D	0.04	0.05	0.05	-5.6	0.1265	-93.9	<0.05	
07Jan09	MG2D	0.14	0.15	0.14	-2.9	0.0936	42.8	0.78	-137
	MG13D	0.25	0.29	0.27	-15.3	0.1326	68.4	0.17	45.7
	MG7D	0.25	0.26	0.25	-2.9	0.0644	119	<0.05	
	MG16D	0.08	0.09	0.09	-10.6	0.0136	147	<0.05	
	MG22D	0.06	0.06	0.06	-8.0	0.0236	88.1	0.23	-116
09Jan09	MG3D	0.03	0.03	0.03	-13.6	0.0024	168	0.1	-114
	MG14D	0.12	0.13	0.13	-10.8	0.0060	182	<0.05	
10Jan09	MG29D	0.02	0.03	0.03	-24.5	0.0075	115	1.43	-192
	MG27D	0.35	0.36	0.35	-1.5	0.0070	192	<0.05	
	MG37D	11.9	12.0	12.0	-1.6	11.9439	0.1	13.5	-12.2
	MG35D	0.16	0.17	0.16	-6.7	0.1552	4.4	0.11	38.3
13Jan09	MG36D	0.04	0.04	0.04	-6.2	0.0223	55.2	<0.05	
	MG19	0.04	0.05	0.04	-11.0	0.0054	156	<0.05	
	MG34D	0.04	0.04	0.04	-16.3	0.0156	84.8	<0.05	
	MG32D	0.08	0.09	0.09	-8.0	0.1420	-49.1	0.12	-33.0
17Jan09	MG30D	0.10	0.10	0.10	-1.1	0.0907	10.6	<0.05	
	MG31D	0.06	0.06	0.06	-4.9	0.0212	95.9	<0.05	
	MG26D	0.04	0.05	0.04	-13.8	0.0255	52.1	0.59	-173
	MG28D	5.42	5.58	5.50	-2.9	5.7557	-4.5	4.96	10.3
19Jan09	MG24D	0.09	0.10	0.09	-10.5	0.0823	11.1	0.11	-17.9
	MG1	0.02	0.02	0.02	-27.0	<2 ppb		<0.05	
07Jun09	MG9D[d]	20.6	20.6	20.6	-0.1	22.5382	-8.9	55.6	-200
01Jul09	MG9D[d]	7.60	7.61	7.60	-0.1	8.4664	-10.8	8.43	-205
27Jul09	MG40D	222	224	223	-0.9	226.6017	-1.7	ND	
Ave. of Absolute % Mean Differences =				9.5			76.1		98.4
SD (σ) of Absolute % Mean Differences =				11.3			64.5		71.2

[a] AAS, [b] without acid inhibition, [c] injection wells for separated brine, [d] with acid inhibition, ND- not determined

TABLE 15: Li determination

Date	Well	ICP-AES				EDC[a]	ICP-AES vs EDC
		Trial 1	Trial 2	Ave.	% Mean Difference	mg/kg	% Mean Difference
		mg/kg	mg/kg	mg/kg			
11Dec08	MG9D[b]	6.27	6.26	6.26	0.2	5.86	6.6
18Dec08	MN3RD[c]	6.27	6.21	6.24	1.0	ND	
19Dec08	MG9RD[c]	7.10	7.05	7.07	0.7	ND	
26Dec08	MG18D	5.72	5.68	5.70	0.7	5.88	-3.1
	MG23D	4.70	4.68	4.69	0.4	4.72	-0.6
	MG39D	8.57	8.33	8.45	2.8	8.8	-4.0
07Jan09	MG2D	7.10	7.02	7.06	1.1	7.94	-11.8
	MG13D	7.93	7.45	7.69	6.2	7.62	0.9
	MG7D	7.81	7.69	7.75	1.6	8.24	-6.1
	MG16D	8.11	8.65	8.38	-6.5	8.5	-1.4
	MG22D	8.14	7.98	8.06	2.0	8.0	0.5
09Jan09	MG3D	5.86	5.82	5.84	0.7	5.86	-0.4
	MG14D	9.89	10.81	10.35	-8.8	10.3	0.5
10Jan09	MG29D	7.99	7.30	7.64	9.1	7.4	3.2
	MG27D	3.36	3.27	3.32	2.7	3.06	8.0
	MG37D	15.3	15.1	15.2	1.8	15.3	-0.8
	MG35D	8.65	8.54	8.59	1.2	8.98	-4.4
13Jan09	MG36D	5.63	5.09	5.36	10.1	5.06	5.7
	MG19	7.82	7.74	7.78	1.1	7.78	0.0
	MG34D	6.16	5.88	6.02	4.6	6	0.3
	MG32D	1.34	1.34	1.34	0.4	1.49	-10.7
17Jan09	MG30D	6.99	6.91	6.95	1.1	7.06	-1.6
	MG31D	7.65	7.58	7.61	0.9	7.74	-1.7
	MG26D	4.11	4.12	4.12	-0.2	4.04	1.8
	MG28D	5.78	5.72	5.75	0.9	5.82	-1.2
19Jan09	MG24D	4.24	4.23	4.23	0.3	4.2	0.3
	MG1	3.96	3.91	3.93	1.4	3.96	-0.6
07Jun09	MG9D[d]	6.22	6.22	6.22	-0.02	6.52	-4.7
01Jul09	MG9D[d]	6.45	6.49	6.47	-0.6	7.0	-8.0
27Jul09	MG40D	12.1	12.1	12.1	-0.02		
Ave. of Absolute % Mean Differences =					2.3		3.2
SD (σ) of Absolute % Mean Differences =					2.9		3.4

[a] AAS, [b] without acid inhibition, [c] injection wells for separated brine, [d] with acid inhibition, ND- not determined

TABLE 16: Sr determination

Date	Well	ICP-AES				ICP-MS[a]				ICP-AES vs ICP-MS
		Trial 1	Trial 2	Ave.	% Mean Difference	Trial 1	Trial 2	Ave.	% Mean Difference	% Mean Difference
		mg/kg	mg/kg	mg/kg		mg/kg	mg/kg	mg/kg		
11Dec08	MG9D[c]	0.104	0.105	0.104	-1.1	0.1103	0.1123	0.1113	-1.7	-6.5
18Dec08	MN3R[d]	0.655	0.658	0.656	-0.5	0.6745	0.6879	0.6812	-2.0	-3.7
19Dec08	MG9R[d]	0.546	0.548	0.547	-0.5	0.5678	0.5480	0.5579	3.5	-2.0
26Dec08	MG18D	0.255	0.257	0.256	-0.9	0.2624	0.2680	0.2652	-2.1	-3.4
	MG23D	0.429	0.433	0.431	-1.0	0.4483	0.4542	0.4512	-1.3	-4.6
	MG39D	0.437	0.434	0.435	0.7	0.4373	0.4828	0.4601	-9.9	-5.5
07Jan09	MG2D	0.507	0.508	0.507	-0.4	0.5188	0.5359	0.5274	-3.2	-3.8
	MG13D	0.160	0.157	0.158	1.9	0.1589	0.1598	0.1594	-0.6	-0.8
	MG7D	0.815	0.815	0.815	0.0	0.8338	0.8202	0.8270	1.6	-1.5
	MG16D	0.647	0.672	0.659	-3.8	0.6755	0.6796	0.6775	-0.6	-2.7
	MG22D	0.667	0.665	0.666	0.3	0.6737	0.7115	0.6926	-5.5	-3.9
09Jan09	MG3D	0.706	0.714	0.710	-1.0	0.7205	0.8495	0.7850	-16.4	-10.0
	MG14D	1.960	2.068	2.014	-5.4	2.1080	2.0254	2.0667	4.0	-2.6
10Jan09	MG29D	0.699	0.665	0.682	5.0	0.6819	0.6957	0.6888	-2.0	-1.0
	MG27D	0.181	0.181	0.181	-0.1	0.1840	0.1847	0.1843	-0.4	-1.8
	MG37D	4.647	4.576	4.611	1.5	4.8540	4.8053	4.8297	1.0	-4.6
	MG35D	0.629	0.632	0.630	-0.4	0.6657	0.6592	0.6625	1.0	-5.0
13Jan09	MG36D	0.396	0.376	0.386	5.2	0.3808	0.3957	0.3882	-3.9	-0.7
	MG19	0.468	0.467	0.467	0.1	0.4728	0.4847	0.4787	-2.5	-2.4
	MG34D	0.623	0.609	0.616	2.3	0.6205	0.6330	0.6268	-2.0	-1.8
	MG32D	0.147	0.149	0.148	-1.1	0.1491	0.1434	0.1462	3.9	1.1
17Jan09	MG30D	0.751	0.751	0.751	-0.1	0.7752	0.8279	0.8015	-6.6	-6.5
	MG31D	0.765	0.767	0.766	-0.2	0.7908	0.7928	0.7918	-0.3	-3.3
	MG26D	0.449	0.454	0.451	-1.1	0.4357	0.5066	0.4711	-15.1	-4.3
	MG28D	0.317	0.318	0.318	-0.3	0.3226	0.3325	0.3276	-3.0	-3.0
19Jan09	MG24D	0.374	0.378	0.376	-1.2	0.3541	0.3828	0.3684	-7.8	2.0
	MG1	0.254	0.254	0.254	-0.1	0.2584	0.2860	0.2722	-10.1	-6.8
07Jun09	MG9D[e]	0.080	0.081	0.081	-0.9	0.0851	0.0828	0.0839	2.7	-3.8
01Jul09	MG9D[e]	0.116	0.116	0.116	-0.1	0.1174	0.1203	0.1189	-2.4	-2.2
27Jul09	MG40D	4.882	4.911	4.896	-0.6	4.6367	4.7060	4.6714	-1.5	4.7
Ave. of Absolute % Mean Differences =					1.3				4.0	3.5
SD (σ) of Absolute % Mean Differences =					1.5				4.1	2.1

[a] readings mostly above standard values, [b] titrimetry (mannitol), [c] without acid inhibition, [d] injection wells for separated brine, [e] with acid inhibition

TABLE 17: As determination

Date	Well	ICP-AES				ICP-MS	ICP-AES vs ICP-MS
		Trial 1	Trial 2	Ave.	% Mean Difference	mg/kg	% Mean Difference
		mg/kg	mg/kg	mg/kg			
11Dec08	MG9D[a]	nil	nil			0.1415	
18Dec08	MN3RD[b]	2.46	2.62	2.54	-6.5	2.5436	-0.2
19Dec08	MG9RD[b]	4.24	4.38	4.31	-3.3	3.7715	13.3
26Dec08	MG18D	3.63	3.69	3.66	-1.7	3.4657	5.4
	MG23D	3.46	3.50	3.48	-1.1	3.0734	12.3
	MG39D	4.35	4.40	4.38	-1.0	3.8752	12.2
07Jan09	MG2D	4.15	4.22	4.18	-1.5	3.6749	13.0
	MG13D	3.68	3.77	3.73	-2.4	3.5513	4.8
	MG7D	4.80	4.93	4.87	-2.7	4.1394	16.1
	MG16D	4.63	4.71	4.67	-1.7	4.2027	10.5
	MG22D	4.92	4.98	4.95	-1.2	4.2015	16.4
09Jan09	MG3D	3.58	3.80	3.69	-6.1	3.6218	1.8
	MG14D	3.70	3.96	3.83	-6.8	3.4115	11.7
10Jan09	MG29D	2.85	2.86	2.85	-0.2	2.4816	13.9
	MG27D	1.69	1.60	1.65	5.6	1.5474	6.2
	MG37D	4.11	4.21	4.16	-2.4	3.5270	16.4
	MG35D	3.02	3.21	3.12	-5.9	3.3245	-6.5
13Jan09	MG36D	2.90	2.96	2.93	-1.8	2.5259	14.8
	MG19	3.98	4.04	4.01	-1.6	3.2991	19.5
	MG34D	2.47	2.51	2.49	-1.5	2.8104	-12.2
	MG32D	0.20	0.16	0.18	21.8	0.6190	-109.5
17Jan09	MG30D	3.60	3.68	3.64	-2.1	3.2941	10.0
	MG31D	3.08	3.29	3.19	-6.6	2.8976	9.6
	MG26D	2.80	2.85	2.83	-1.9	2.3078	20.2
	MG28D	3.55	3.55	3.55	0.1	2.9097	19.9
19Jan09	MG24D	0.86	0.84	0.85	2.2	1.5084	-55.9
	MG1	2.20	2.28	2.24	-3.7	1.9473	13.9
07Jun09	MG9D[c]	3.93	4.04	3.99	-2.8	3.7169	7.1
01Jul09	MG9D[c]	4.19	4.04	4.11	3.7	3.6394	12.3
27Jul09	MG40D	5.23	5.34	5.28	-2.0	4.4314	17.5
Ave. of Absolute % Mean Differences =					3.5		16.7
SD (σ) of Absolute % Mean Differences =					4.0		20.3

[a] without acid inhibition, [b] injection wells for separated brine, [c] with acid inhibition, nil- not detectable

TABLE 18: Ba determination

Date	Well	ICP-AES				ICP-MS				ICP-AES vs ICP-MS
		Trial 1	Trial 2	Ave.	% Mean	Trial 1	Trial 2	Ave.	% Mean	% Mean Difference
		µg/kg	µg/kg	µg/kg	Difference	µg/kg	µg/kg	µg/kg	Difference	
11Dec08	MG9D[a]	155.4	153.2	154.3	1.4	82.3	87.3	84.8	-5.8	58.1
18Dec08	MN3R[b]	197.9	197.1	197.5	0.4	192.4	206.6	199.5	-7.1	-1.0
19Dec08	MG9R[b]	93.5	103.3	98.4	-9.9	83.9	79.6	81.8	5.3	18.5
26Dec08	MG18D	51.5	54.3	52.9	-5.3	44.1	40.6	42.4	8.2	22.1
	MG23D	16.5	17.2	16.9	-4.5	16.1	12.2	14.2	27.2	17.2
	MG39D	48.7	53.9	51.3	-10.2	48.2	53.9	51.0	-11.3	0.5
07Jan09	MG2D	51.2	50.1	50.6	2.2	33.1	29.6	31.3	11.2	47.1
	MG13D	100.3	95.9	98.1	4.6	94.7	97.5	96.1	-3.0	2.0
	MG7D	92.2	109.7	101.0	-17.3	69.3	64.5	66.9	7.2	40.6
	MG16D	53.4	61.2	57.3	-13.6	32.3	32.6	32.4	-0.7	55.3
	MG22D	54.2	61.2	57.7	-12.2	39.5	33.7	36.6	15.9	44.7
09Jan09	MG3D	155.1	152.9	154.0	1.5	153.2	189.5	171.4	-21.2	-10.7
	MG14D	1333.4	1358.8	1346.1	-1.9	1449.3	1497.6	1473.5	-3.3	-9.0
10Jan09	MG29D	135.2	125.1	130.1	7.8	116.4	121.2	118.8	-4.1	9.1
	MG27D	61.4	70.4	65.9	-13.5	51.3	49.8	50.5	3.0	26.4
	MG37D	2204.6	2128.1	2166.3	3.5	2402.1	2577.2	2489.7	-7.0	-13.9
	MG35D	171.8	170.6	171.2	0.7	187.8	196.4	192.1	-4.5	-11.5
13Jan09	MG36D	75.0	73.7	74.4	1.8	58.0	56.6	57.3	2.4	26.0
	MG19	65.6	69.2	67.4	-5.3	47.2	48.8	48.0	-3.3	33.6
	MG34D	442.7	420.1	431.4	5.3	457.7	481.9	469.8	-5.2	-8.5
	MG32D	35.8	36.2	36.0	-1.3	41.6	39.6	40.6	5.0	-12.0
17Jan09	MG30D	103.0	113.4	108.2	-9.6	88.9	92.5	90.7	-3.9	17.6
	MG31D	280.8	275.9	278.3	1.8	274.3	288.5	281.4	-5.0	-1.1
	MG26D	259.4	253.3	256.4	2.4	259.8	297.9	278.8	-13.7	-8.4
	MG28D	207.7	203.2	205.5	2.2	213.6	224.2	218.9	-4.8	-6.3
19Jan09	MG24D	132.7	142.7	137.7	-7.3	113.4	122.7	118.1	-7.8	15.3
	MG1	32.0	38.7	35.3	-19.0	25.4	26.2	25.8	-3.1	31.1
07Jun09	MG9D[c]	135.2	133.3	134.3	1.4	130.9	129.2	130.1	1.2	3.2
01Jul09	MG9D[c]	237.5	238.2	237.8	-0.3	237.8	245.4	241.6	-3.2	-1.6
27Jul09	MG40D	1924.8	1940.8	1932.8	-0.8	1327.9	1376.9	1352.4	-3.6	35.3
Ave. of Absolute % Mean Differences =					5.6				6.9	19.6
SD (σ) of Absolute % Mean Differences =					5.3				5.9	16.7

[a]- without acid inhibition, [b]-injection wells for separated brine,[c]-with acid inhibition

TABLE 19: Be determination

Date	Well	ICP-MS			
		Trial 1	Trial 2	Ave.	% Mean
		µg/kg	µg/kg	µg/kg	Difference
11Dec08	MG9D[a]	5.5028	3.7051	4.6039	39.0
18Dec08	MN3RD[b]	3.1088	0.2459	1.6774	170.7
19Dec08	MG9RD[b]	4.0948	0.1558	2.1253	185.3
26Dec08	MG18D	4.5080	0.3479	2.4279	171.3
	MG23D	3.2563	0.1390	1.6977	183.6
	MG39D	4.4478	0.3115	2.3797	173.8
07Jan09	MG2D	4.2612	0.1663	2.2137	185.0
	MG13D	4.6460	0.3436	2.4948	172.5
	MG7D	4.5793	0.2111	2.3952	182.4
	MG16D	4.7623	0.2288	2.4956	181.7
	MG22D	4.3395	0.2377	2.2886	179.2
09Jan09	MG3D	3.4543	0.2348	1.8446	174.5
	MG14D	4.6437	0.2788	2.4612	177.3
10Jan09	MG29D	2.6026	0.1296	1.3661	181.0
	MG27D	2.2246	0.1219	1.1733	179.2
	MG37D	5.4162	0.5663	2.9912	162.1
	MG35D	6.2318	0.6512	3.4415	162.2
13Jan09	MG36D	2.8834	0.1278	1.5056	183.0
	MG19	3.9724	0.1750	2.0737	183.1
	MG34D	5.9143	0.6004	3.2573	163.1
	MG32D	2.1036	0.2697	1.1867	154.5
17Jan09	MG30D	2.7698	0.1310	1.4504	181.9
	MG31D	3.8060	0.3451	2.0755	166.7
	MG26D	3.1011	0.5020	1.8016	144.3
	MG28D	4.2792	0.8199	2.5495	135.7
19Jan09	MG24D	2.1569	0.1160	1.1364	179.6
	MG1	2.8366	0.0939	1.4652	187.2
07Jun09	MG9D[c]	4.7315	0.9144	2.8229	135.2
01Jul09	MG9D[c]	4.3896	0.8899	2.6397	132.6
27Jul09	MG40D	5.7247	0.7269	3.2258	154.9
Ave. of Absolute % Mean Differences =					165.4
SD (σ) of Absolute % Mean Differences =					28.7

[a] without acid inhibition, [b] injection wells for separated brine, [c] with acid inhibition

TABLE 20: Br determination

Date	Well	ICP-AES			
		Trial 1	Trial 2	Ave.	% Mean
		mg/kg	mg/kg	mg/kg	Difference
11Dec08	MG9D[a]	14.52	14.93	14.73	-2.8
18Dec08	MN3RD[b]	15.61	16.33	15.97	-4.5
19Dec08	MG9RD[b]	17.34	18.25	17.80	-5.1
26Dec08	MG18D	16.98	17.20	17.09	-1.3
	MG23D	14.17	14.40	14.29	-1.7
	MG39D	18.24	18.90	18.57	-3.6
07Jan09	MG2D	17.24	17.50	17.37	-1.5
	MG13D	16.78	17.35	17.06	-3.3
	MG7D	19.00	19.58	19.29	-3.0
	MG16D	20.02	19.54	19.78	2.4
	MG22D	19.36	19.81	19.59	-2.3
09Jan09	MG3D	17.42	18.13	17.77	-4.0
	MG14D	26.80	24.78	25.79	7.9
10Jan09	MG29D	16.27	17.23	16.75	-5.8
	MG27D	9.42	9.00	9.21	4.6
	MG37D	37.41	38.57	37.99	-3.1
	MG35D	19.34	19.79	19.57	-2.3
13Jan09	MG36D	11.90	12.44	12.17	-4.4
	MG19	16.14	16.65	16.39	-3.1
	MG34D	18.08	18.52	18.30	-2.4
	MG32D	3.64	3.53	3.58	3.1
17Jan09	MG30D	17.22	17.45	17.33	-1.3
	MG31D	19.11	19.52	19.31	-2.1
	MG26D	12.44	12.50	12.47	-0.4
	MG28D	17.06	17.16	17.11	-0.6
19Jan09	MG24D	12.19	12.60	12.40	-3.4
	MG1	10.56	10.68	10.62	-1.1
07Jun09	MG9D[c]	17.11	17.50	17.31	-2.3
01Jul09	MG9D[c]	17.15	17.38	17.27	-1.4
27Jul09	MG40D	33.88	35.89	34.89	-5.8
Ave. of Absolute % Mean Differences =					3.0
SD (σ) of Absolute % Mean Differences =					1.7

[a] without acid inhibition, [b] injection wells for separated brine, [c] with acid inhibition

TABLE 21: Cs determination

Date	Well	ICP-MS			
		Trial 1	Trial 2	Ave.	% Mean Difference
		mg/kg	mg/kg	mg/kg	
11Dec08	MG9D[a]	0.66972	0.59326	0.63149	12.1
18Dec08	MN3RD[b]	0.73911	0.67168	0.70539	9.6
19Dec08	MG9RD[b]	1.02446	0.86026	0.94236	17.4
26Dec08	MG18D	0.98862	0.86488	0.92675	13.4
	MG23D	0.80197	0.70819	0.75508	12.4
	MG39D	1.12917	1.05932	1.09424	6.4
07Jan09	MG2D	1.02913	0.89562	0.96238	13.9
	MG13D	1.06951	0.93897	1.00424	13.0
	MG7D	1.07408	0.92512	0.99960	14.9
	MG16D	1.14296	0.97711	1.06004	15.6
	MG22D	1.12373	1.01639	1.07006	10.0
09Jan09	MG3D	0.68494	0.71534	0.70014	-4.3
	MG14D	1.15310	0.96879	1.06094	17.4
10Jan09	MG29D	0.80776	0.70679	0.75728	13.3
	MG27D	0.41345	0.36801	0.39073	11.6
	MG37D	1.19747	1.01085	1.10416	16.9
	MG35D	1.07743	0.91211	0.99477	16.6
13Jan09	MG36D	0.61644	0.54287	0.57965	12.7
	MG19	0.96807	0.82542	0.89675	15.9
	MG34D	1.07642	0.92122	0.99882	15.5
	MG32D	0.28100	0.23929	0.26014	16.0
17Jan09	MG30D	0.79360	0.74117	0.76739	6.8
	MG31D	0.99691	0.84611	0.92151	16.4
	MG26D	0.55387	0.54574	0.54981	1.5
	MG28D	0.67707	0.59037	0.63372	13.7
19Jan09	MG24D	0.48183	0.43576	0.45880	10.0
	MG1	0.54153	0.50297	0.52225	7.4
07Jun09	MG9D[c]	0.80863	0.67709	0.74286	17.7
01Jul09	MG9D[c]	0.77060	0.69099	0.73080	10.9
27Jul09	MG40D	1.00869	0.85242	0.93055	16.8
Ave. of Absolute % Mean Differences =					12.7
SD (σ) of Absolute % Mean Differences =					4.2

[a] without acid inhibition, [b] injection wells for separated brine, [c] with acid inhibition, ND- not determined

TABLE 22: Mn determination

Date	Well	ICP-AES				ICP-MS	ICP-AES vs ICP-MS
		Trial 1	Trial 2	Ave.	% Mean Difference	µg/kg	% Mean Difference
		µg/kg	µg/kg	µg/kg			
11Dec08	MG9D[a]	12145	12482	12313	-2.7	10388	17.0
18Dec08	MN3RD[b]	396	409	402	-3.2	391.43	2.8
19Dec08	MG9RD[b]	77.6	78.4	78.0	-1.0	80.869	-3.6
26Dec08	MG18D	32.0	31.7	31.8	1.0	70.315	-75.3
	MG23D	13.4	15.8	14.6	-16.2	14.826	-1.3
	MG39D	49.6	50.8	50.2	-2.3	47.74	5.0
07Jan09	MG2D	58.7	59.7	59.2	-1.7	53.923	9.4
	MG13D	60.0	61.8	60.9	-2.9	51.317	17.1
	MG7D	94.1	95.1	94.6	-1.1	65.963	35.7
	MG16D	73.1	72.4	72.7	0.9	68.213	6.4
	MG22D	62.3	61.7	62.0	1.0	57.9	6.8
09Jan09	MG3D	404	412	408	-2.0	370.16	9.7
	MG14D	1800	1772	1786	1.6	1742.0	2.5
10Jan09	MG29D	74.1	73.5	73.8	0.8	80.4	-8.5
	MG27D	17.2	16.7	17.0	3.0	20.847	-20.5
	MG37D	14231	14431	14331	-1.4	13607.3	5.2
	MG35D	2039	2076	2058	-1.8	2018.9	1.9
13Jan09	MG36D	34.5	34.5	34.5	-0.1	32.629	5.6
	MG19	47.6	48.7	48.1	-2.4	46.714	3.0
	MG34D	142	142	142	-0.4	131.18	7.9
	MG32D	21.3	20.8	21.0	2.6	22.994	-8.8
17Jan09	MG30D	57.9	57.7	57.8	0.2	63.375	-9.2
	MG31D	182	184	183	-1.3	166.44	9.3
	MG26D	38.4	38.2	38.3	0.5	35.917	6.4
	MG28D	2723	2770	2747	-1.7	2538.4	7.9
19Jan09	MG24D	214	217	215	-1.3	176.0	20.1
	MG1	16.3	16.3	16.3	0.1	16.606	-1.8
07Jun09	MG9D[c]	1980	1981	1980	-0.1	2005	-1.2
01Jul09	MG9D[c]	3204	3206	3205	-0.1	2983.2	7.2
27Jul09	MG40D	51646	51886	51766	-0.5	42441	19.8
Ave. of Absolute % Mean Differences =					1.9		11.2
SD (σ) of Absolute % Mean Differences =					2.9		14.3

[a] without acid inhibition, [b] injection wells for separated brine, [c] with acid inhibition

TABLE 23: Mo determination

Date	Well	ICP-MS			
		Trial 1	Trial 2	Ave.	% Mean Difference
		µg/kg	µg/kg	µg/kg	
11Dec08	MG9D[a]	45.9	20.6	33.2	76.0
18Dec08	MN3RD[b]	51.1	22.2	36.6	78.8
19Dec08	MG9RD[b]	59.8	26.9	43.3	75.7
26Dec08	MG18D	51.7	21.5	36.6	82.3
	MG23D	44.5	19.6	32.1	77.6
	MG39D	49.8	17.1	33.4	98.0
07Jan09	MG2D	57.5	27.7	42.6	70.1
	MG13D	48.7	18.3	33.5	90.9
	MG7D	62.0	27.7	44.8	76.6
	MG16D	55.1	18.2	36.7	100.8
	MG22D	56.0	22.5	39.3	85.5
09Jan09	MG3D	44.5	14.1	29.3	103.8
	MG14D	57.8	5.2	31.5	167.0
10Jan09	MG29D	46.6	16.6	31.6	94.8
	MG27D	33.0	19.1	26.1	53.6
	MG37D	83.2	6.5	44.9	171.1
	MG35D	51.1	13.8	32.4	115.0
13Jan09	MG36D	41.1	20.8	31.0	65.7
	MG19	43.1	14.8	29.0	97.8
	MG34D	58.0	22.8	40.4	87.3
	MG32D	14.6	10.6	12.6	31.7
17Jan09	MG30D	47.0	19.6	33.3	82.1
	MG31D	47.2	12.9	30.0	114.1
	MG26D	39.9	23.3	31.6	52.4
	MG28D	34.3	3.1	18.7	167.2
19Jan09	MG24D	30.8	12.2	21.5	86.7
	MG1	33.0	17.3	25.1	62.5
07Jun09	MG9D[c]	46.8	12.5	29.7	115.4
01Jul09	MG9D[c]	39.7	5.4	22.6	152.1
27Jul09	MG40D	79.8	16.8	48.3	130.4
Ave. of Absolute % Mean Differences =					95.4
SD (σ) of Absolute % Mean Differences =					34.4

[a] without acid inhibition, [b] injection wells for separated brine, [c] with acid inhibition

TABLE 24: Pb determination

Date	Well	ICP-MS			
		Trial 1	Trial 2	Ave.	% Mean Difference
		µg/kg	µg/kg	µg/kg	
11Dec08	MG9D[a]	10.727	12.033	11.380	-11.5
18Dec08	MN3RD[b]	0.894	0.607	0.751	38.2
19Dec08	MG9RD[b]	0.494	0.396	0.445	21.9
26Dec08	MG18D	1.132	0.905	1.018	22.3
	MG23D	0.460	0.512	0.486	-10.7
	MG39D	0.403	0.490	0.447	-19.6
07Jan09	MG2D	0.402	0.383	0.392	4.9
	MG13D	0.321	0.328	0.324	-2.1
	MG7D	0.260	0.291	0.276	-11.1
	MG16D	0.275	0.293	0.284	-6.1
	MG22D	0.289	0.333	0.311	-14.4
09Jan09	MG3D	0.213	0.261	0.237	-20.1
	MG14D	0.393	0.375	0.384	4.9
10Jan09	MG29D	0.249	0.242	0.246	2.8
	MG27D	0.289	0.305	0.297	-5.4
	MG37D	0.620	0.620	0.620	0.0
	MG35D	0.332	0.350	0.341	-5.3
13Jan09	MG36D	0.434	0.464	0.449	-6.7
	MG19	0.234	0.276	0.255	-16.8
	MG34D	1.027	0.792	0.909	25.8
	MG32D	0.582	0.535	0.558	8.4
17Jan09	MG30D	0.339	0.338	0.338	0.3
	MG31D	0.536	0.498	0.517	7.3
	MG26D	0.839	0.837	0.838	0.2
	MG28D	0.342	0.422	0.382	-21.0
19Jan09	MG24D	0.471	0.515	0.493	-8.9
	MG1	0.571	0.626	0.598	-9.1
07Jun09	MG9D[c]	177.965	176.206	177.086	1.0
01Jul09	MG9D[c]	114.064	119.379	116.721	-4.6
27Jul09	MG40D	190.242	192.731	191.486	-1.3
Ave. of Absolute % Mean Differences =					10.4
SD (σ) of Absolute % Mean Differences =					9.2

[a] without acid inhibition, [b] injection wells for separated brine, [c] with acid inhibition

TABLE 25: Rb determination

Date	Well	ICP-MS			
		Trial 1	Trial 2	Ave.	% Mean Difference
		mg/kg	mg/kg	mg/kg	
11Dec08	MG9D[a]	1.8139	1.6992	1.7565	6.5
18Dec08	MN3RD[b]	2.1579	2.0099	2.0839	7.1
19Dec08	MG9RD[b]	2.7375	2.4402	2.5889	11.5
26Dec08	MG18D	2.3384	2.1549	2.2467	8.2
	MG23D	2.0792	1.9311	2.0052	7.4
	MG39D	3.0483	3.0637	3.0560	-0.5
07Jan09	MG2D	2.6962	2.5531	2.6246	5.5
	MG13D	3.1196	2.9423	3.0310	5.8
	MG7D	2.8736	2.6627	2.7682	7.6
	MG16D	3.0987	2.8651	2.9819	7.8
	MG22D	3.0361	2.9441	2.9901	3.1
09Jan09	MG3D	1.9036	2.0474	1.9755	-7.3
	MG14D	3.6169	3.2909	3.4539	9.4
10Jan09	MG29D	2.4086	2.2481	2.3284	6.9
	MG27D	1.0535	1.0178	1.0356	3.5
	MG37D	6.6689	6.1991	6.4340	7.3
	MG35D	2.9871	2.6936	2.8404	10.3
13Jan09	MG36D	1.7161	1.6030	1.6596	6.8
	MG19	2.5898	2.4198	2.5048	6.8
	MG34D	2.6496	2.4609	2.5552	7.4
	MG32D	0.6031	0.5671	0.5851	6.1
17Jan09	MG30D	2.2133	2.2094	2.2114	0.2
	MG31D	2.6351	2.4444	2.5398	7.5
	MG26D	1.5157	1.5798	1.5477	-4.1
	MG28D	2.0164	1.8415	1.9290	9.1
19Jan09	MG24D	1.8517	1.7927	1.8222	3.2
	MG1	1.3297	1.3131	1.3214	1.3
07Jun09	MG9D[c]	2.2587	2.0305	2.1446	10.6
01Jul09	MG9D[c]	2.2894	2.1640	2.2267	5.6
27Jul09	MG40D	5.0139	4.6983	4.8561	6.5
Ave. of Absolute % Mean Differences =					6.4
SD (σ) of Absolute % Mean Differences =					2.8

[a] without acid inhibition, [b] injection wells for separated brine, [c] with acid inhibition, ND- not determined

TABLE 26: Sb determination

Date	Well	ICP-MS			
		Trial 1	Trial 2	Ave.	% Mean Difference
		µg/kg	µg/kg	µg/kg	
11Dec08	MG9D[a]	9.6	10.3	10.0	-7.9
18Dec08	MN3RD[b]	15.6	15.2	15.4	2.5
19Dec08	MG9RD[b]	62.5	59.9	61.2	4.3
26Dec08	MG18D	58.7	57.1	57.9	2.7
	MG23D	51.3	49.8	50.5	3.0
	MG39D	25.5	27.1	26.3	-6.0
07Jan09	MG2D	56.9	56.9	56.9	0.1
	MG13D	28.3	27.1	27.7	4.4
	MG7D	89.2	86.5	87.9	3.2
	MG16D	19.7	19.2	19.4	2.7
	MG22D	97.4	100.6	99.0	-3.3
09Jan09	MG3D	5.0	5.7	5.3	-14.1
	MG14D	1.2	1.1	1.2	5.7
10Jan09	MG29D	17.2	16.7	17.0	2.9
	MG27D	26.1	25.3	25.7	3.1
	MG37D	3.1	3.1	3.1	-0.1
	MG35D	1.7	1.7	1.7	-1.1
13Jan09	MG36D	55.1	53.8	54.5	2.4
	MG19	7.9	8.8	8.4	-11.3
	MG34D	6.8	6.1	6.4	10.9
	MG32D	20.1	18.9	19.5	6.0
17Jan09	MG30D	66.9	70.6	68.7	-5.3
	MG31D	4.6	4.3	4.4	8.1
	MG26D	66.5	73.1	69.8	-9.4
	MG28D	1.7	1.9	1.8	-6.9
19Jan09	MG24D	13.4	13.6	13.5	-1.5
	MG1	17.4	17.6	17.5	-0.9
07Jun09	MG9D[c]	18.3	16.9	17.6	7.9
01Jul09	MG9D[c]	79.3	79.1	79.2	0.3
27Jul09	MG40D	62.3	60.2	61.3	3.3
Ave. of Absolute % Mean Differences =					4.7
SD (σ) of Absolute % Mean Differences =					3.6

[a] without acid inhibition, [b] injection wells for separated brine, [c] with acid inhibition

TABLE 27: W determination

Date	Well	ICP-MS			
		Trial 1	Trial 2	Ave.	% Mean
		µg/kg	µg/kg	µg/kg	Difference
11Dec08	MG9D[a]	7.6	7.5	7.6	1.3
18Dec08	MN3RD[b]	10.5	10.4	10.4	0.8
19Dec08	MG9RD[b]	10.7	10.2	10.4	4.4
26Dec08	MG18D	10.4	10.2	10.3	2.0
	MG23D	11.2	11.1	11.1	0.6
	MG39D	8.1	9.0	8.6	-10.5
07Jan09	MG2D	8.4	8.6	8.5	-2.2
	MG13D	9.5	9.6	9.5	-1.5
	MG7D	10.2	10.1	10.2	1.2
	MG16D	10.3	10.4	10.3	-0.3
	MG22D	8.7	9.4	9.0	-7.7
09Jan09	MG3D	2.3	2.7	2.5	-16.7
	MG14D	4.2	4.2	4.2	0.0
10Jan09	MG29D	8.5	8.9	8.7	-4.1
	MG27D	10.8	11.0	10.9	-2.5
	MG37D	4.1	4.2	4.2	-1.2
	MG35D	7.2	7.3	7.2	-1.0
13Jan09	MG36D	10.4	10.7	10.6	-3.0
	MG19	8.2	8.4	8.3	-2.0
	MG34D	13.0	11.7	12.4	10.4
	MG32D	6.9	6.7	6.8	3.1
17Jan09	MG30D	7.5	8.3	7.9	-10.5
	MG31D	8.7	8.8	8.7	-1.6
	MG26D	12.8	14.5	13.7	-12.4
	MG28D	3.2	3.2	3.2	-1.1
19Jan09	MG24D	7.7	8.1	7.9	-5.7
	MG1	9.6	10.6	10.1	-9.5
07Jun09	MG9D[c]	2.9	2.8	2.9	3.2
01Jul09	MG9D[c]	2.7	2.8	2.7	-2.1
27Jul09	MG40D	8.3	8.6	8.4	-3.1
Ave. of Absolute % Mean Differences =					4.2
SD (σ) of Absolute % Mean Differences =					4.3

[a] without acid inhibition, [b] injection wells for separated brine,
[c] with acid inhibition